AD-A040 180 IIT RESEARCH INST CHICAGO ILL F/G 18/3
A BIBLIOGRAPHY ON THE RESPONSE OF EARTH MEDIA AND BURIED STRUCT--ETC(U)
JUN 67 R L CHIAPETTA, C J COSTANTINO DACA39-67-C-0015
UNCLASSIFIED WES-CR-3-168 NL

1 OF 2
AD
A040 180

Contract Report No. 3-168

A BIBLIOGRAPHY ON THE RESPONSE OF EARTH ME AND BURIED STRUCTURES TO GROUND SHOCK LOAD

IITRI Project M6177
Final Report

for

Waterways Experiment Station
Corps of Engineers
Department of the Army
Vicksburg, Mississippi

A BIBLIOGRAPHY ON THE RESPONSE OF EARTH MEDIA AND BURIED STRUCTURES TO GROUND SHOCK LOADING

IITRI Project M6177
Final Report

for

Waterways Experiment Station
Corps of Engineers
Department of the Army
Vicksburg, Mississippi

CONTRACT REPORT NO. 3-168

IIT Research Institute
Technology Center
Chicago, Illinois 60616

(1)

AD-A040180

A BIBLIOGRAPHY ON THE RESPONSE OF EARTH MEDIA AND BURIED STRUCTURES TO GROUND SHOCK LOADING

IITRI Project M6177
Final Report

Prepared by

R. L. Chiapetta
C. J. Costantino

for

Waterways Experiment Station
Corps of Engineers
Department of the Army
Vicksburg, Mississippi

Under
Contract No. DACA39-67-C-0015

June 1967

ABSTRACT

Brief descriptions are presented of several of IIT Research Institute's analyses and associated computer codes relating to shock wave propagation through earth media and to the response of buried structures to ground shock loading.

CONTENTS

ILLUSTRATIONS

ILLUSTRATIONS (Contd)

ILLUSTRATIONS (Contd)

I. INTRODUCTION

This report contains a compilation of summaries of analyses developed at IIT Research Institute pertaining to wave propagation through earth media and soil-structure interaction as a result of nuclear detonation or other high intensity wave sources.

The summaries can basically be divided into two groups. The first group describes analyses which were concerned with determination of the free-field behavior of earth media subjected to shock wave propagation through it. The second group is composed of studies devoted to the prediction of horizontal and/or vertical response of buried tunnel and missile-silo structures to ground shock loading.

References for each analysis are cited by number immediately following the title. The corresponding reference information is contained in the list of references at the end of the report.

II. FREE-FIELD ENVIRONMENT

The studies associated with determination of the free-field behavior of the earth media have been separated either into a category in which the analyses are based on a hydrodynamic description of material behavior, or one in which the analyses characterize the soil as a solid. There is no essential difference between the two approaches for one-dimensional problems.

A. Hydrodynamic Models

1. SWIMM Code (Ref. 1)

The SWIMM (Stress Waves in Multilayered Media) Code was written in FORTRAN II for use on an IBM 7094 digital computer. The purpose of the code is to calculate one-dimensional uniaxial stress wave attenuation in layered media. The main uses thus far of the code have been in accomplishing calculations involved

in the analysis of various blast shield designs for use with a nuclear reactor in the advent of a malfunction due to overheating. However, the code can also be directly applied to predict the air-induced ground shock environment created by an H.E. or nuclear explosion.

The media may contain from one to forty separate layers, as illustrated in Fig. 1, with a prescribed loading at the top surface and a base boundary condition corresponding either to a rigid wall (i.e., velocity equal to zero), or to a free surface (i.e., stress or pressure equal to zero). This enables the code to handle a wide variety of stress wave problems.

Each layer may exhibit different material properties as characterized by a stress-specific volume relationship accommodating elastic, plastic and compactible ranges as shown in Fig. 2. This relationship is represented by a piecewise linear approximating function consisting of a number (maximum of 30) of connected straight line segments. Provision is also included to allow for unloading from any stress state. A maximum of four linear unloading paths can be specified for various ranges of the function.

The computer code can handle two types of applied loadings. First, the loading upon the top surface of the material may be an arbitrary pressure-time function which is represented in the form of a stepwise series of values as shown in Fig. 3. Up to 75 steps may be specified, thereby providing a relatively good fit to most arbitrarily desired curves (at least to the extent required by the SWIMM Code). The second method of surface loading is supplied by the specification of the velocity of a second moving body which impacts the layered media. In this manner problems such as a projectile striking a fixed surface may be analyzed.

The wave diagram in Fig. 4 presents a qualitative picture of the propagation of various wave fronts in the layered media. The numbered areas indicate distinct zones of a uniform state.

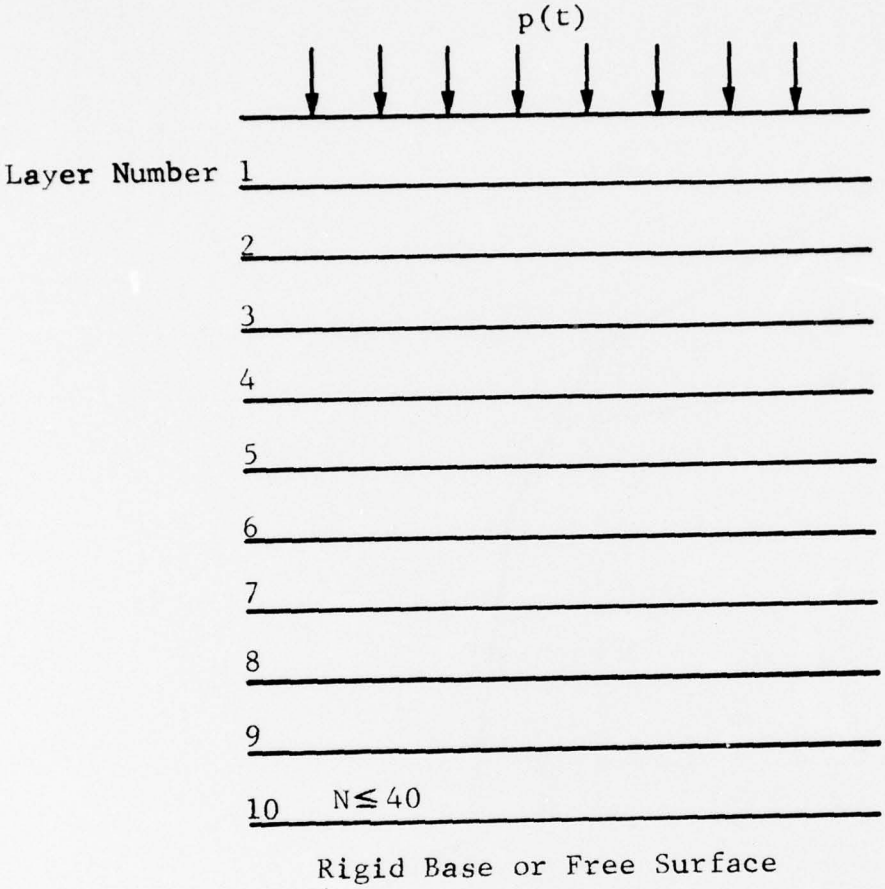

FIG. 1 ONE-DIMENSIONAL MODEL FOR SWIMM CODE

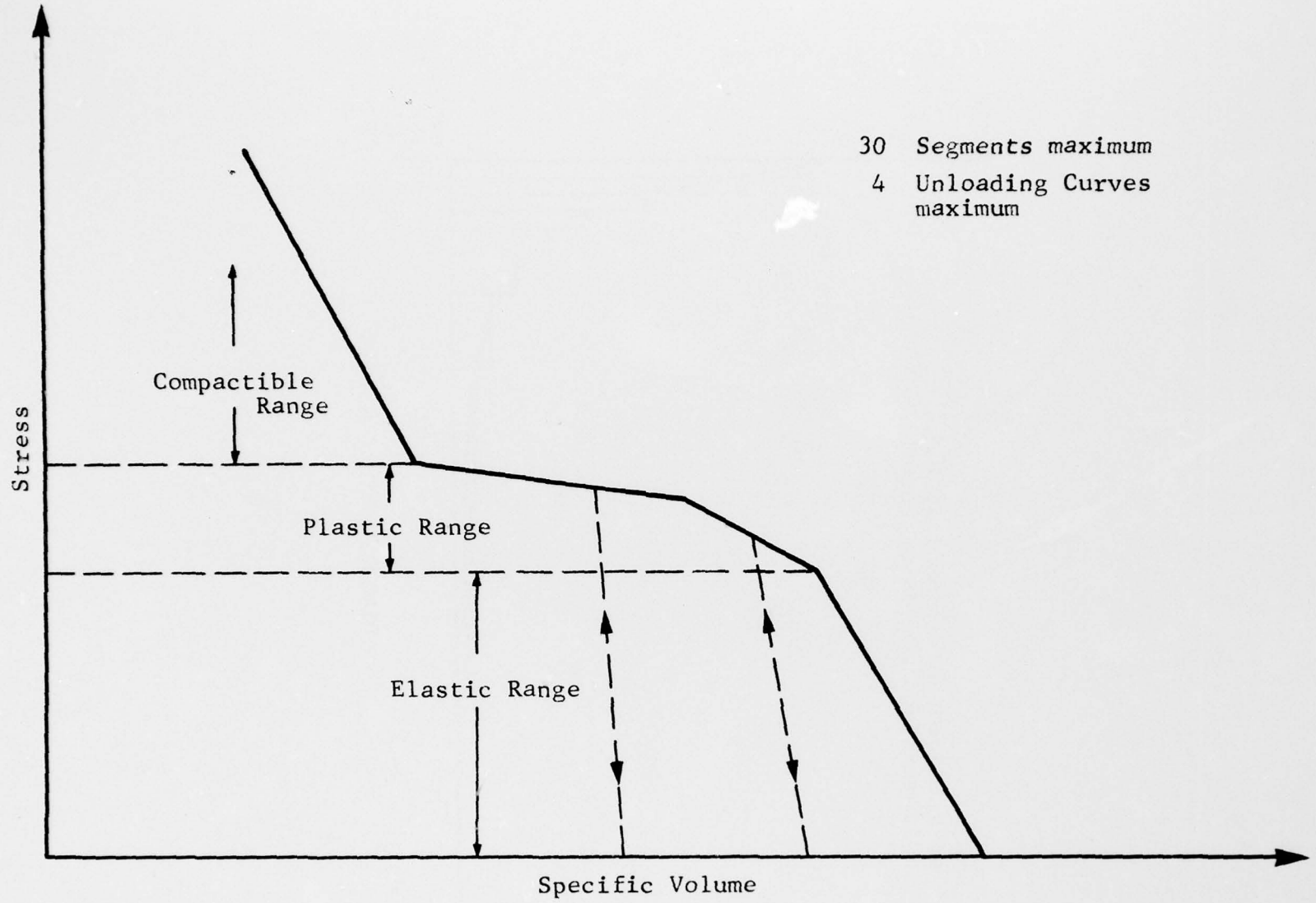

FIG. 2 STRESS-SPECIFIC VOLUME CURVE FOR A TYPICAL LAYER

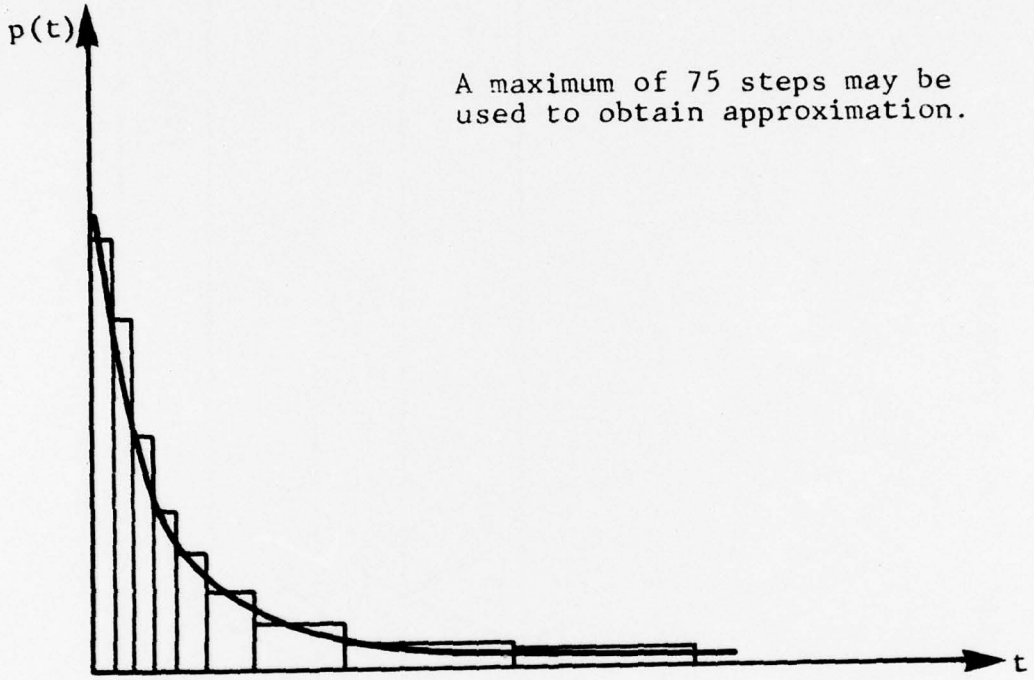

FIG. 3 SURFACE LOADING

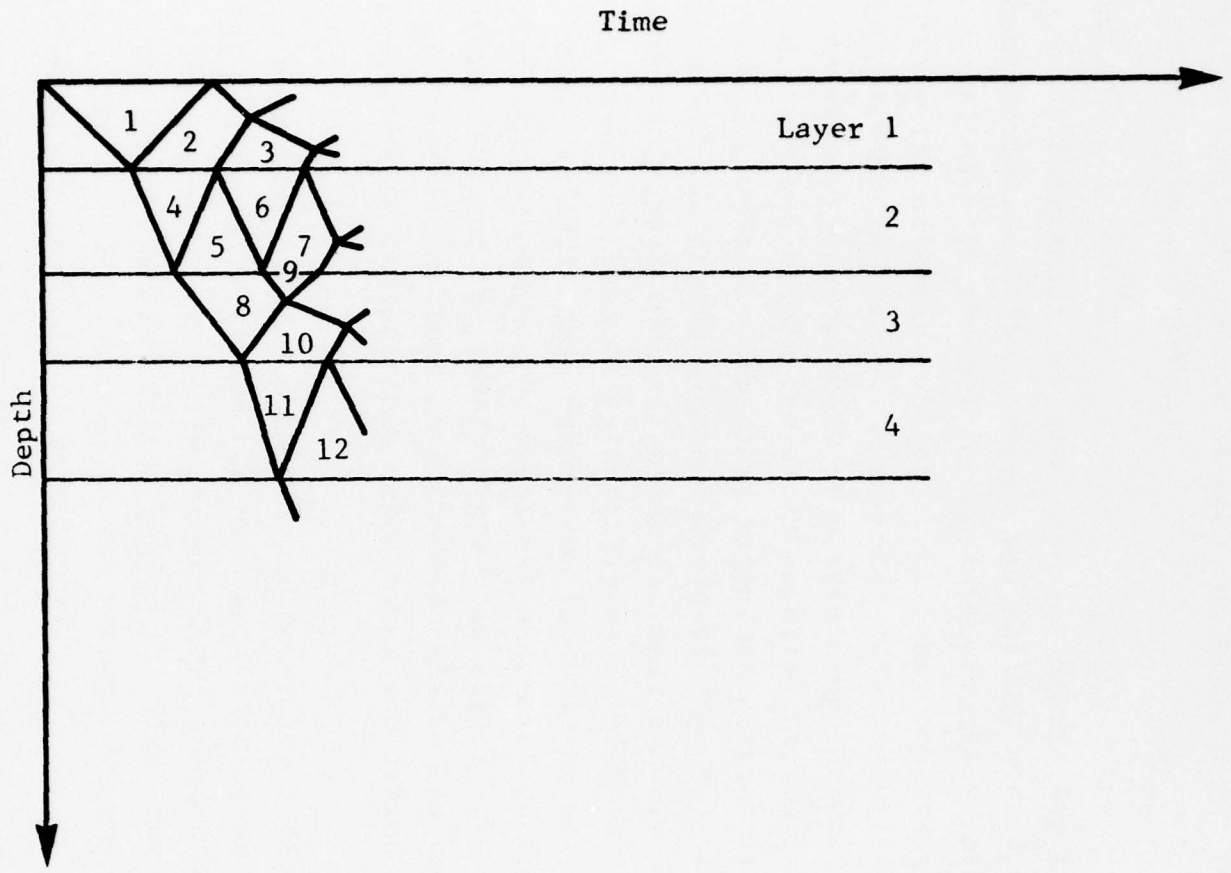

FIG. 4 WAVE DIAGRAM

When SWIMM Code is run on the IBM 7094 computer, storage capacity considerations limit the number of such zones which can be analyzed to approximately 1000.

2. SHALLOW Code (Ref. 2)

A hydrodynamic model was developed for predicting the ground shock environment from surface and shallow-buried nuclear explosions. In general for a shallow-buried explosion at early times the direct ground shock will be completely contained as indicated in Fig. 5. A computer code was written to solve the one-dimensional problem of determining the environment at the shock and within the shock-engulfed region. The soil can have a completely arbitrary Hugoniot relation (the loading phase of the pressure-volume curve of Fig. 6.), but it is restricted to expand (unload) along the same curve. This implies that the soil behaves essentially as a nonlinear, elastic media. An additional assumption is that the material density distribution behind the shock has a prescribed form. The specific form used for the model is given in Fig. 7. The incorporation of these assumptions into the code allows the computation of pressure, density and particle velocity at and behind the shock front.

This approach was used primarily to determine media behavior at the shock front and has been applied successfully for this purpose. However, while the predicted gross characteristics of the shock engulfed region behind the front may be reasonable, the use of this model is not recommended when local response behind the front is of importance.

At a certain time after burst, the direct ground shock will strike the surface and initiate the propagation of a rarefaction front into the previously shocked region as illustrated in Fig. 8a. The rarefaction front will eventually catch up with the one-dimensional shock wave and from that point on will increase the decay rate of the shock (Fig. 8b).

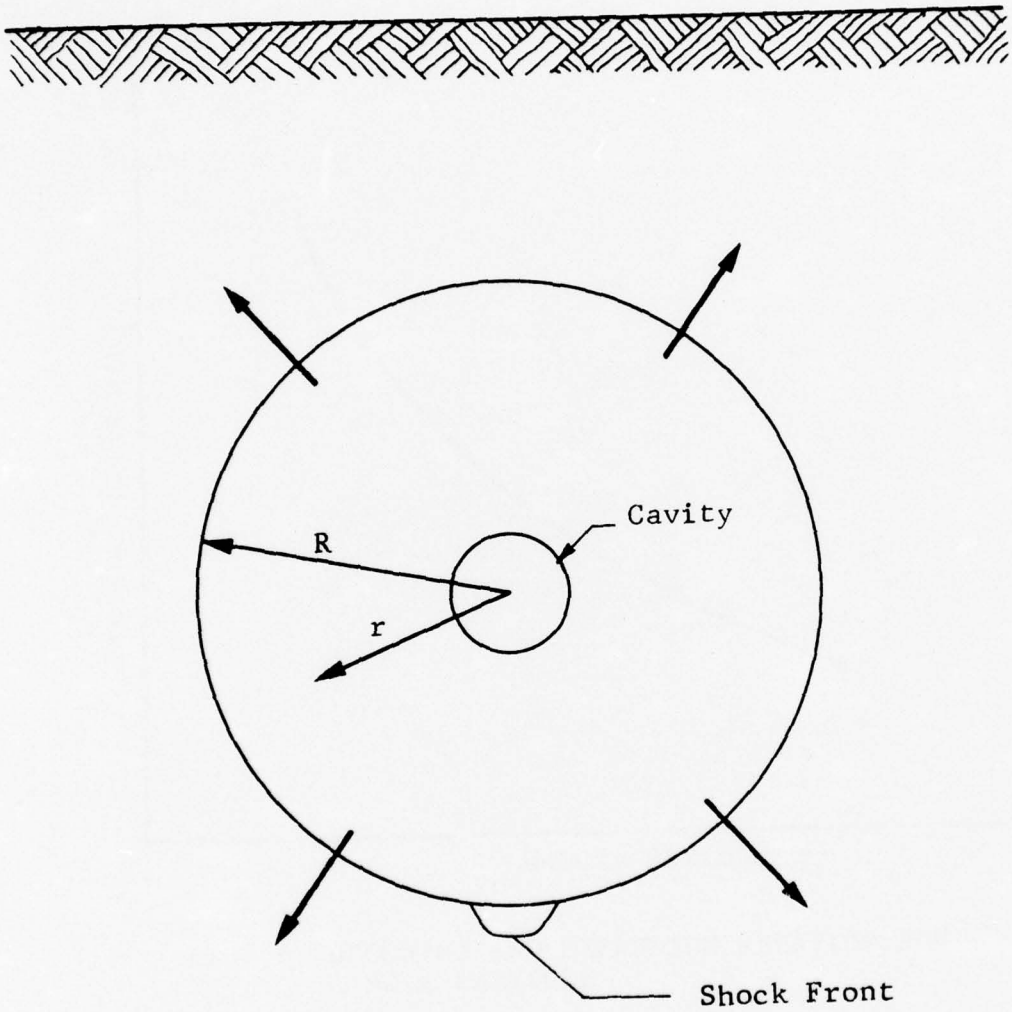

FIG. 5 COMPLETELY CONTAINED SHOCK, EARLY TIMES

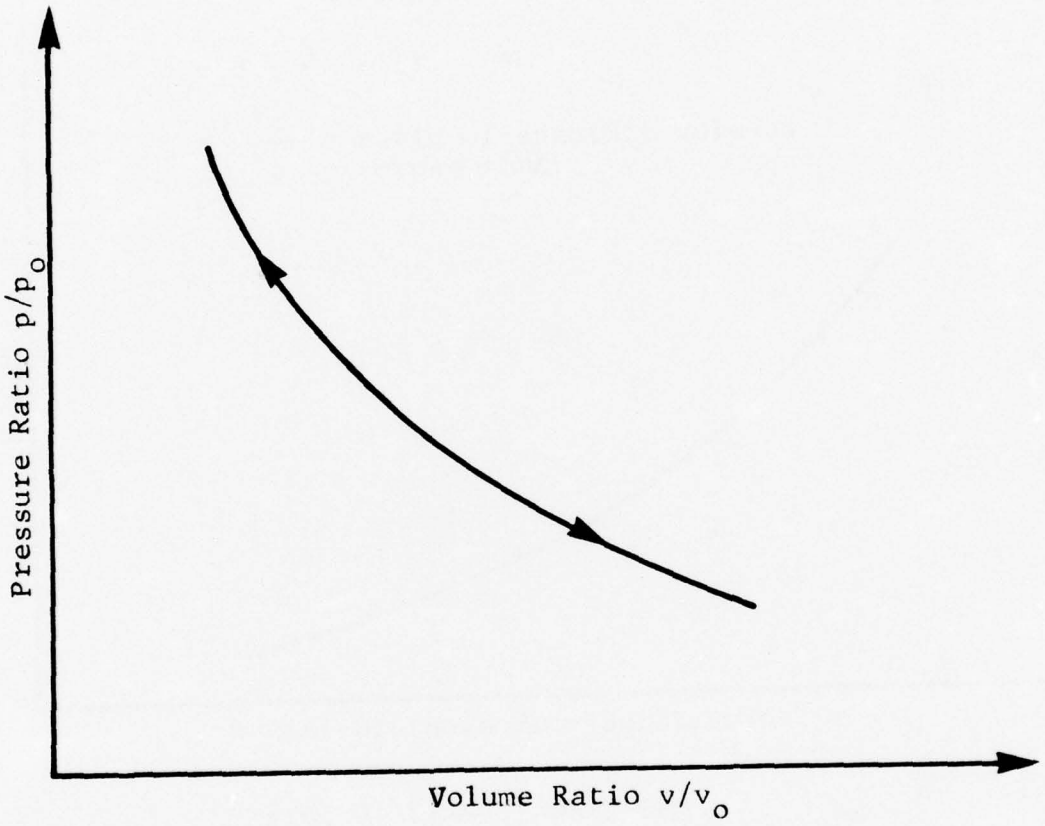

FIG. 6 HUGONIOT AND EXPANSION RELATION FOR A SOIL PARTICLE

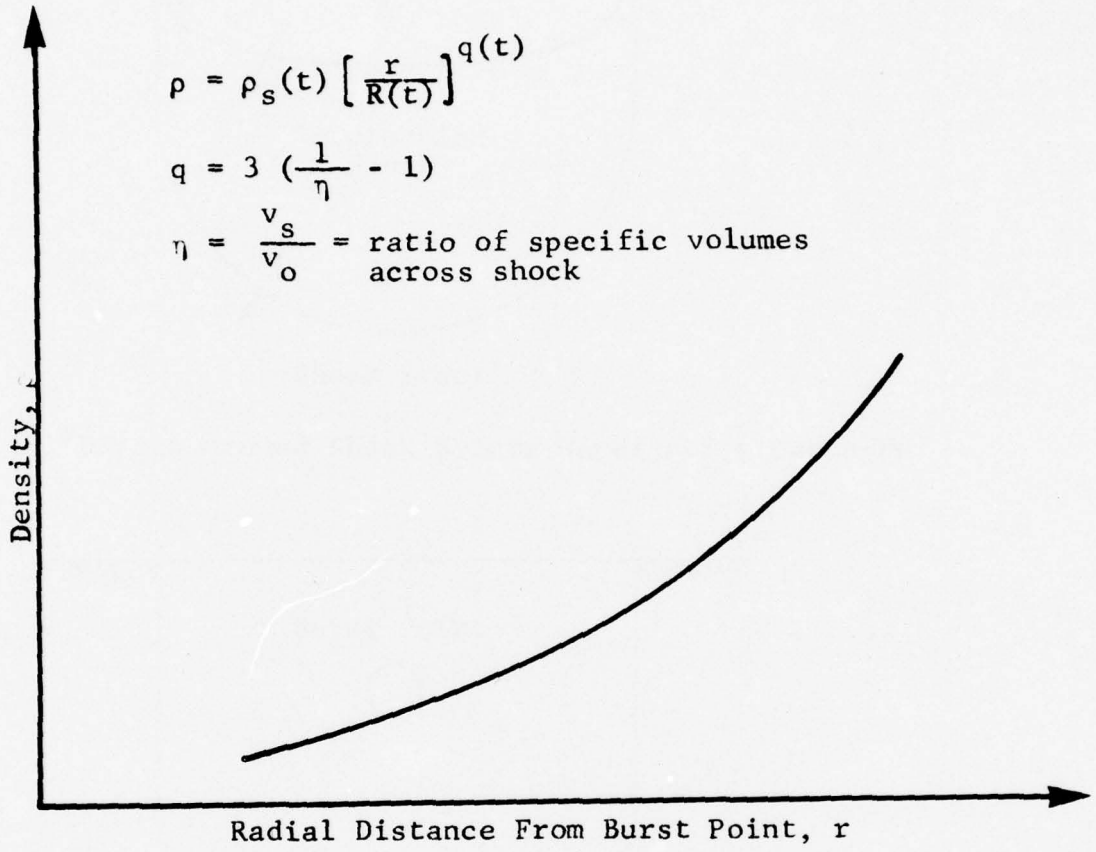

FIG. 7 DENSITY WAVEFORM

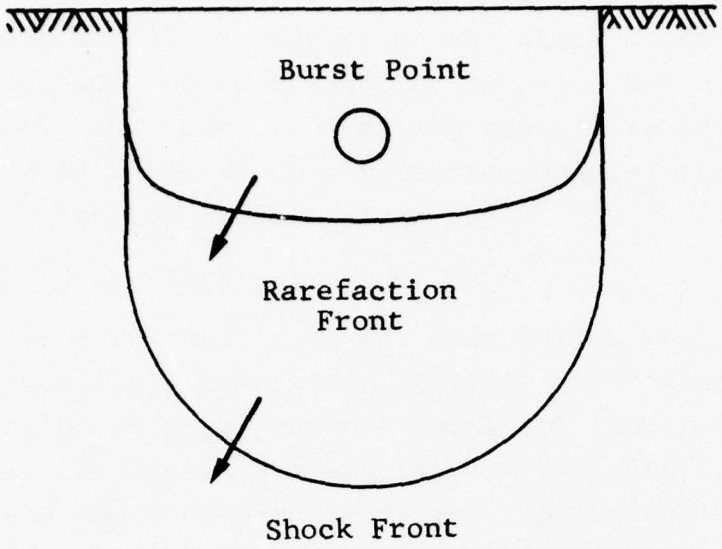

(a) Direct Ground Shock Before Rarefaction Catch-Up

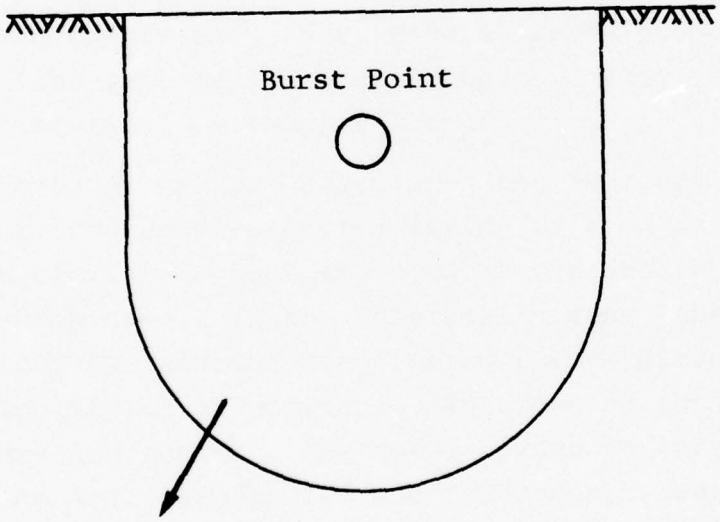

(b) Direct Ground Shock After Rarefaction Catch-Up

FIG. 8 GROUND SHOCK STRUCTURE
AT LATER TIMES

With the use of additional simplifications, a method was developed for surface bursts, to predict the characteristics of the rarefaction front and of the direct ground shock front after rarefaction catch up. Calculations for behavior behind the fronts are not made. The code also has the capability of determining the air-induced shock front parameters assuming there is no interaction with the direct ground shock.

3. MULTIPLE Code (Ref. 3)

This is a computer code for calculating the crater size produced by multiple underground nuclear explosions. It permits the computation of total earth removal for two explosions horizontally displaced as a function of the displacement distance, the depth of burst, and the explosive yield. Figure 9 portrays the three zones which must be considered - the shock engulfed region of (1) the first burst, (2) the second burst and (3) their interaction. Also included in the computer model is the effect of lag time between the initiation of the first explosion and the second. Very general earth properties can be handled (the same as for SHALLOW Code). They can be specified in either analytical or tabular form.

The computer program calculates the emergent one-dimensional shock history and shock engulfed field for each of the explosions in a manner similar to that employed in the SHALLOW Code for the contained shock case. In the interaction zone, the shock details are determined by reducing the problem to one dimension by means of simplifying assumptions. When one of the shock fronts first reaches the surface, the total upward non-negative momentum of the soil is computed and a resultant crater size (not profile) is estimated. The results indicate that the interaction of the two shock waves produces an enhancement of the upward momentum and consequently of the earth removal capability.

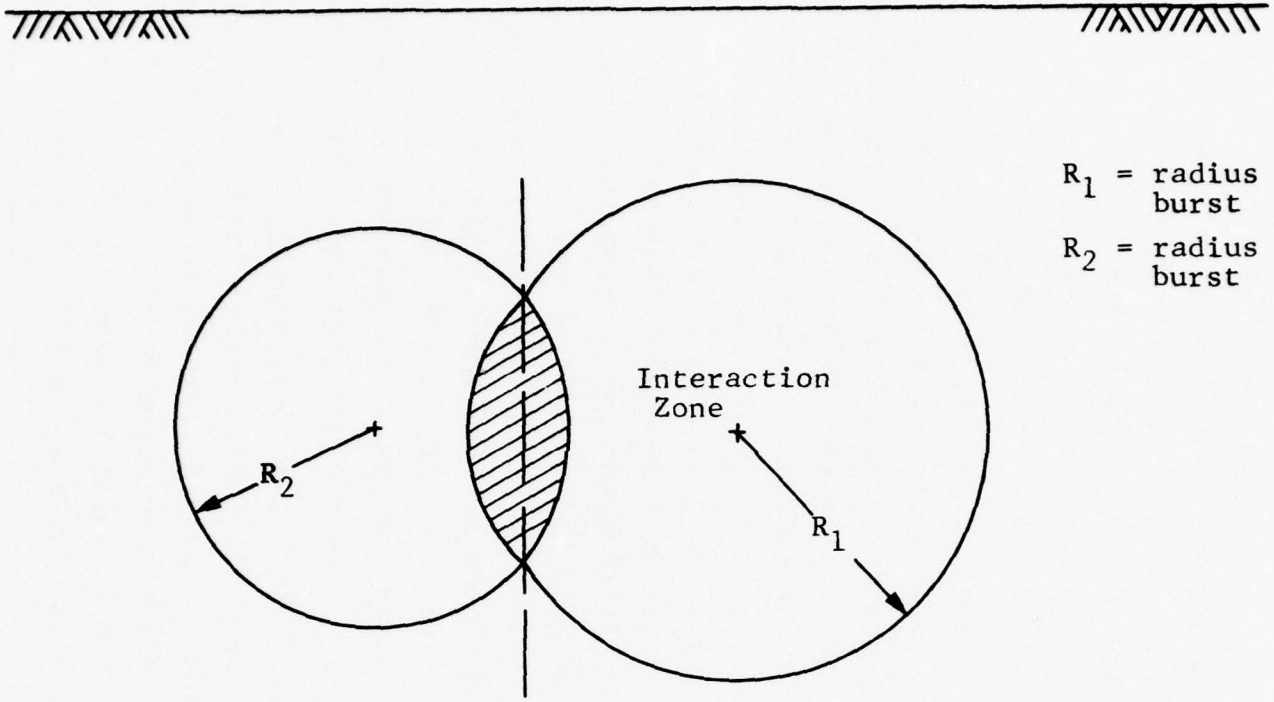

R_1 = radius for first burst

R_2 = radius for second burst

FIG. 9 MULTIPLE BURSTS

4. Stress Wave Propagation in Regions of Variable Modulus of Deformation (Ref. 4)*

A series of analytic solutions was obtained for a class of air-induced ground shock problems. These exact solutions deal with layered media in which the modulus of deformation of the soil increases with depth in a prescribed manner. The analysis includes both a one-dimensional nonsteady solution and a two-dimensional quasi-steady solution, Fig. 10. The latter solution is limited to the superseismic regions and yields details of both the horizontal and vertical motions.

The equation of state (See Fig. 11) which is used to describe the material behavior is a linear and reversible one, i.e., a constant modulus of deformation at any one depth. The density of the media is assumed constant throughout the entire region. In the one-dimensional nonsteady treatment no additional materials characteristics need be specified; however for the two-dimensional quasi-steady treatment the shear capacity of the media must be examined. As a preliminary part of this latter treatment the stress along the initial disturbance front (the dilatation wave) was determined for both an elastic and a hydrodynamic media. There was little difference between the two cases except in the extreme regions where the onset of subseismic wave propagation occurs. Thus the hydrodynamic model was used to derive the complete wave propagation solution for the two-dimensional quasi-steady problem.

The problem is further limited to small strains; however this condition is generally satisfied with most soils and rocks in the pressure ranges of general interest. Thus the problem is linear and the principle of superposition is used. Exact basic solutions have been obtained (Fig. 12 and 13) for a unit surface or blast wave load (i.e., a simple step pulse shown in

---

* Reference 4 is presented as the Appendix to this report.

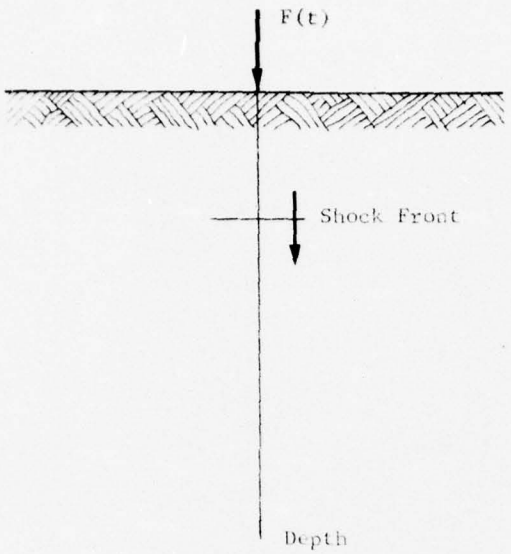

(a) One-Dimensional Nonsteady Wave Propagation

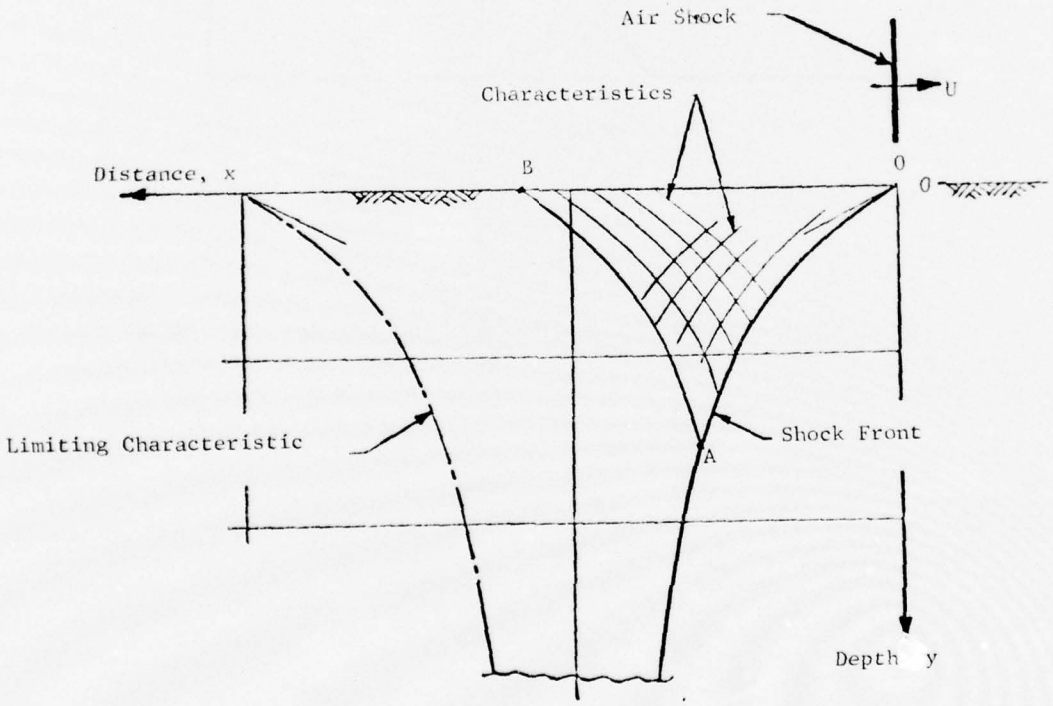

(b) Two-Dimensional Quasi-Steady Motion

FIG. 10 WAVE PROPAGATION GEOMETRY

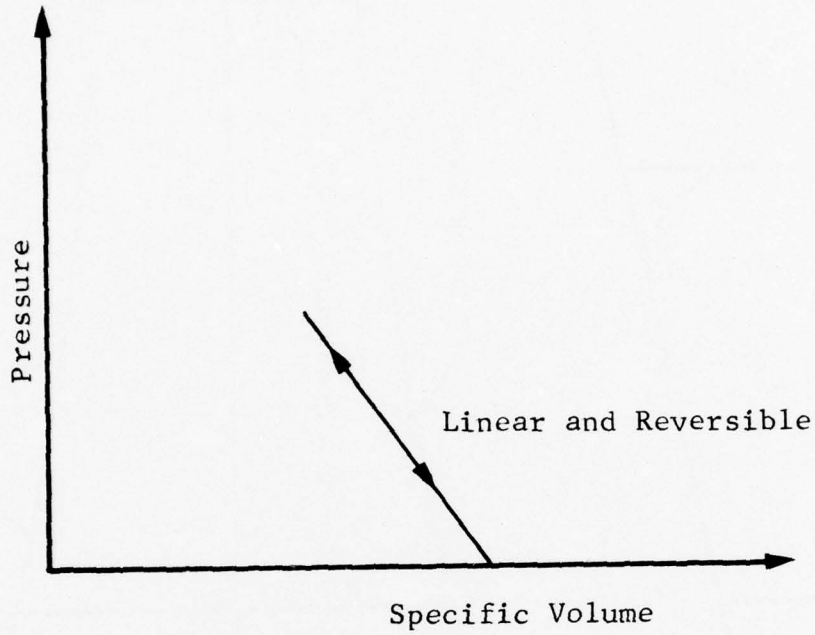

FIG. 11 MATERIAL EQUATION-OF-STATE RELATION

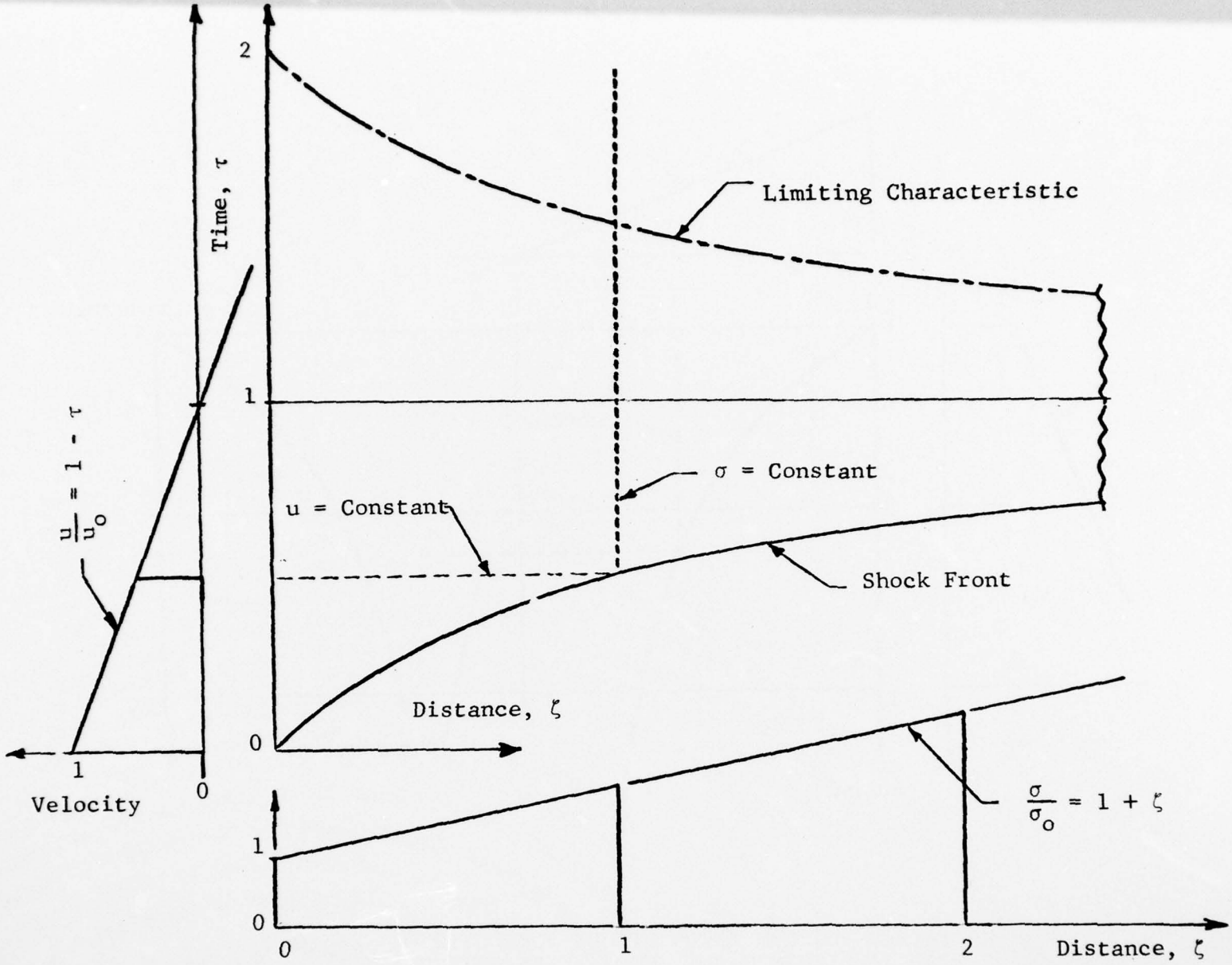

FIG. 12 SOLUTION FOR FOURTH POWER MODULUS VARIATION AND STEP PULSE LOAD, ONE-DIMENSIONAL CASE

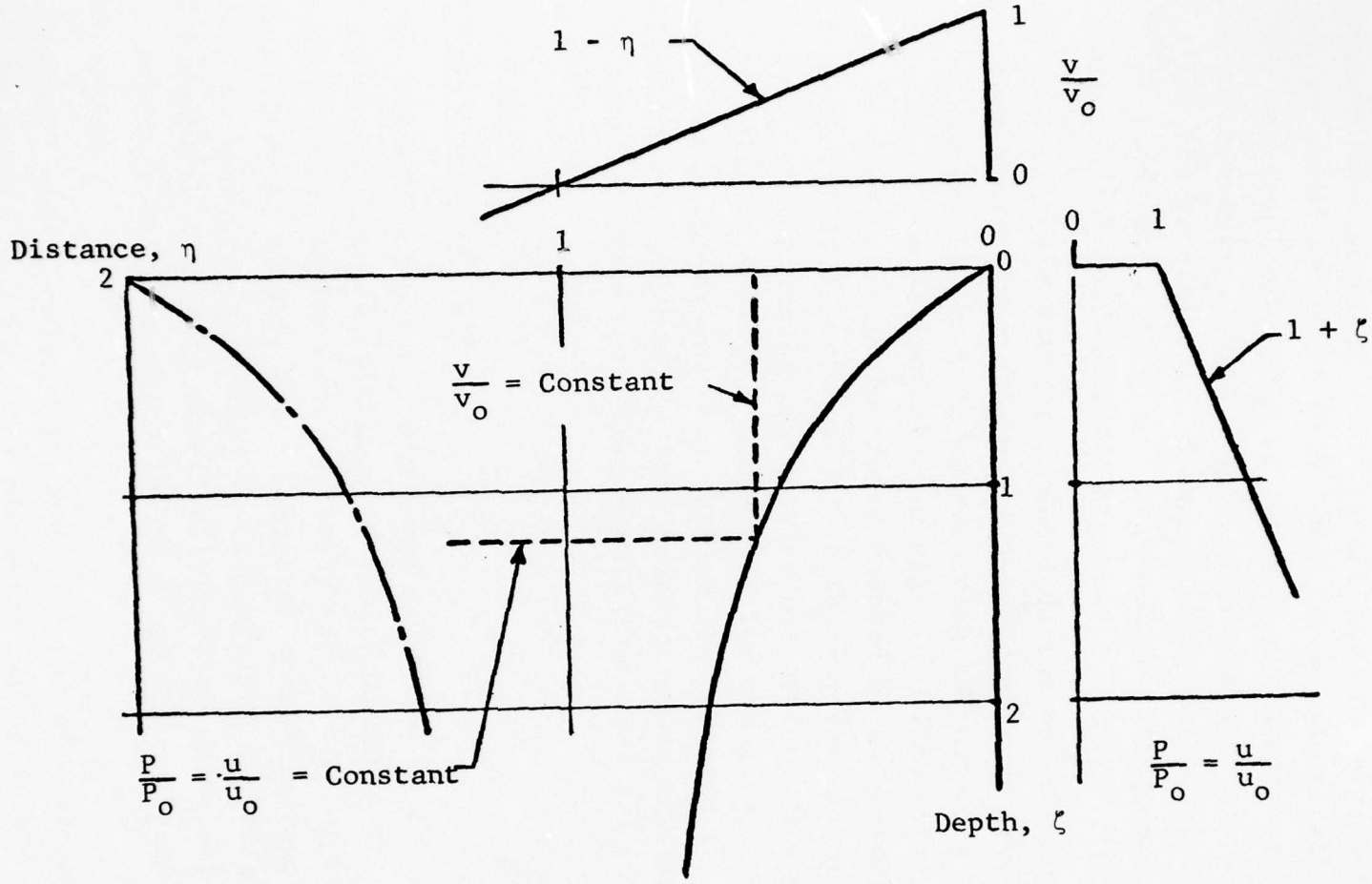

FIG. 13 SOLUTION FOR FOURTH POWER MODULUS VARIATION AND STEP PULSE LOAD, TWO-DIMENSIONAL CASE

Fig. 14a) and a requirement on the modulus of deformation variation with depth was determined for both the one-dimensional and two-dimensional problems. The result was that a relatively simple fourth power variation with depth (shown quantitatively in Fig. 15) was required. This can be fitted to most actual site data quite readily. Simple integral equations were then developed for the general case of an arbitrary surface load. Specific solutions are also given for the more common case of a simple exponential surface load, Fig. 14b.

The analyses were further extended to include the more realistic case where a variable modulus surface layer overlaps an infinite homogeneous base layer requiring the use of a modified molulus form as indicated in Fig. 16. This configuration gives rise to distinct solution zones bounded by the reverberation of the initial disturbance within the surface or variable modulus layer. The solution was carried out to include approximately four solution zones and programmed for a digital computer. The zones for the one-dimensional problem are depicted in Fig. 17. The surface load is defined for this calculation as the sum of three exponential terms (to coincide with the usual air blast loading profile).

B. Solid Models

1. DISCRETE Code (Ref. 5)*

The DISCRETE computer program was developed to obtain approximate time-history solutions for the free-field vertical component of soil displacement, velocity and stress for representative Titan II missile sites subjected to surface air blast loading. It is coded in FORTRAN IV language and utilizes the IBM 7094 computer to obtain numerically integrated solutions for a discrete system approximation of a one-dimensional continuous system.

The soil model employed is that of a one-dimensional layered media with quite general piecewise linear stress-strain

*Reference 5 was prepared for WES and issued as a separate report on this contract.

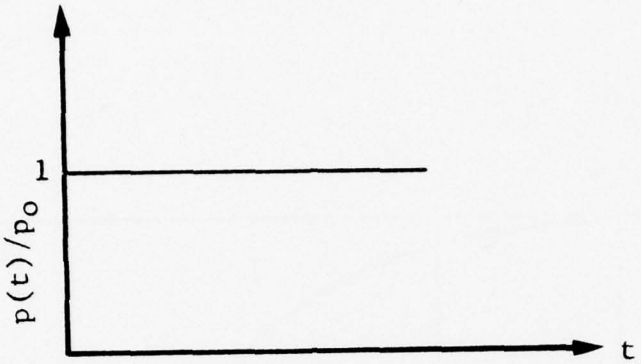

(a) Step Pulse

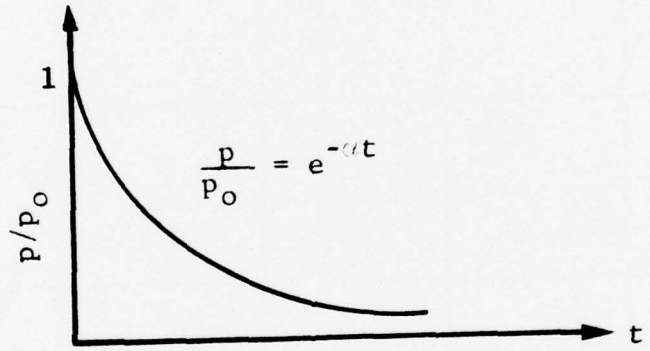

(b) Exponential Load

FIG. 14 SURFACE LOADINGS

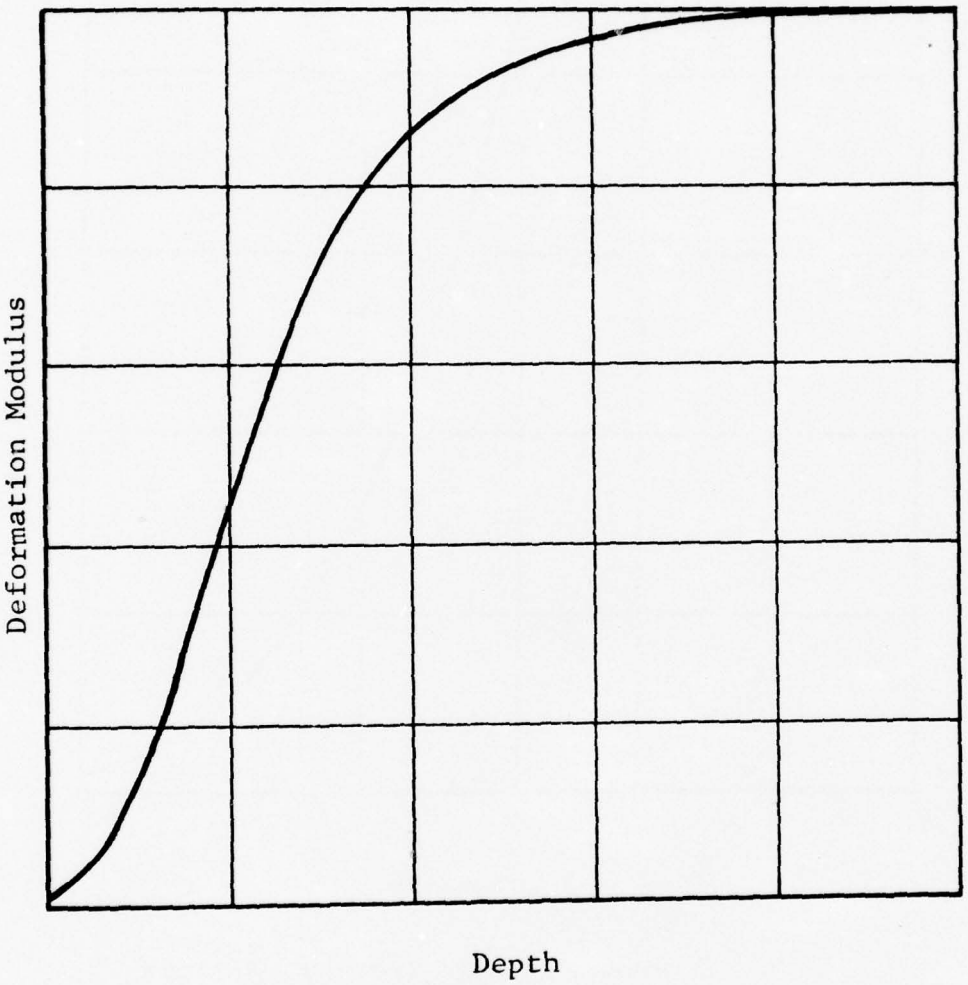

FIG. 15 PRESCRIBED MODULUS VARIATION FORM

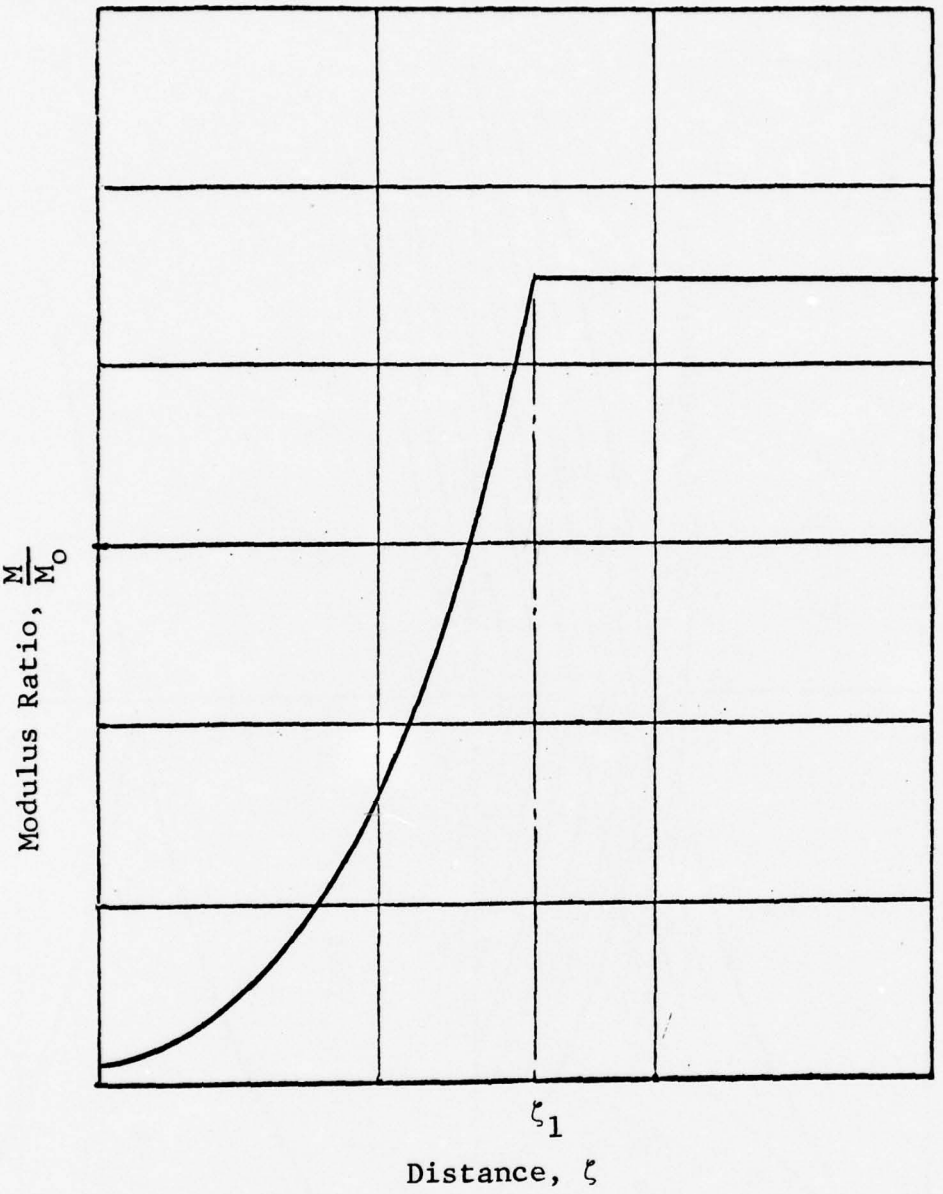

FIG. 16 MODIFIED MODULUS FORM

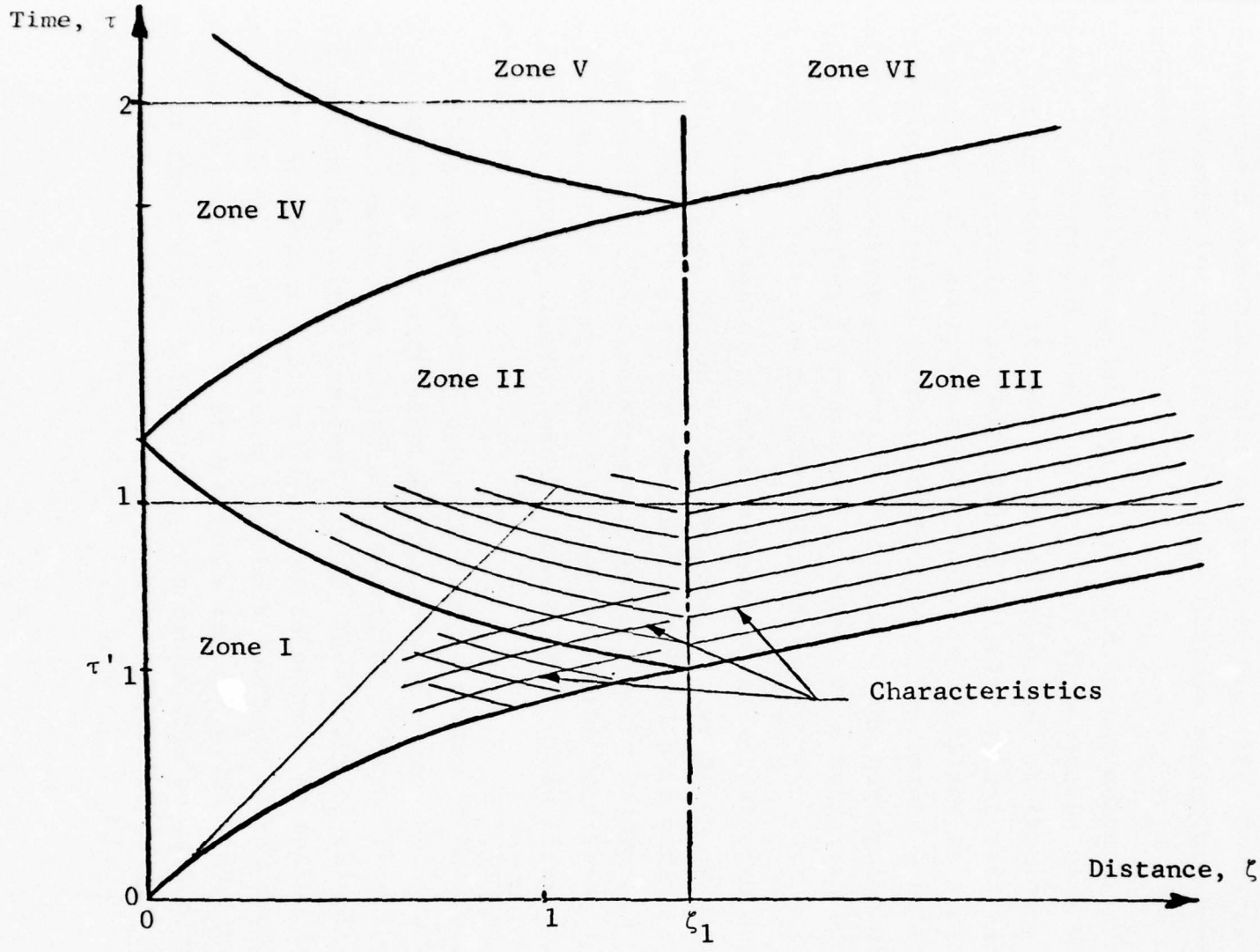

FIG. 17 WAVE DIAGRAM, MODIFIED MODULUS FORM, EXPONENTIAL LOAD

characteristics specified for each material layer. Each of the layers can possess independent loading and unloading/reloading stress-strain characteristics as shown in Fig. 18. There is also provision for specification of a maximum admissible tension for each layer.

The idealized model (Fig. 19) coded by the computer program considers a vertical column of soil that is subjected to a known loading function at its upper end and connected at the lower end to a linear elastic base material of infinite extent with known properties. The continuous soil column is idealized as a discrete element system in which each element represents a soil layer with constant properties throughout. The assumption of constant properties is reasonably accurate if a sufficient number of layers are selected for the soil model.

Consideration of spatial attenuation of stress with depth is included as an option in the program. Attenuation effects are introduced by altering the one-dimensional soil parameters automatically within the program. The parameter values are altered based on an approximate solution to the Boussinesq problem of static loading on the free surface of an elastic half space.

The response of the discrete element system is obtained by solution of the differential equations of motion using a Runge-Kutta method of numerical integration. Output from the program includes the transient stress, acceleration, velocity and displacement of arbitrarily selected nodes. An option is also provided for determining the shock spectrum and/or tape output of the motion and stress variables for given time increments at the nodes. This latter information can be used directly as free-field data input to soil-structure interaction computer codes.

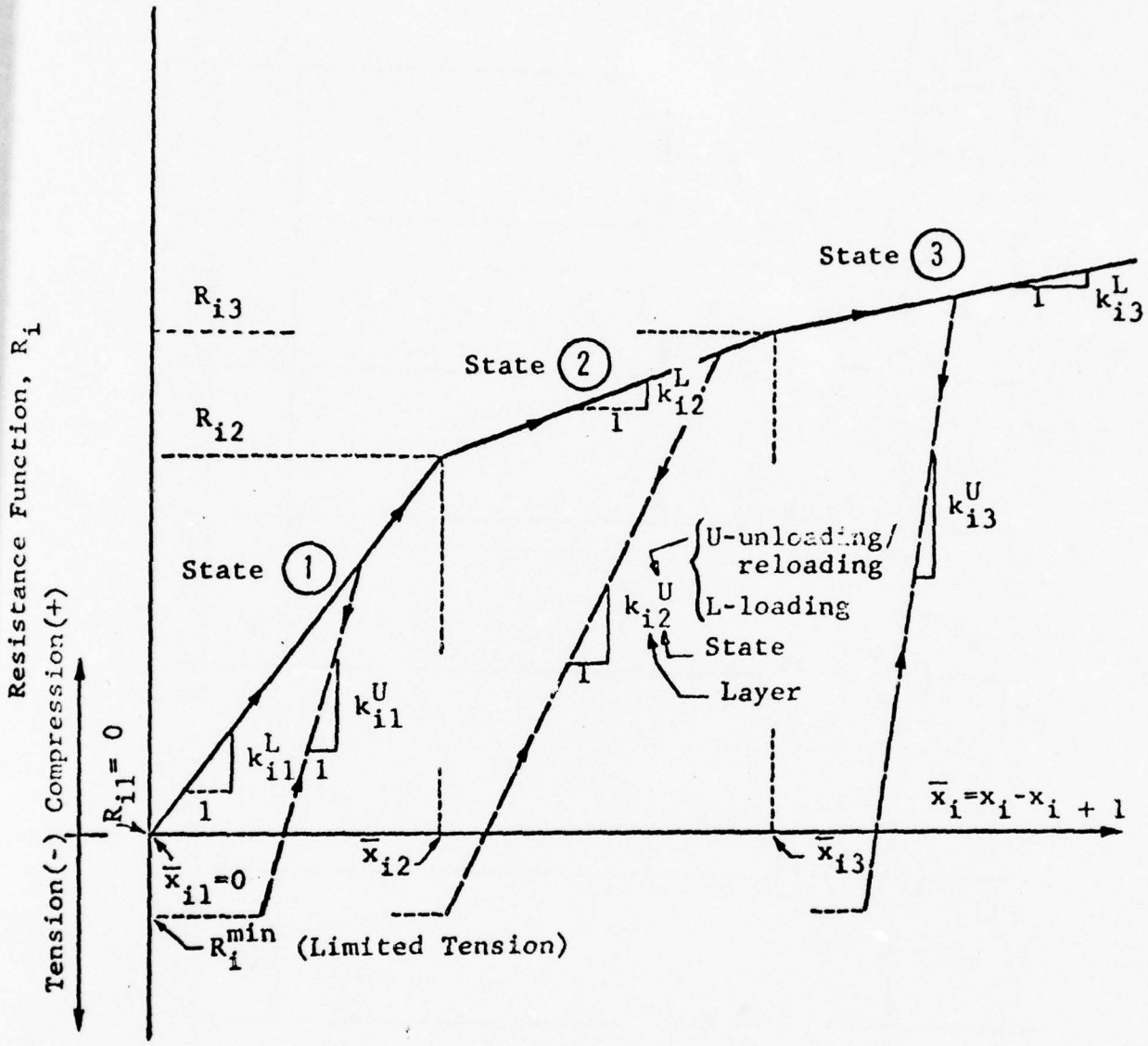

FIG. 18 RESISTANCE FUNCTION

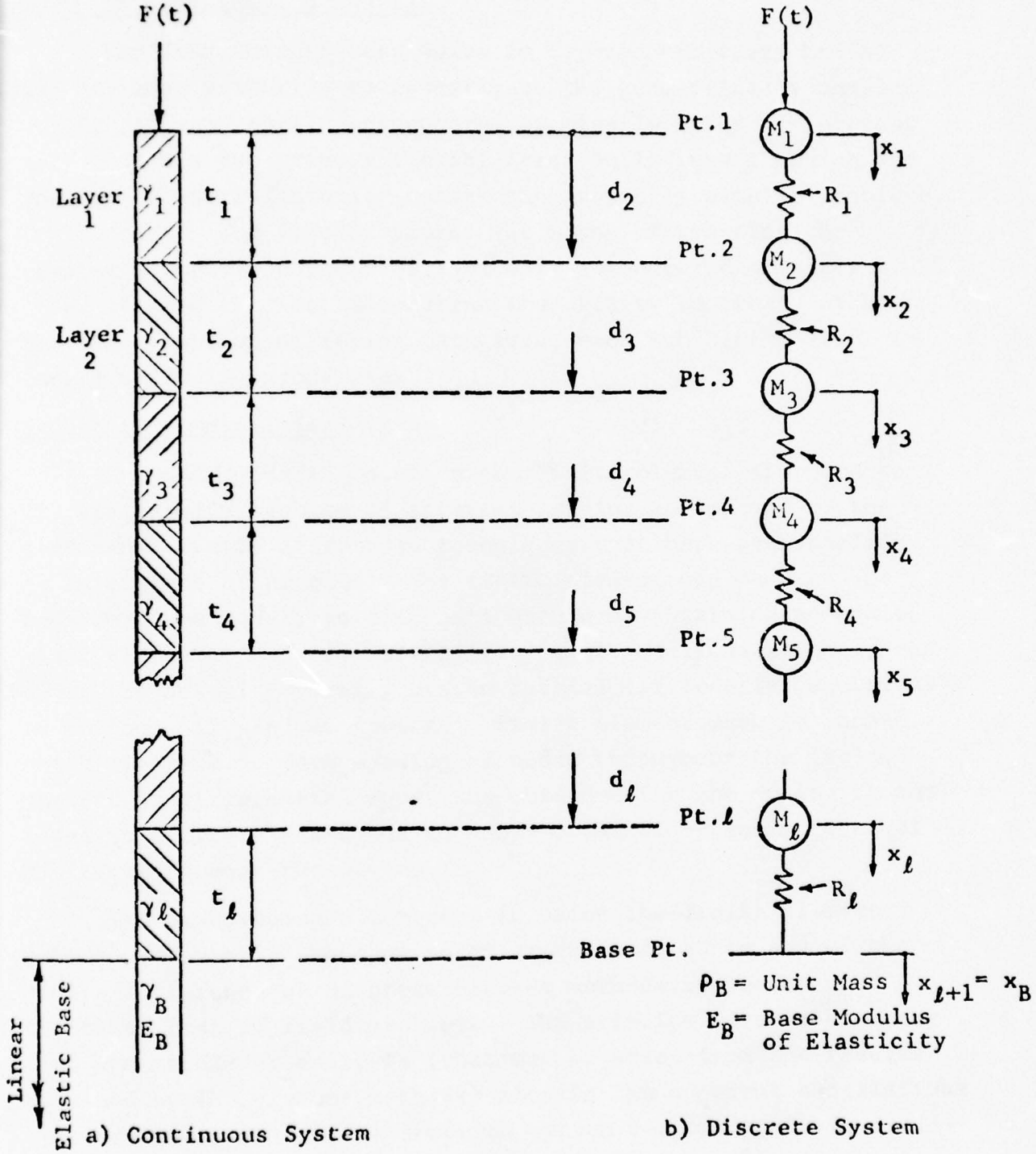

FIG. 19 ONE-DIMENSIONAL MODEL PARAMETERS

2. SLAM Code (Ref. 6 and 7)

The SLAM Code (Stress Waves in Layered Arbitrary Media) was designed primarily to investigate the geometrically complex configurations usually encountered at missile sites of interest. This code has two primary flexibilities built into it which are required to satisfactorily attack the generally complex problems of interest. The first concerns the means of treating the complex geometric boundaries typically encountered at sites of interest, and the second concerns the ability to treat, within the same problem, differing materials, each exhibiting significantly differing properties.

Geometric Complexities

The SLAM Code is based on the finite element approach to the stress wave problem of interest herein, as opposed to the more usual finite difference techniques that have been applied to this class of problem. The finite element approach can be considered as merely an alternate method of obtaining an equivalent finite set of ordinary differential equations which approximate the actual governing system partial differential equations of motion. If, in particular, a finite element mesh is chosen which yields a uniform spacing of nodes throughout the field, the set of differential equations obtained for the motion of the nodes is entirely analogous to those obtained by the more usual finite difference techniques.

The disadvantages inherent in using the finite element method are exactly the same as those encountered in any of the finite difference or discrete element methods typically used for this class of field problems. The principal drawback of any discrete method of analysis (that may be noted from the results obtained by the various methods) lies in the apparent oscillations that are induced into the computed system response. These oscillations come about simply from the fact that the actual system under study contains an infinite set of system frequencies where-

as the approximating set contains only a finite set of these frequencies.

The primary advantage of the finite element method, however, over the finite difference formulation lies in the means of treating the complex geometries typically encountered. For example, a general complex site geometry is shown in Fig. 20. Since the site boundaries and interfaces are generally non-uniform, the use of finite difference formulations is made quite difficult by the relative uniformity of mesh point spacing required by the method. The use of the finite element method however, completely eliminates this problem, since the spacing of nodes throughout the free-field is completely arbitrary and can be made to satisfy the system geometry. This is indicated in Fig. 21.

As a further example of the flexibility allowed by this method, consider the problem shown in Fig. 22 which consists of a three layered material zone which passes through a fault that can be used to approximate the system as shown in Fig. 23. It may be noted how simply the finite element mesh can be matched to the complex boundary and interface conditions of this problem.

As another example of the flexibility of the method, a finite element mesh for a uniform half-space problem is shown in Fig. 24. It is clear of course that for this simple problem, a finite difference formulation can be used. However, in this problem it is desired to have a relatively fine mesh at the several ground ranges of interest (shown by the circles in Fig. 24) to allow for sufficient description of the motion history, while to obtain a long enough duration of the results, the mesh boundaries must be placed sufficiently far so that they will not interfere with the computed results during the times of interest. The uniformity of mesh spacing required by the finite difference method would generally require an excessively large number of node points in the mesh leading to a longer computer running time.

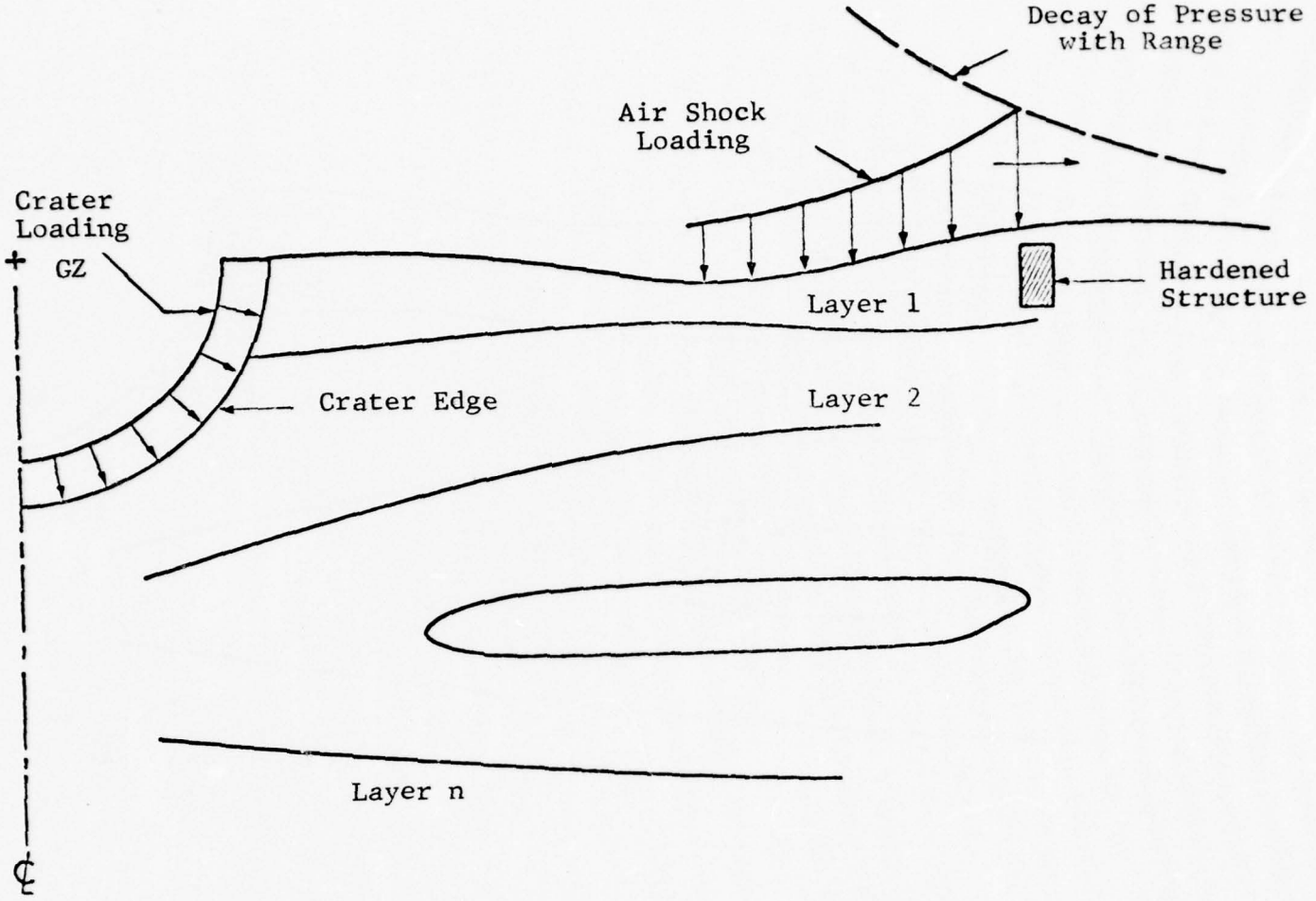

FIG. 20 GENERAL CONFIGURATION OF SITES OF INTEREST

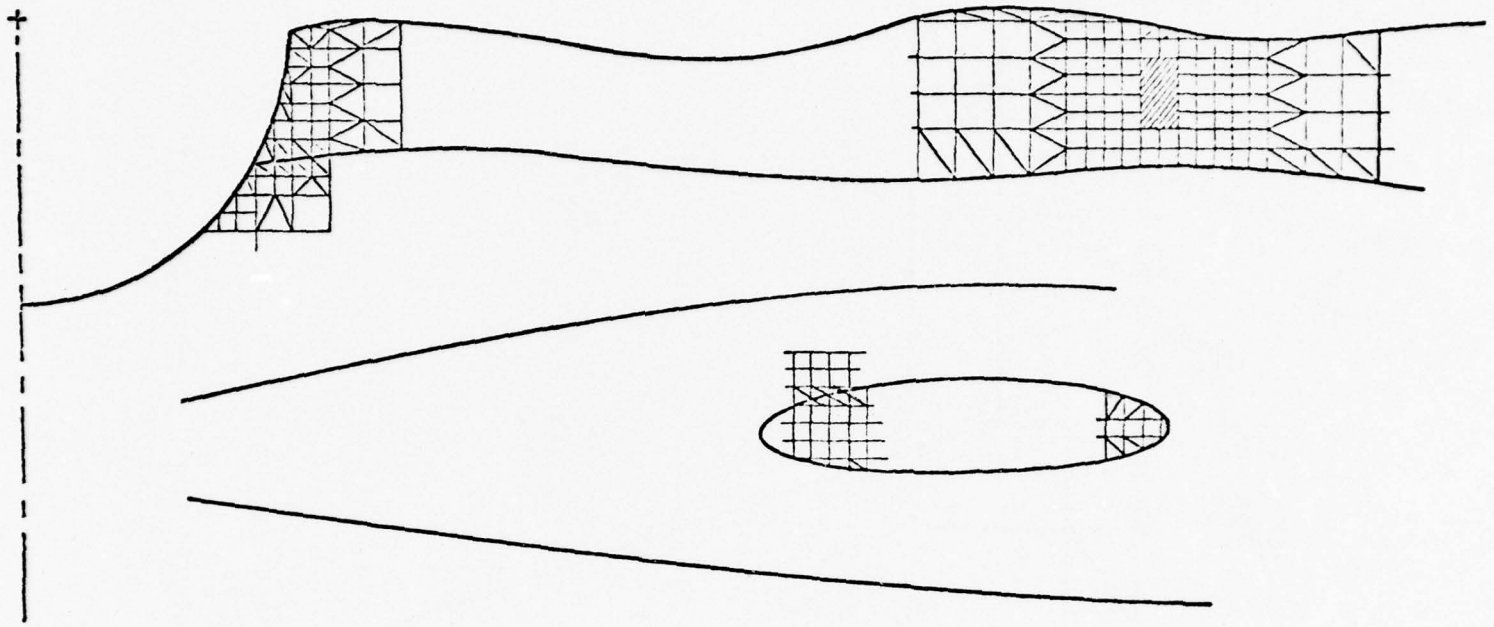

FIG. 21 FINITE ELEMENT IDEALIZATION OF SITE CONFIGURATION

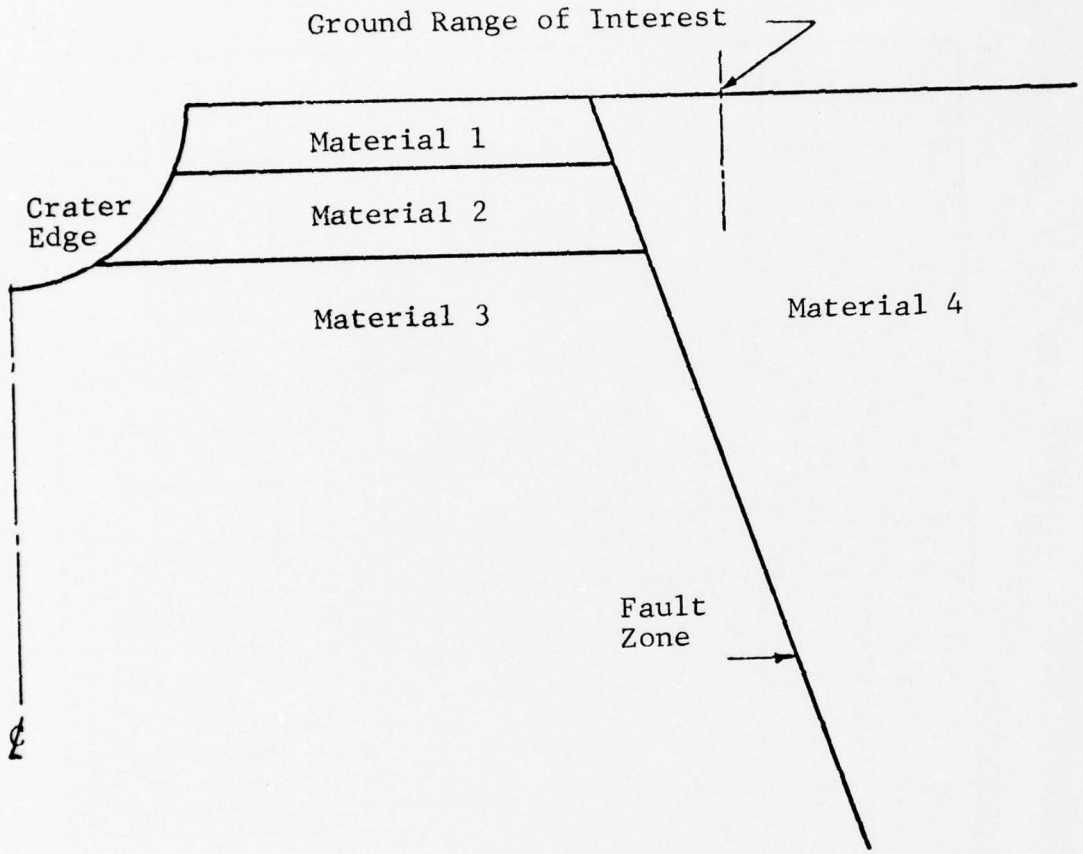

FIG. 22 SITE CONFIGURATION FOR PROBLEM EXHIBITING A FAULT ZONE

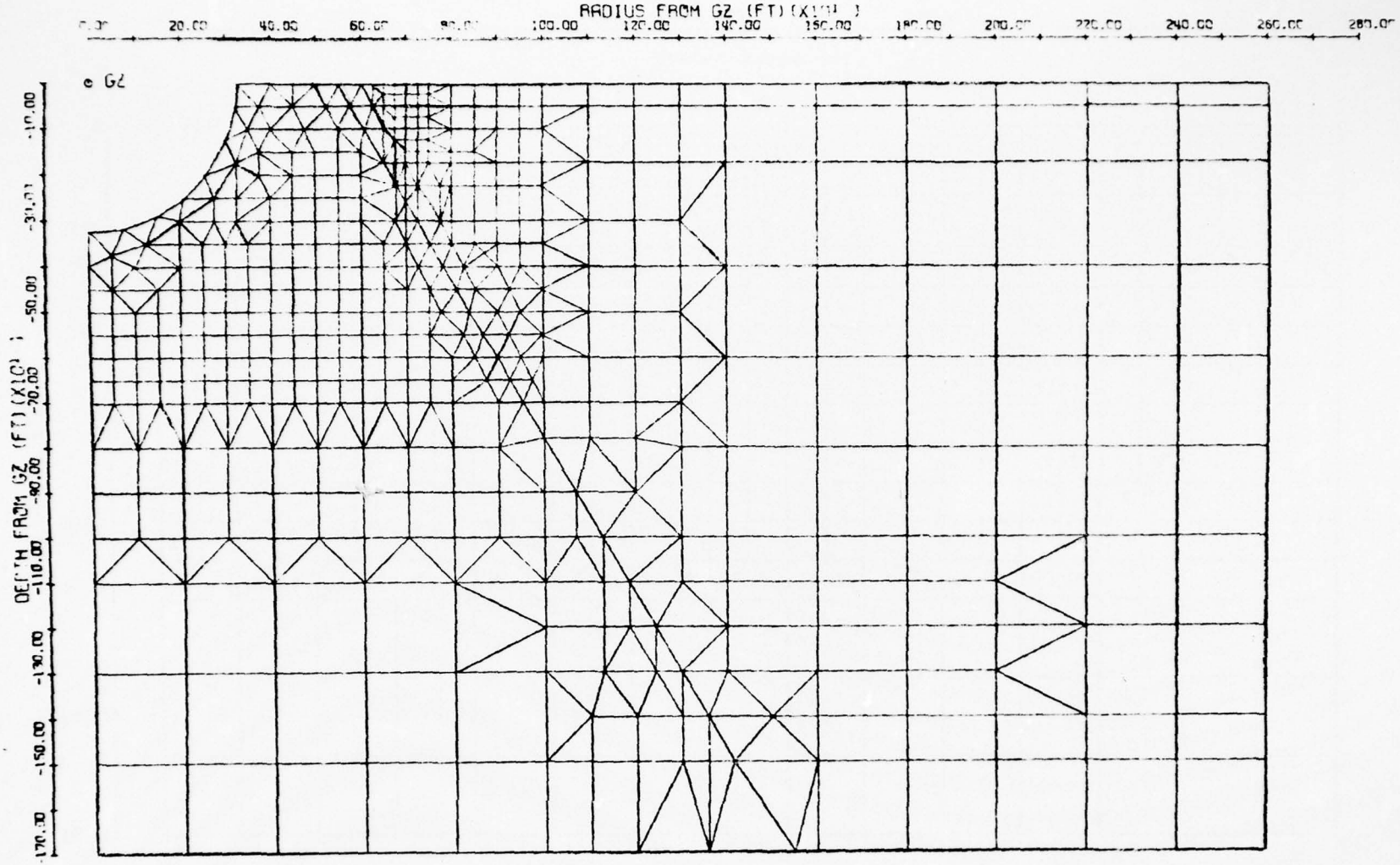

FIG. 23 DEMONSTRATION PROBLEM NO. 2, CANTED BOUNDARY

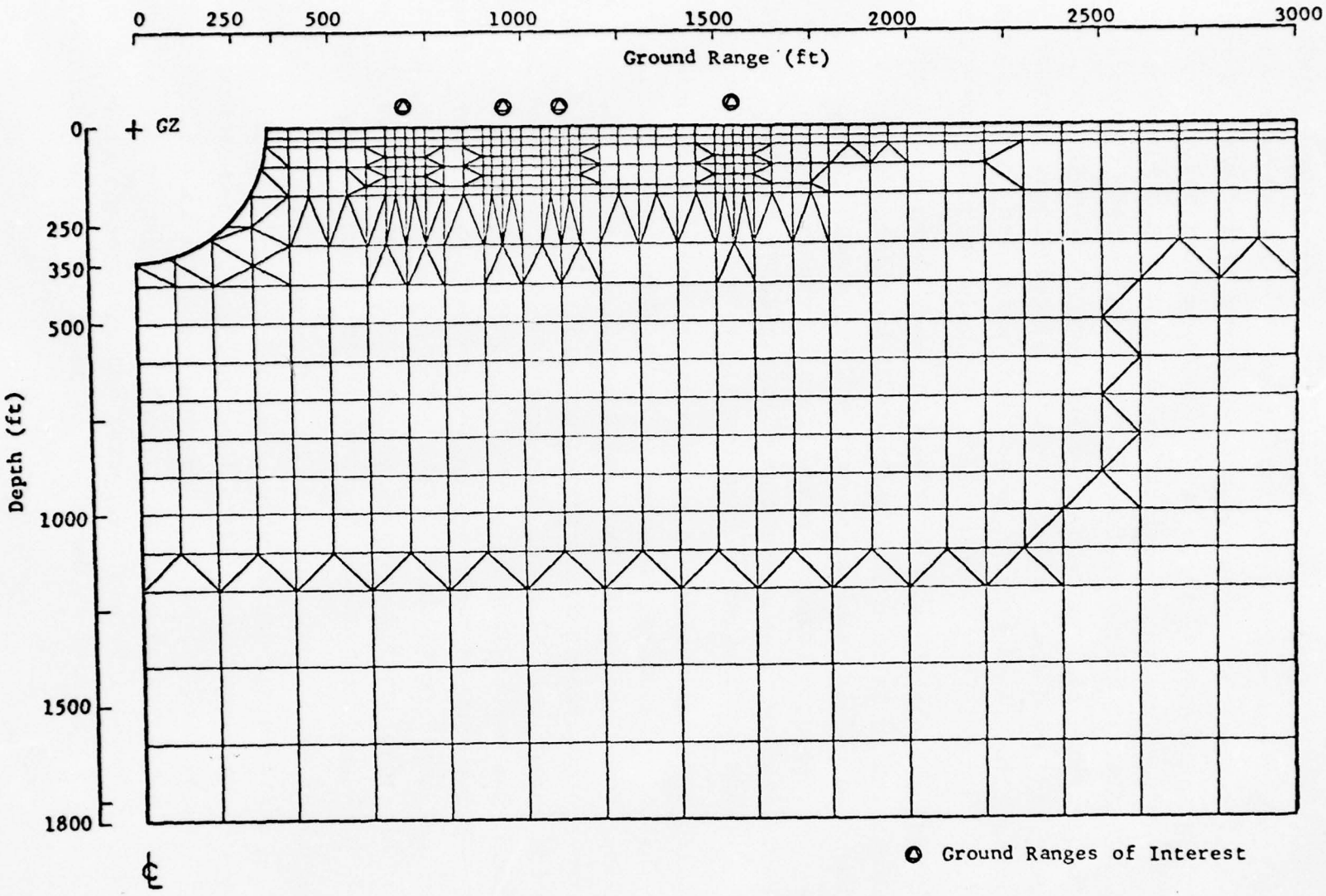

FIG. 24 TYPICAL ELEMENT MESH FOR UNIFORM HALF SPACE PROBLEMS

With the finite element method, the mesh can be easily expanded away from the zones of interest allowing for a reduced number of node points requiring consideration and leading to a shorter computer running time. These zones between areas of primary interest and the area boundaries act primarily as mechanisms to absorb the wave without introducing reflected waves from any more closely spaced boundaries. Several methods for treating boundaries to eliminate reflections have been proposed, but none have been found to be satisfactory, particularly for the nonlinear problem.

As can be noted from the meshes of Fig. 23 and 24, the element meshes considered in the SLAM Code consist of triangular and rectangular elements. The fine rectangular meshes are used in the zones of primary interest where computed response is desired. Coarser grids are used in zones away from these areas while the triangular elements are used to merge these areas.

Missile site configurations can be divided into two classes of problems, (1) those made up of uniform horizontally bedded one, two and three layered problems, and (2) unusual configurations. For the first class, no further mesh considerations need be mentioned. In fact, the same mesh shown in Fig. 24 for the uniform half-space problem can be used to analyze two and three layered problems by merely changing the property data for the various zones of interest. The second class of problems indicates the wide versatility of the method over other techniques. A typical mesh for one of these problems is shown in Fig. 25.

It should also be mentioned that the actual mesh formation for specific problems is highly dependent upon the material properties of the system. The usual criteria (encountered in finite difference methods also) that must be followed is that the time for propagation of the stress pulse across the element must be small compared to the response times of interest in the particular problem, at least in the zones of interest.

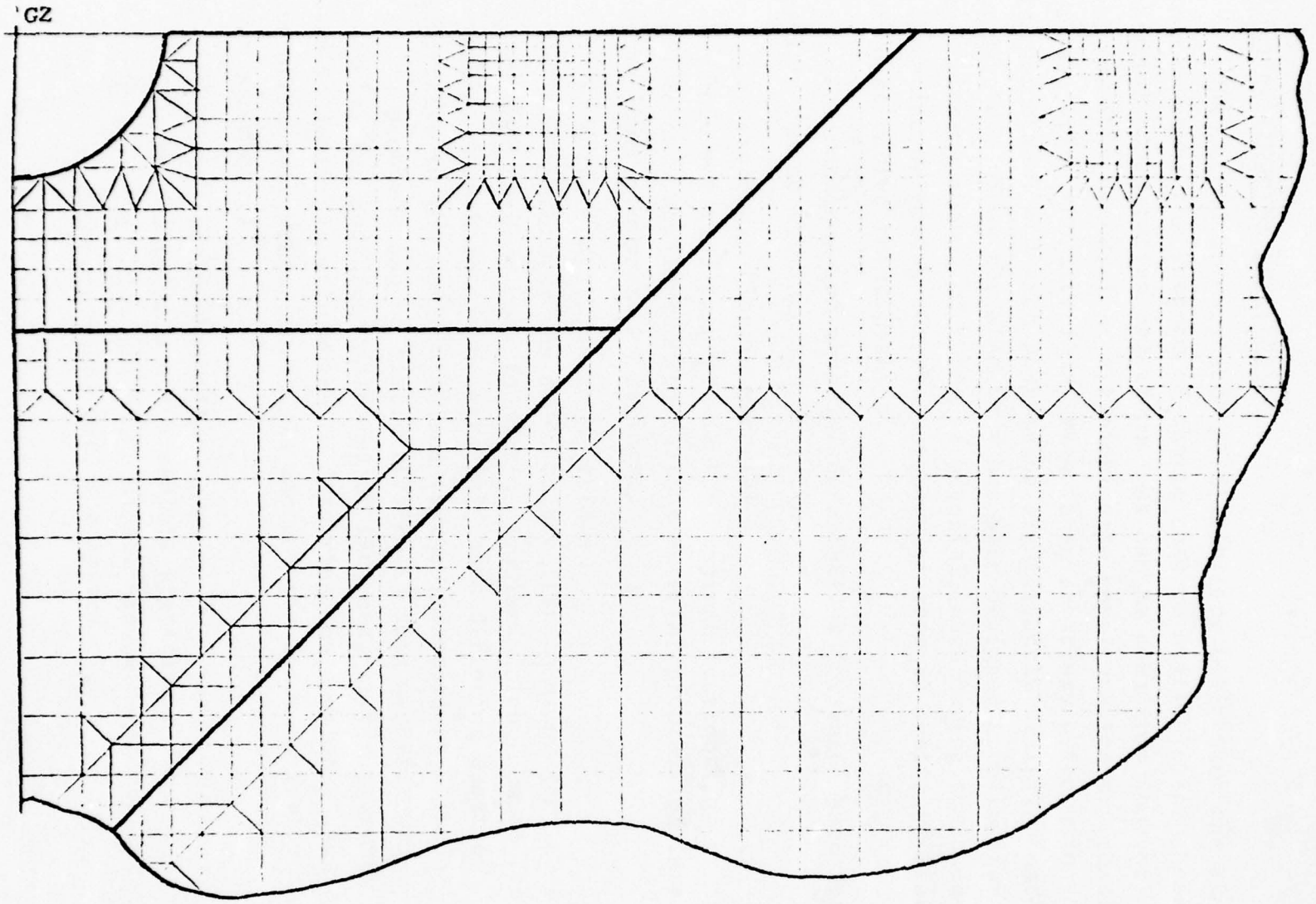

FIG. 25 TYPICAL ELEMENT MESH FOR A FAULT ZONE SITE CONFIGURATION

Material Property Description

The second primary area of flexibility built into the SLAM Code concerns the freedom of choice that is available for choosing material constitutive relations. As can be seen from some of the previous discussion, a typical site configuration may consist of many different materials, each in an arbitrary orientation to each other, and each possessing significantly differing material properties. Thus the SLAM Code has been designed to allow for an arbitrary number of zones of material, each having the capability for selecting material properties from an arbitrary list of constitutive relationships.

The catalogue of material descriptions for which numerical results can be obtained are as follows:

- Isotropic Elastic Material

This material property is the simplest to treat, of course, and does have application to various material problems of interest in the lower overpressure regimes.

- Anisotropic Elastic Materials

This capability was added to the list to allow for investigation of various rock foundation problems which, due to the method of formation of the material, have differing elastic properties in the horizontal and vertical directions. These bedding problems can be easily treated in this manner. Unfortunately, for most rock material of interest, little property data is available with which to determine the necessary constants. (Unfortunately, this problem is encountered for many real soil/rock materials.)

- Viscoelastic Materials

To treat materials which exhibit significant damping characteristics (i.e. clay soils), a simple viscoelastic constitutive model has been incorporated into the system.

- Compressible Fluid

Since the SLAM Code has been used to investigate configurations in which stress wave propagation from solid to water and vice versa was of interest, a linear compressible fluid model was incorporated.

- Elastic-Mises Plastic, Arbitrary Strain Hardening Material

To account for nonlinear material behavior, one of the constitutive relations incorporated into the code is an elastic-plastic material in which plastic flow is governed by the Prandt-Reuss relations and the initial yield is based upon the Mises yield criteria. As seen in Fig. 26, the yield surface considered is a cylindrical surface in principal stress space, with an axis (Λline of Fig. 26a) that makes equal angles with the principal stress axes. When the stress state reaches a point on the yield surface, initial plastic flow can occur. This point corresponds to the point, σ_o, on the effective stress-strain relation of Fig. 26b. As further straining occurs the material becomes stronger (strain hardens) and the diameter of the yield surface increases. For unloading, recovery of the material takes place elastically. The effective stress-strain curve of Fig. 26b can be obtained from the results of an unconfined compression test. In the SLAM Code, any arbitrary strain hardening law can be used as data input to the code by considering it in the form of a series of points along the effective stress-strain curve of the material.

This plastic behavior model was initially developed for metal materials in which two primary characteristics are apparent: (1) the material behaves similarly in both tension and compression, and (2) no plastic volume change occurs (hydrostatic stress states, states on the Λline, produce only elastic volume changes). Some rock materials at the lower overpressure ranges do exhibit this behavior under compressive loadings. However, under tensile loadings, they exhibit a much different

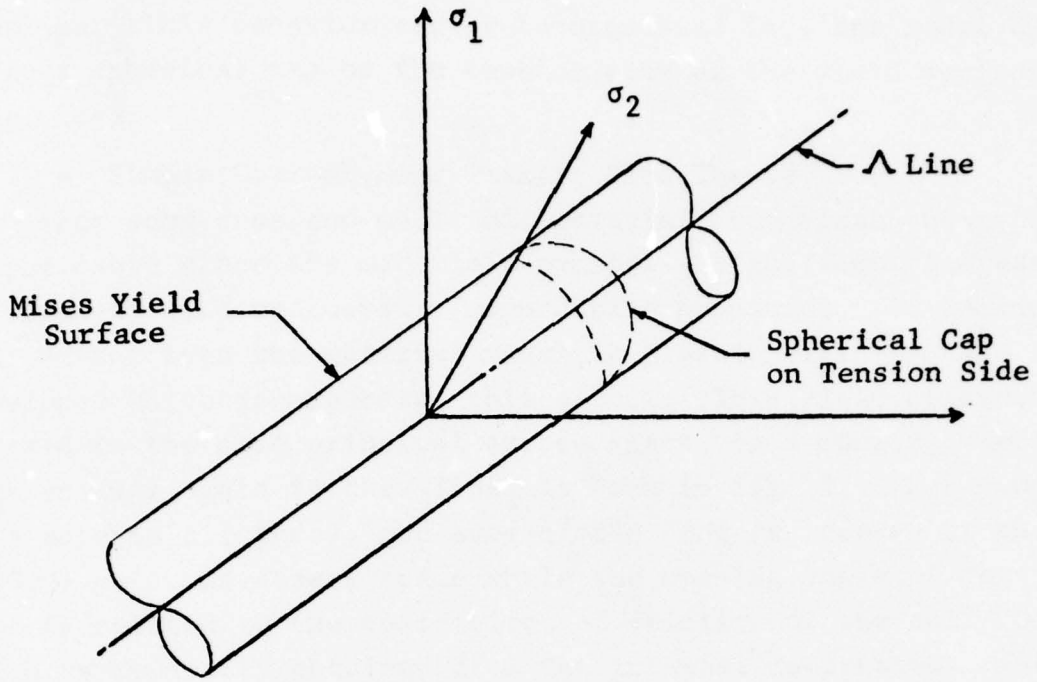

(a) Yield Surface for Mises Yield Condition

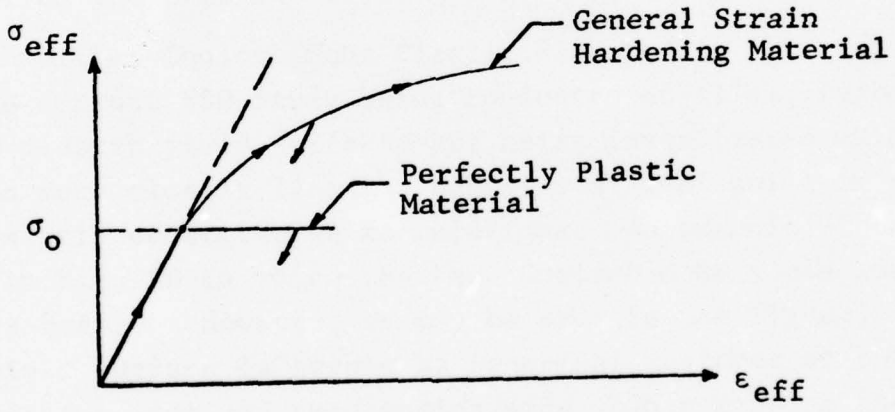

(b) Strain Hardening Characteristics

FIG. 26 ELASTIC-PLASTIC BEHAVIOR OF MISES MATERIAL

behavior so that plastic flow occurs even under hydrostatic tensile loadings. This behavior can be incorporated into the model by using a spherical cap on the tension side of the yield surface (Fig. 26a).

- Simple Coulomb-Mohr Plastic Flow Theory

For some rock and most soil materials the Mises theory is inapplicable since the materials exhibit a significant increase in strength with hydrostatic compressive pressures. To include this effect into the material model, a plastic yield law was developed which incorporated this effect. This yield criterion, plotted in the same principal stress space, is a conical surface with an axis again in the Λ line, as seen in Fig. 27. For cohesionless materials (sands), the apex of the cone is located at the (0,0,0) point in stress space while the opening angle of the cone is related to the coefficient of friction of the soil/rock which is typically obtained from the triaxial compression test. For cohesive materials, the location of the apex along the Λ line is related to both the coefficient of friction and the cohesion obtained from the triaxial test.

- Modified Coulomb-Mohr Plastic Flow Model

On a current BSD study being conducted at IITRI, improved models of plastic yield surfaces are being investigated which attempt to more closely link the behavior of real soils or rocks to the analytic constitutive formulations. An example of this is shown in Fig. 28 in which the same Coulomb-Mohr yield surface is used as before. However, as may be seen in the figure, the conical yield surface is capped by spherical surfaces at both the compression side and the tension side. This enables two relatively well known properties of soils to be simulated.

First, the result of a series of triaxial tests on a typical cohesive soil is shown in Fig. 29. The linear Mohr envelope applies at relatively low values of confining stress levels. But, from the results of an unconfined triaxial test (no lateral restraining pressures), the cohesive strength C_u, is usually

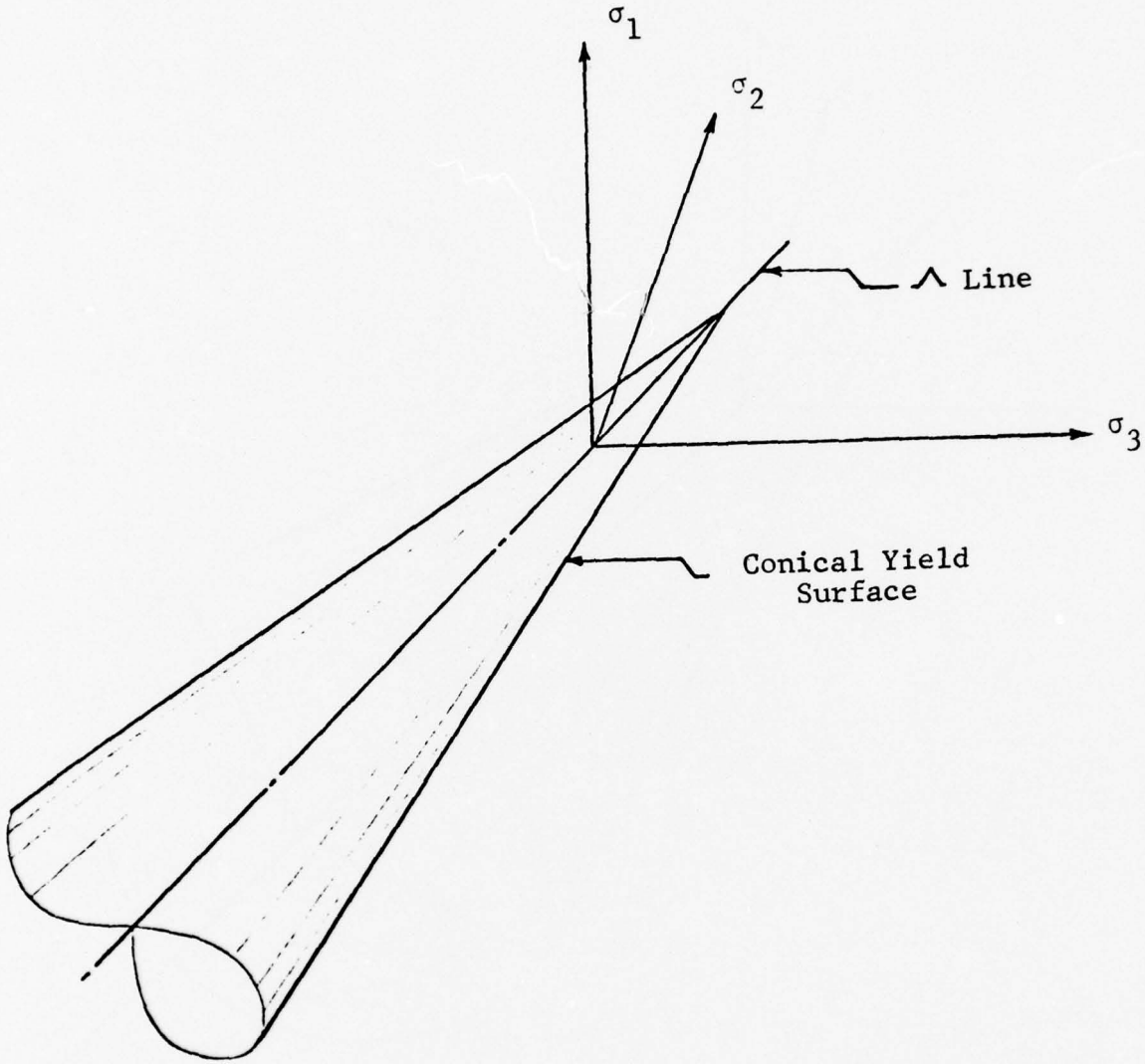

FIG. 27 SIMPLE COULOMB-MOHR YIELD CONDITION

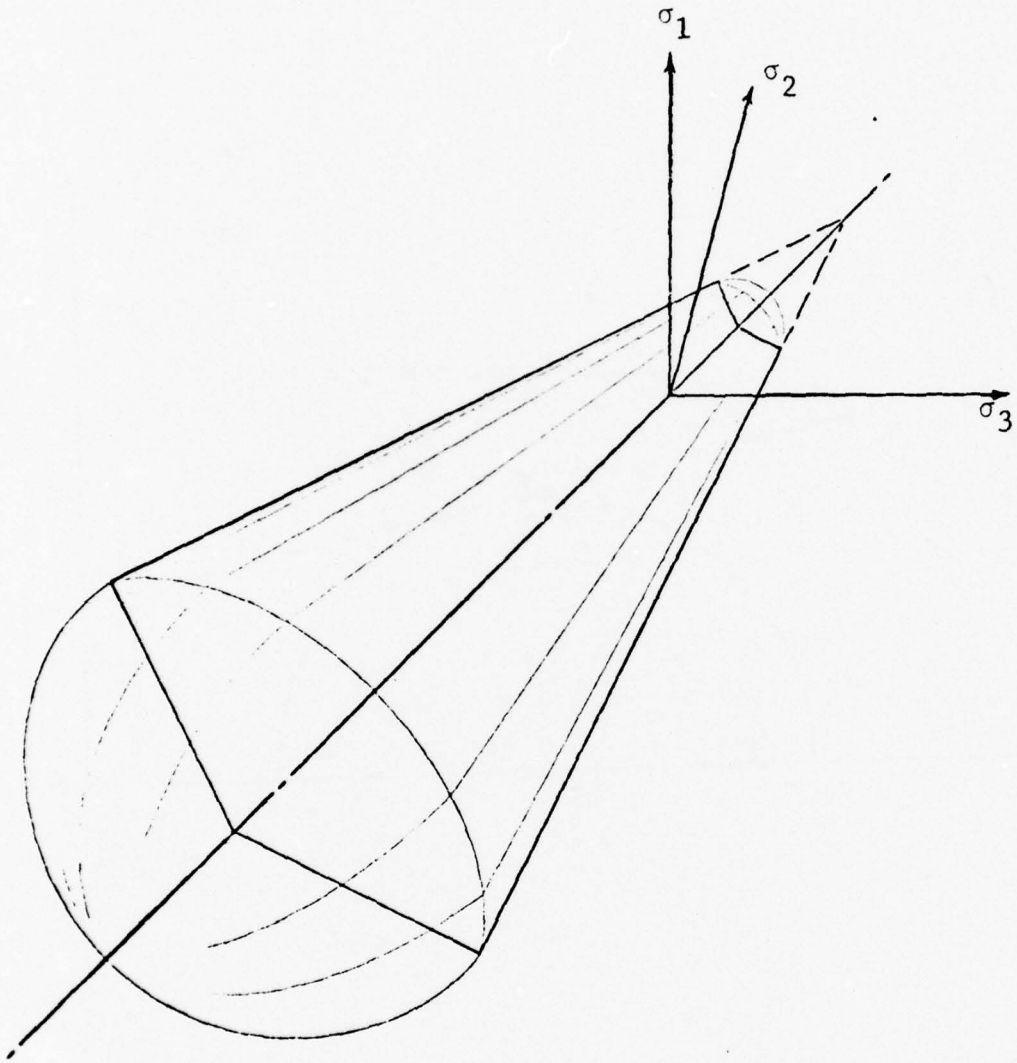

FIG. 28 MODIFIED COULOMB-MOHR YIELD CRITERION

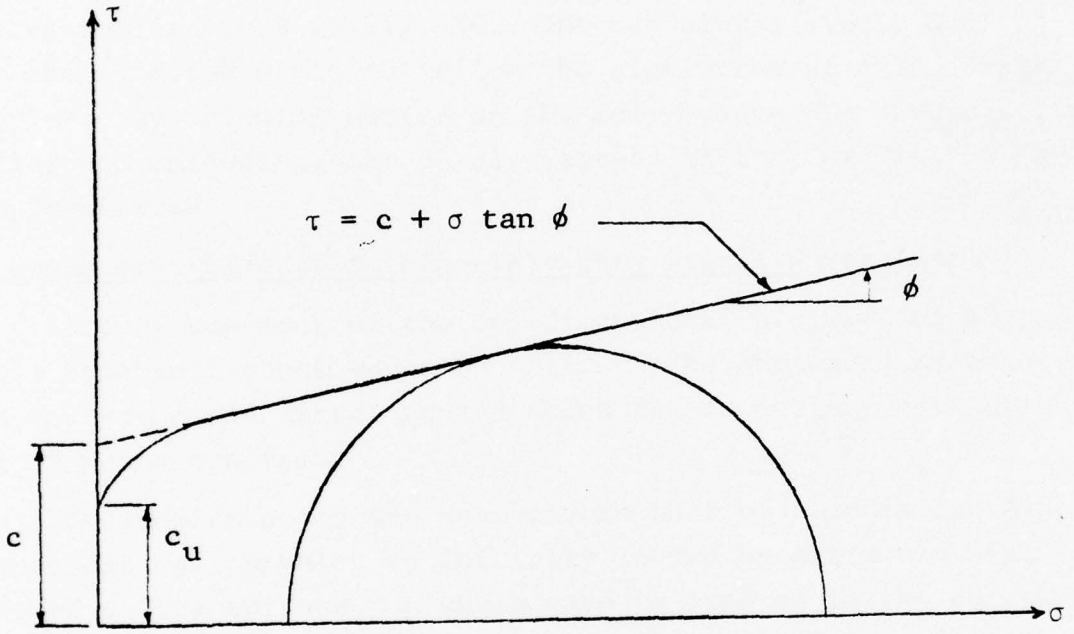

FIG. 29 TYPICAL MOHR ENVELOPE FOR COHESIVE SOIL AT LOW STRESS LEVELS

much lower than the apparent cohesion, C, obtained by extrapolating the envelope to the zero stress line. By placing the cap on the conical yield surface near the apex of the cone, this effect can be relatively easily simulated.

On the other hand, by using the cap at the compressive side of the cone one can then simulate the nonlinear behavior of soils noted in the hydrostatic and confined (consolidation) tests. A typical example of this plastic behavior during confined compression is shown in Fig. 30. The use of the simple Coulomb-Mohr theory alone would not allow the simulation of this complex behavior. By allowing motion of the compressive cap with plastic loading and unloading, the complex stress history of Fig. 30 can be approximated.

3. Deviatoric Effects in High-Intensity Stress Waves (Ref. 8)

A study was made of the one-dimensional propagation of strong spherical shock waves in solids. The phenomena associated with cratering and direct ground shock due to nuclear detonations were of prime concern.

The problem posed and analyzed is that of a media containing a spherical cavity which is initially loaded by extremely high pressure on its surface. A shock wave is created in the surrounding solid forming successive zones of primarily fluid, plastic and elastic behavior as the wave propagates outward and decays (Fig. 31). The fluid and elastic zones have been studied in great detail whereas the plastic zone has been given relatively little attention. The present analysis bridges the gap between the fluid and elastic solutions by consideration of plastic behavior. In fact it affects a continuous transition from one zone to another by using a material description which accommodates all three types of behavior together. In the formulation, the plastic (deviatoric) effects remain the same order of magnitude regardless of stress level; hence at extremely high stress levels a fluid-like behavior dominates. The inclusion of

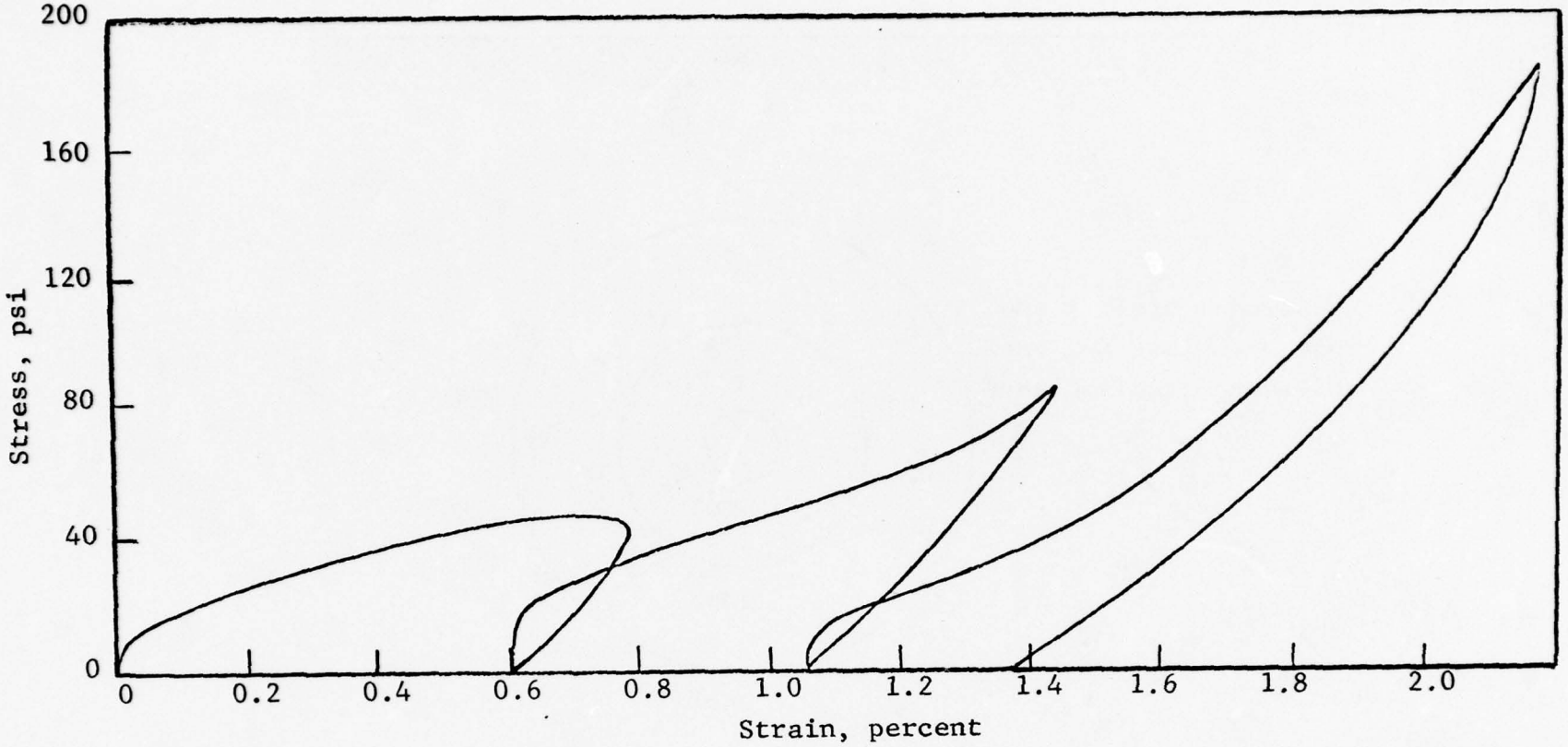

FIG. 30 STRESS-STRAIN RELATION FOR OTTAWA SAND

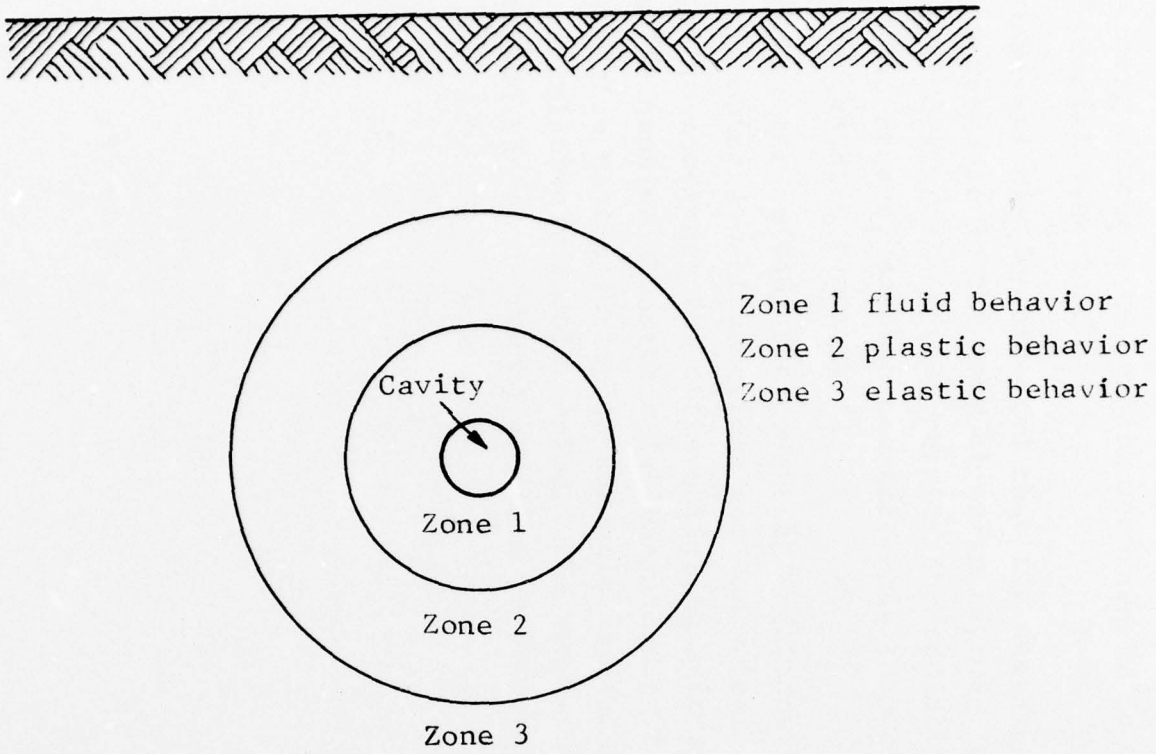

FIG. 31 ZONES OF BASICALLY DIFFERENT BEHAVIOR

deviatoric effects required the development of a rational description of real media applicable to any three-dimensional state of stress. This was done by extending established plasticity theories to include compressibility effects, and by modification of present hardening concepts to conform more nearly to the actual physics of material behavior.

This analysis has demonstrated that the deviatoric effects can alter the response in the very close-in region. In essence the presence of deviatoric stress permits the radial transmission of a compressive stress, despite the fact that the material experiences a hydrostatic tension.

Techniques for solving the governing equations have been outlined. A combination of numerical and analytical procedures was indicated to integrate the differential equations. At the shock front the Rankine-Hugoniot relations are used together with a progressive wave solution to analytically extend the solution into a relatively smooth region. The remainder of the solution (behind the shock front) can then be determined numerically.

III. SOIL-STRUCTURE INTERACTION

A. VIM Code I (Ref. 9)

This program was written to determine the vertical rigid-body motion imparted to the contents of a silo subjected to air blast surface overpressure. In the analysis the silo is idealized as a stepped, rigid, circular cylinder containing two constant-diameter sections to simulate the Titan II Silo configuration as shown in Fig. 32.

The forces acting on the silo which were considered in the vertical response analysis are the vertical cap force F(t), skin friction F_i, vertical loads at the base F_B, and the soil-structure interaction forces F_P at the step in the cylinder.

The time varying cap load was taken to be simply the specified air blast overpressure σ times the cap area. Skin friction forces were computed using the Coulomb friction model which utilizes information on free-field soil stresses and velocities at selected node points along the length of the silo. The silo base-soil interaction vertical resultant force F_B was calculated on the basis of a commonly used soil-structure interaction model (see Fig. 32). This model stipulates that the total force is composed of the sum of three forces due to (1) the free-field stress, (2) the relative displacements of the free-field soil and the structure, and (3) the relative values of the free-field soil velocity and the velocity of the structure. The constant proportionality factor k_B, (spring constant) for the relative displacements is assumed to be equal to a fraction of the spring constant corresponding to the elasticity solution for the displacement of a rigid circular die pressed into the plane boundary of an elastic half space. The calculation of the base damping constant S_B, associated with the interaction forces produced by the relative velocity between the silo and the free-field soil is also based on an elasticity solution. It is taken to be a fraction of the normal stress produced at the end of a bar which

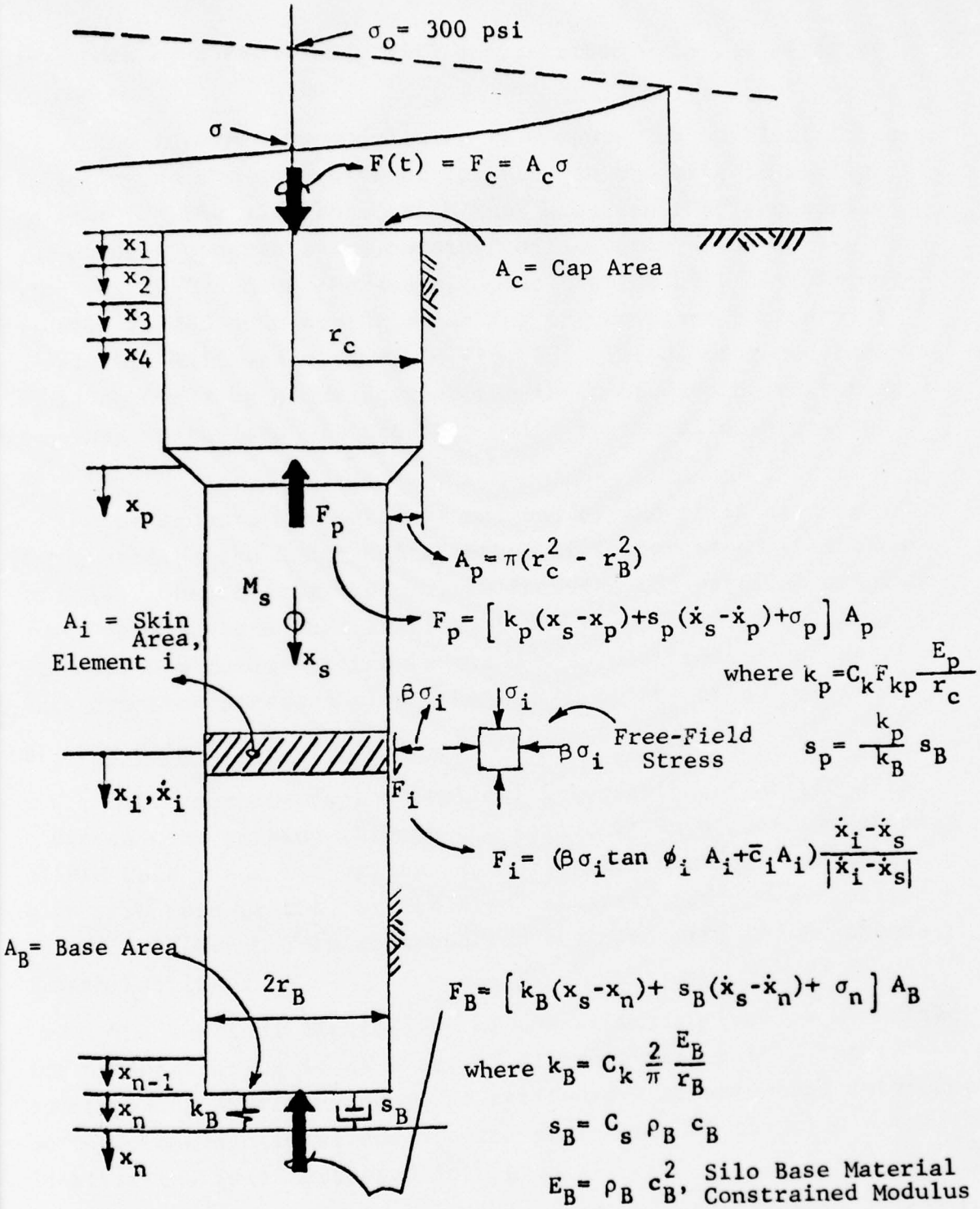

FIG. 32 SILO SKIN FRICTION INTERACTION MODEL

is struck by a rigid body with a prescribed velocity relative to the bar.

The interaction model used to compute the vertical force F_p acting on the underside of the step in the silo is similar to that for the silo base, with the exception that the spring and damping constants are obtained differently. The spring constant k_p is based on the average displacement of a uniform vertically loaded annular region acting on the plane boundary of an elastic half space shown in Fig. 33. The damping constant S_p is obtained by assuming that the ratio of damping to spring constant is the same at the step point in the silo and at the silo base.

The equation of veritcal motion for the rigid silo is integrated by the Runge-Kutta method of integration attributed to Gill. Output from the program includes the vertical displacement, velocity and acceleration of the silo; the interaction stresses and forces at the base and step positions; and the skin friction stresses along the length of the silo.

B. VIM Code II (Ref. 10)

This code treats the vertical interaction of a silo with a stress wave passing through the soil. It is a generalization of VIM Code I and was written specifically to handle the single silo structure or the "articulated" silo structure, as typified by the LER/Launch Tube construction employed with the Minuteman Launch Facility.

The vertical flexibility of the silo structure is accounted for by considering it as a set of discrete mass points interconnected by stiff springs, the stiffnesses of which are determined by the cross-sectional and elastic properties of the silo. The idealization is illustrated in Fig. 34.

The interaction model includes effects of silo skin friction S_{ij}. The skin friction model used is based on the Coulomb soil

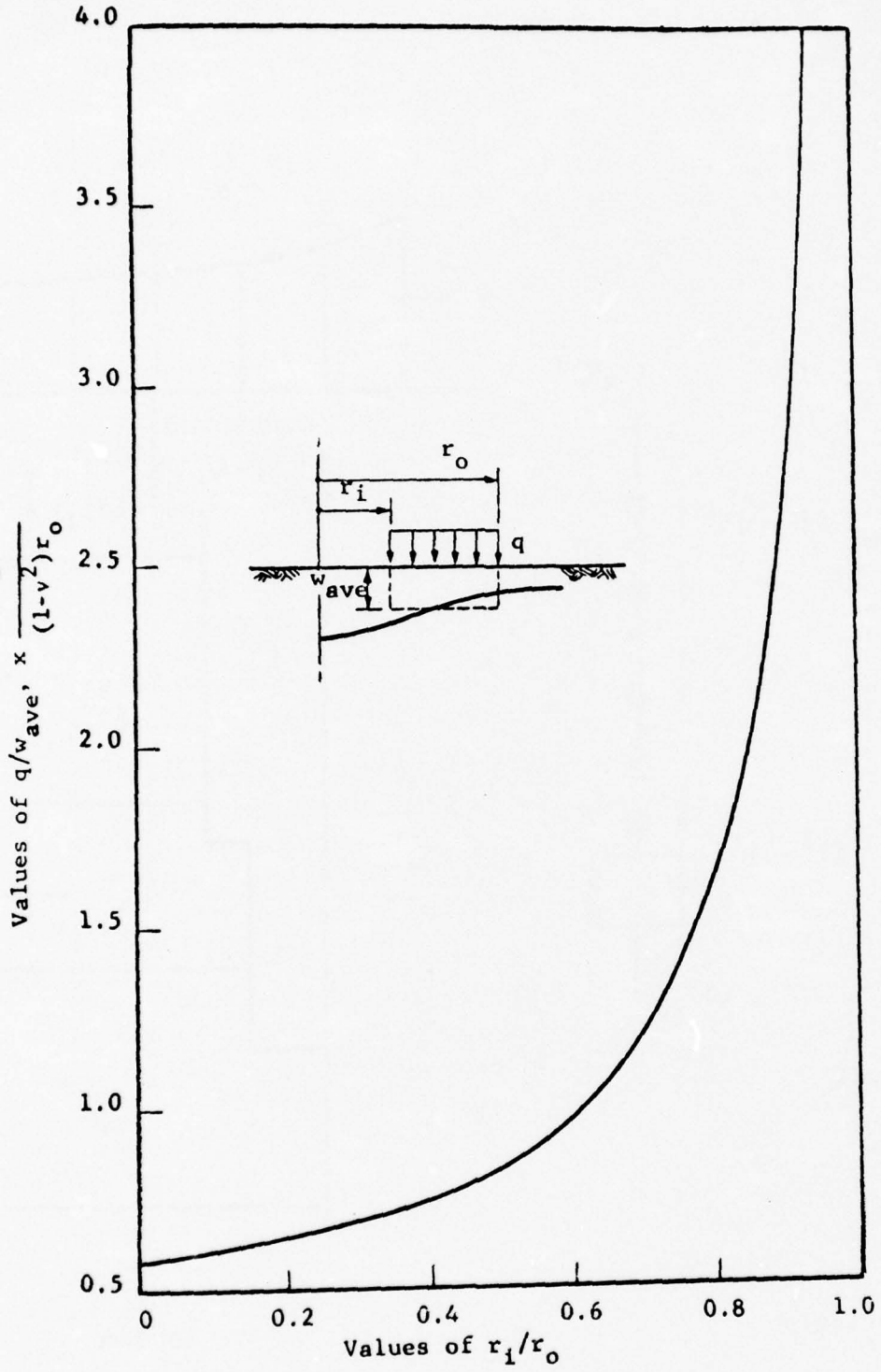

FIG. 33 RATIO OF UNIFORM LOAD TO AVERAGE DISPLACEMENT FOR ANNULARLY LOADED AREA (F_{kp})

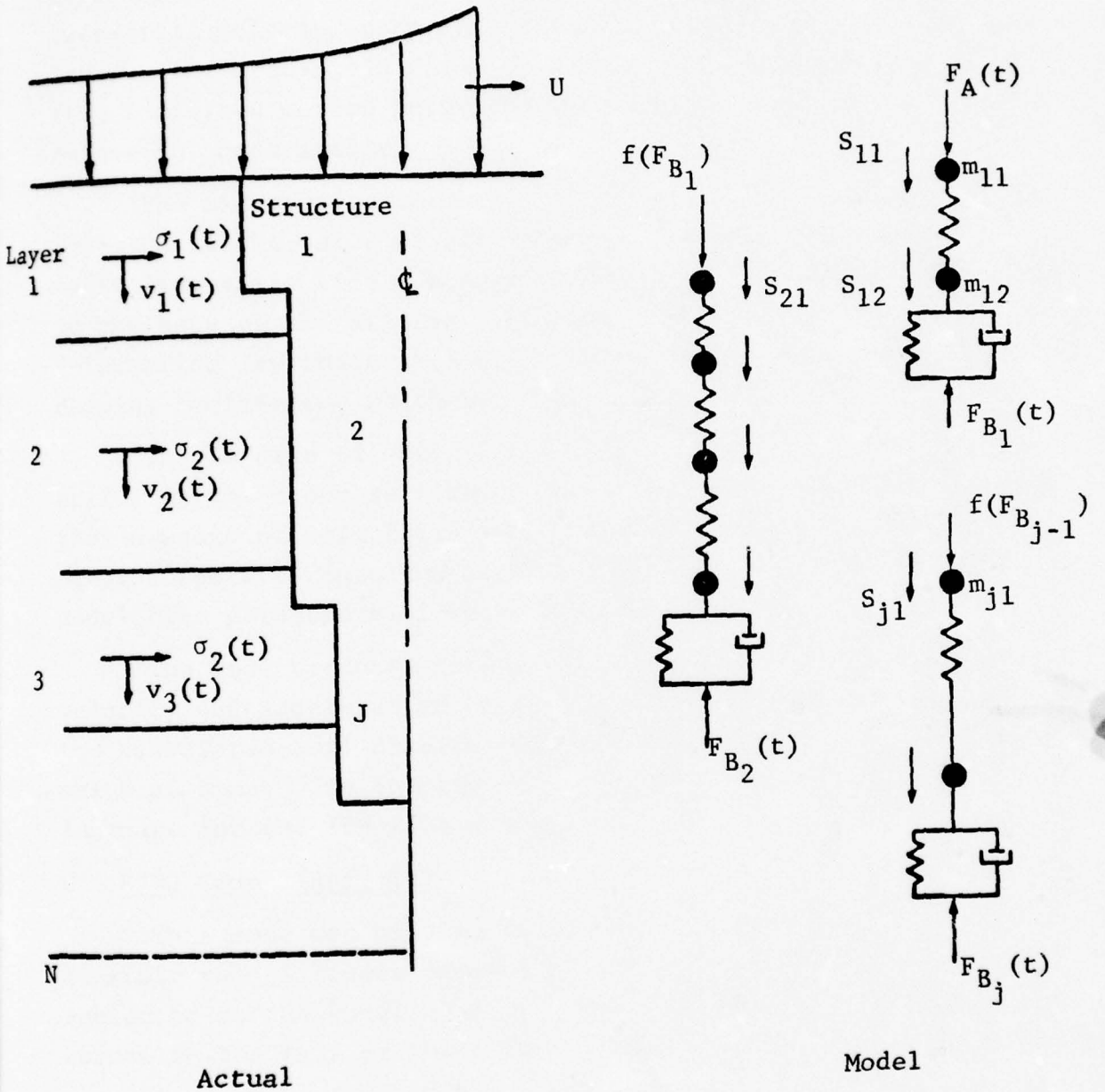

FIG. 34 MODEL USED FOR VERTICAL INTERACTION CODE

shear failure theory. The frictional forces on the silo are computed from free-field inputs which are described at the mid-point of soil "layers" in terms of both vertical velocity and horizontal stress pulses, the layers being chosen so that the free-field pulses can be considered as fairly uniform over each layer. The free-field data can either be read in or determined from idealized motion pulse shapes which are obtained by fitting pulses to shock spectra.

The air overpressure load $F_A(t)$ on the cap of the silo is computed as the value of the overpressure times the cap area, neglecting early time cap engulfment effects. The loading $F_{Bj}(t)$ on the base of the silo is determined by use of a soil-structure interaction law which includes the soil foundation modulus and damping coefficient which are prescribed.

In the case of articulated silos, the base loads $F_{Bi}(t)$ acting on the upper section of the silo are computed by assuming that a wedge of soil fails under its foundation. These loads are incorporated into the code in the form of a spring-dashpot model, the parameters of which must be specified.

The code produces output which includes the displacement, velocity and acceleration of each silo mass point, as well as the associated soil displacement and velocity at each specified value of time. The computer program is written in FORTRAN IV language for the IBM 7094 computer.

C. RING Code (Ref. 11)

This code was written to predict the response of buried flexible tunnel liners encased in crushable foam materials and subjected to the engulfment of a plane compression wave moving normal to the axis of the tunnel. This is demonstrated in Fig. 35.

The soil-structure interaction model on which the code is based uncouples the free-field response from the structural response. The code accepts as input free-field stress and/or motion history data directly in the form of tabulated values at

$\sigma_r = \sigma_o + k\ (w_o - w_f) + s(\dot{w}_o - \dot{w}_f)$

σ_o = radial free-field stress

w = radial displacement

$\dot{w}$ = radial velocity

k,s= parameters

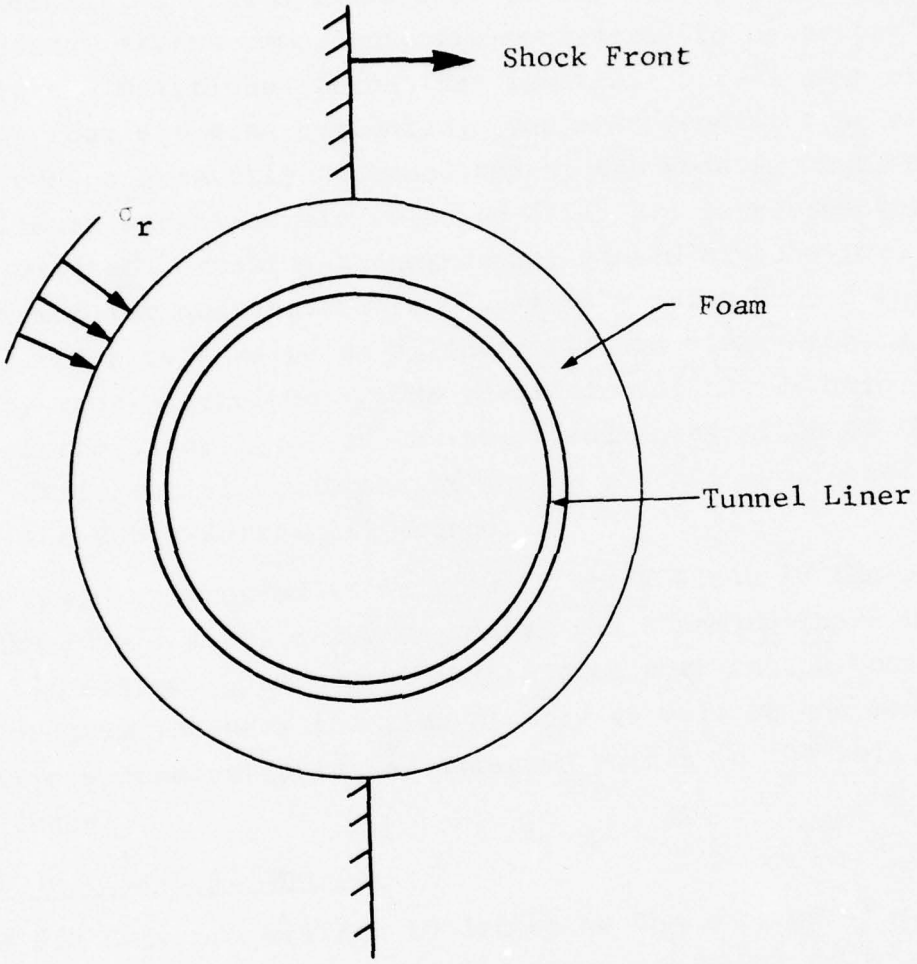

FIG. 35 MODEL FOR RING CODE

various times, or indirectly as parameters of an ideal shock "fitted" to actual spectra data. The soil is characterized by a power-law stress strain curve suggested by experiments and provides for a hysteresis effect during unloading, see Fig. 36. In the interaction model the free-field stresses and those generated by the relative displacement and velocity of the soil and structure constitute the applied load to the outer (foam) structure. Only the normal stress components are considered to be acting on the structure - frictional forces are ignored. Stress wave effects through the foam are also neglected. The most general type of foam that can be presently accommodated by the code is that which has a trilinear stress-strain relation (Fig. 37) corresponding to linear elastic, crushing and hardening phases of behavior, with provision for nonrecoverable plastic straining upon unloading. The tunnel liner is treated as a linear elastic ring which is analyzed by modal techniques. The prediction of the dynamic response of the liner involves the numerical integration of the system of differential equations of motion which is performed by use of the Runge-Kutta-Gill method.

The computer program is written in the FORTRAN IV language for the IBM 7094 digital computer, using the standard IBSYS monitor (version 13) system. The output information that can be obtained from the program includes the time history as well as the maxima of several response variables at selected points in the soil, foam and tunnel.

D. SIM Code (Ref. 12 and 13)

The SIM Code was written to determine the motions of a missile isolated from a hardened silo structure which is subjected to ground shock developed by a nuclear detonation as depicted in Fig. 38. The analysis developed for the system considers beam motions of both the missile and silo. Although the analysis is primarily concerned with horizontal response produced by horizontal loads, the effect of rigid body vertical

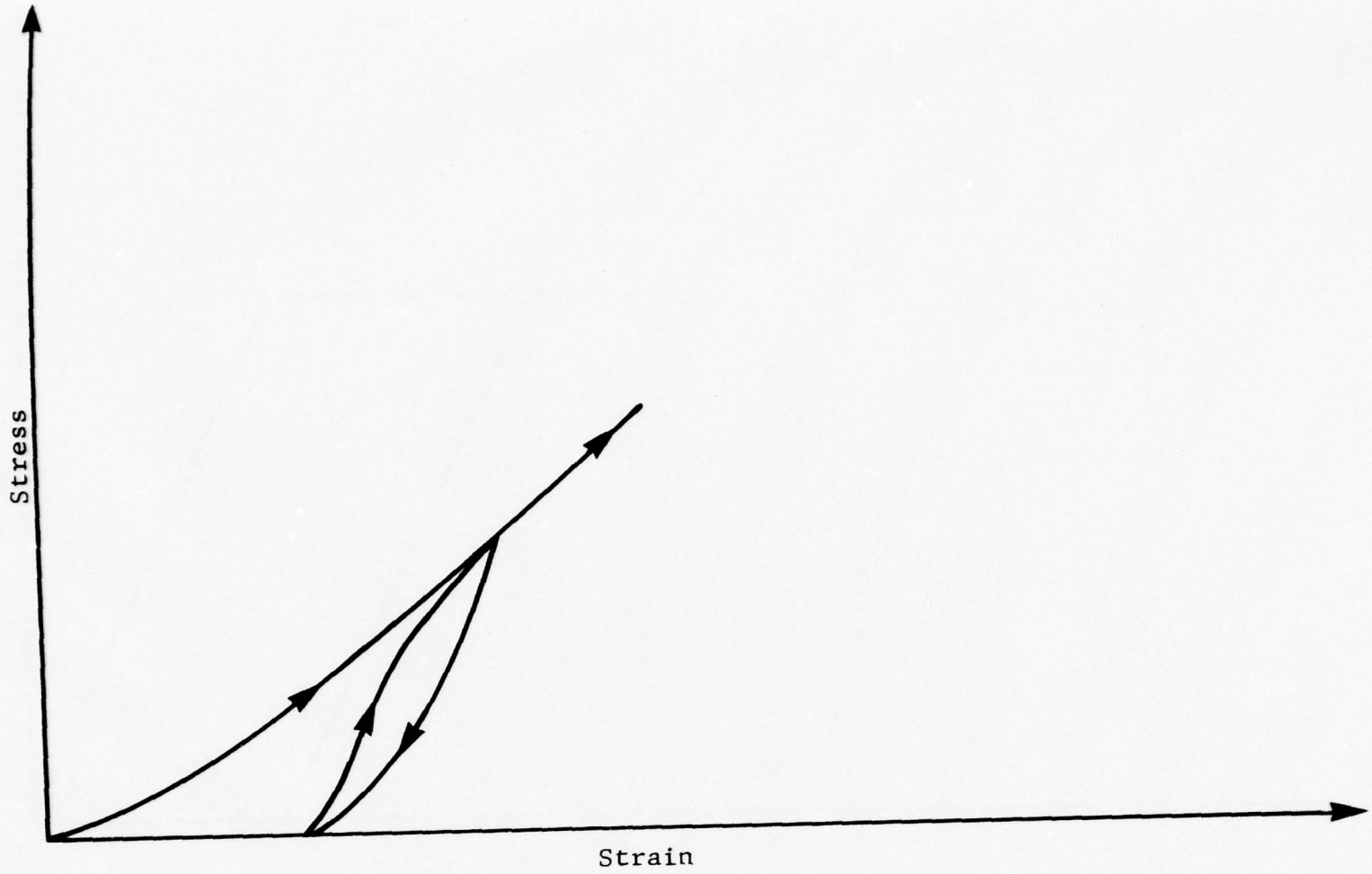

FIG. 36 STRESS-STRAIN RELATIONSHIP FOR SOIL

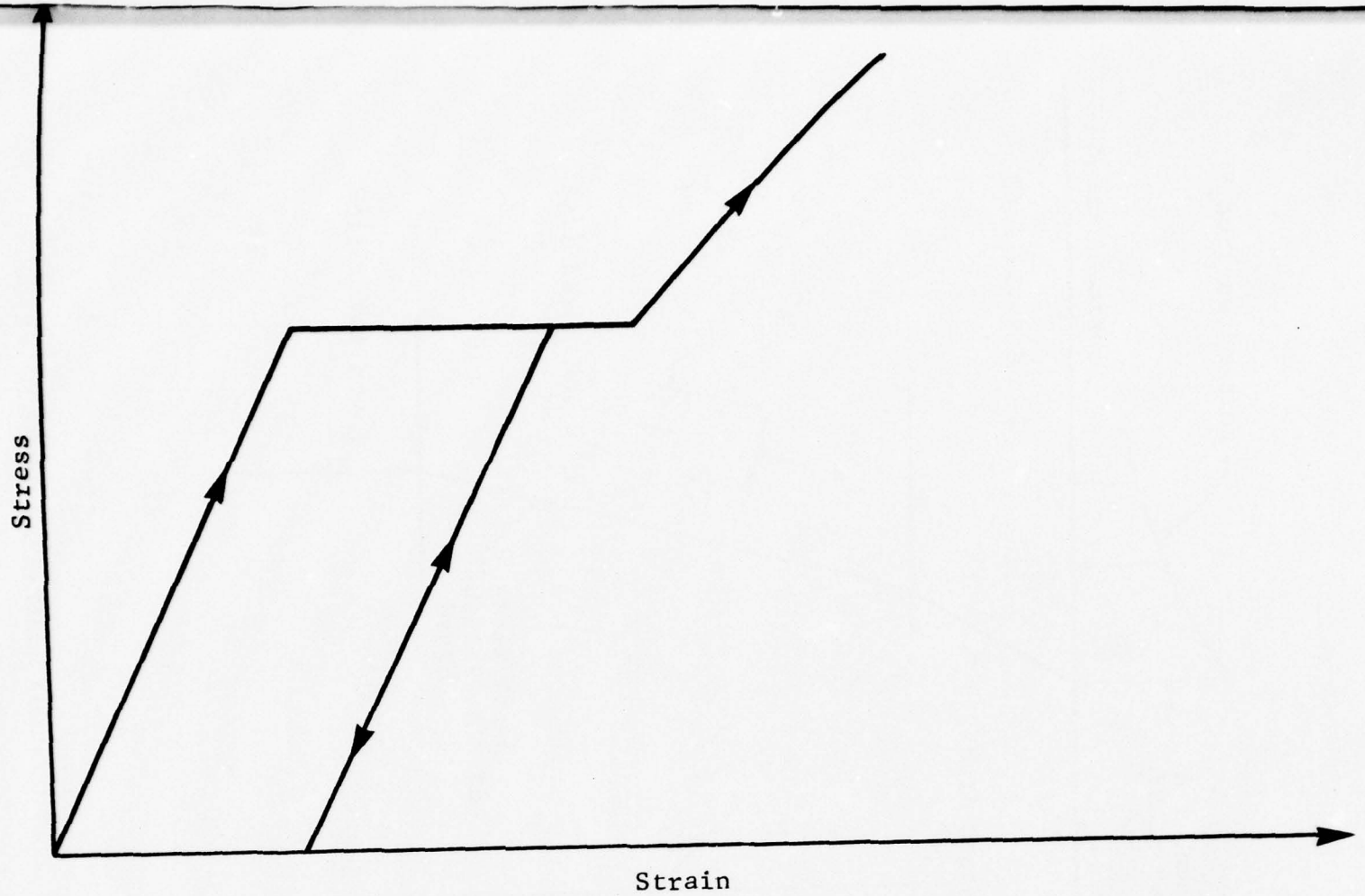

FIG. 37 ASSUMED STRESS-STRAIN CURVE FOR FOAM

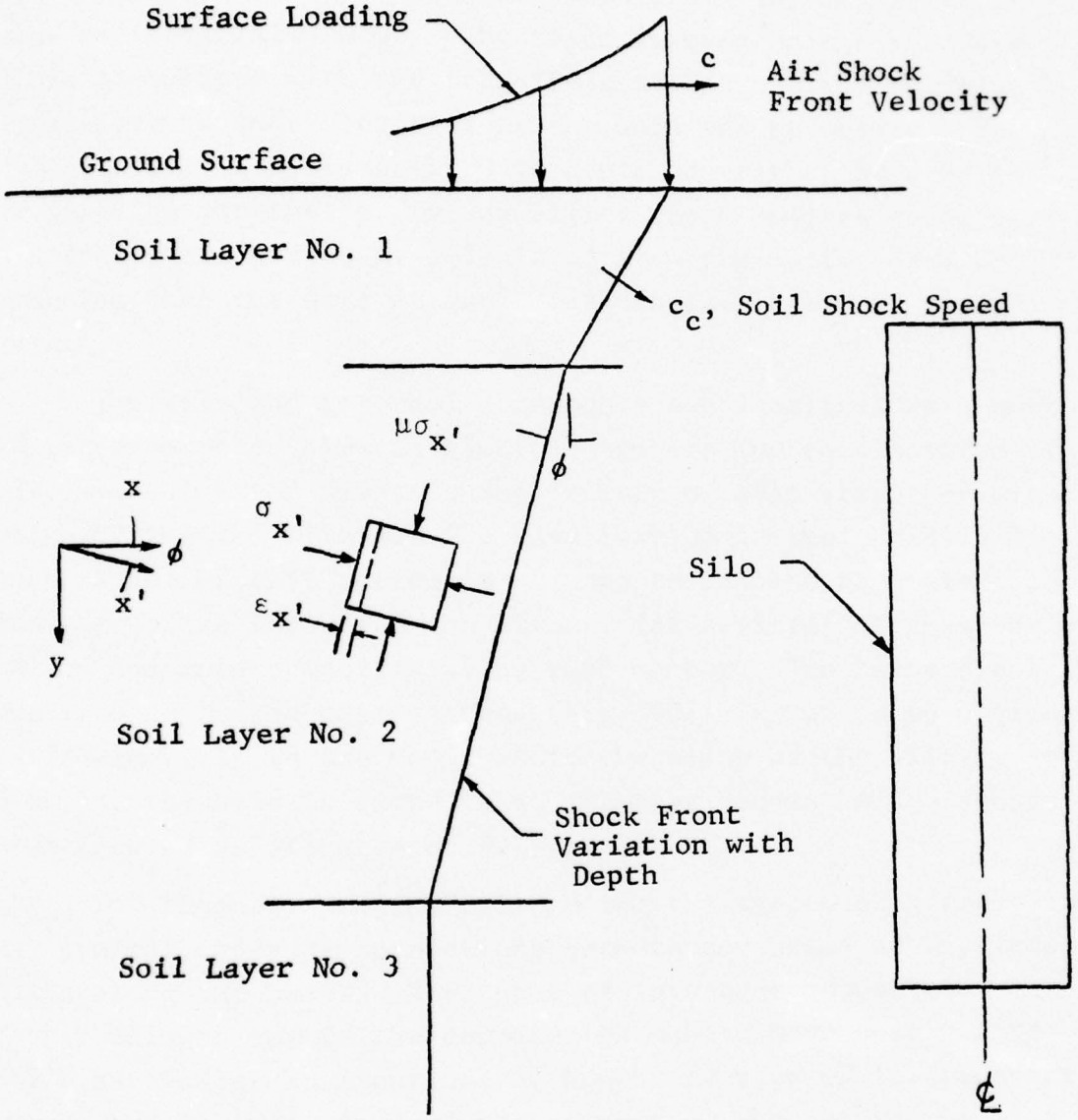

FIG. 38 ASSUMED FREE-FIELD CONDITIONS

motion of the silo on this response can be determined from the program also.

The soil-structure interaction model employed separates the soil and structural response problems. The model is the same as in the RING Code. The loads imposed on the silo are those associated with the free-field stress and the relative displacements and velocities of the soil and structure. The free-field motion histories with depth can either be read in or computed internally from specified shock spectra parameters. The free-field stress is calculated from the motion data by assuming that the soil at each depth is in a state of plane strain.

The silo and internal components are idealized as a number of interconnected elastic flexible members (up to a maximum of five) of which the first is the primary or silo structure with the other housed within. The idealization is indicated in Fig. 39. Each member of this system is assumed to respond as a flexible beam structure including the effects (if desired) of shear deformation and rotary inertia along each member. The beams are analyzed as lumped mass systems (Fig. 40) with up to 60 degrees of freedom. It is assumed that in the plane of the silo cross section, the silo is rigid, that is, ring bending effects have been ignored as illustrated in Fig. 41.

The computer program written for the system of beams allows for general types of connections between any beams at any locations along the beams. The types of interbeam connections currently allowed for in the computation scheme have been geared for a particular application, although any type of interconnection may be considered. For any one connection the general model used is representative of a wide class of practical connectors and consists of a nonlinear spring element, a linear dashpot and a number (up to five) of Maxwell elements in parallel (Fig. 42a). In addition to these force transmission connectors, arbitrary

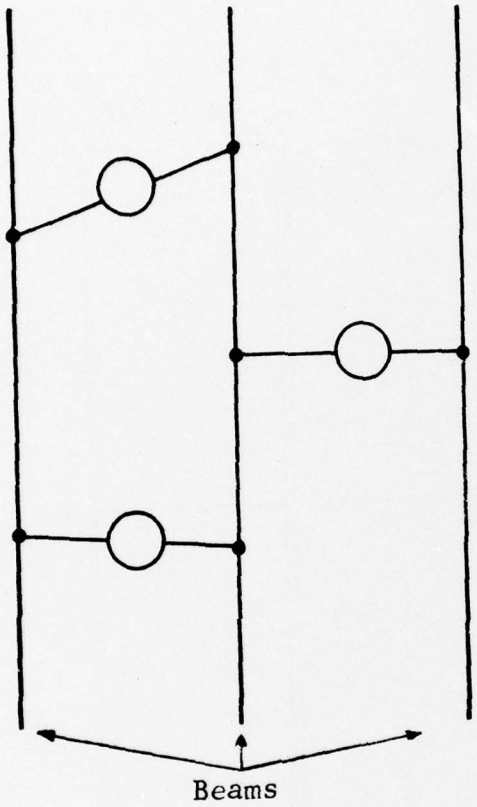

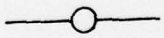

indicates force or moment transmission connector

FIG. 39 IDEALIZATION OF SILO SYSTEM

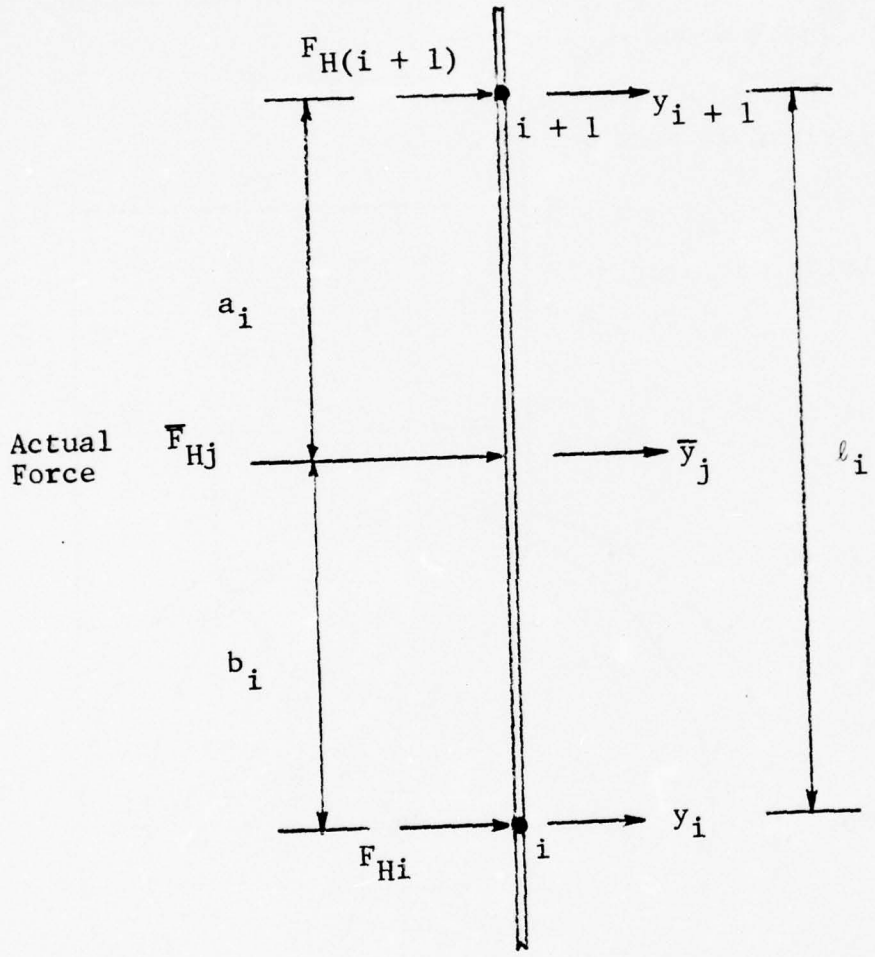

FIG. 40 TYPICAL BEAM ELEMENT WITH APPLIED HORIZONTAL FORCE

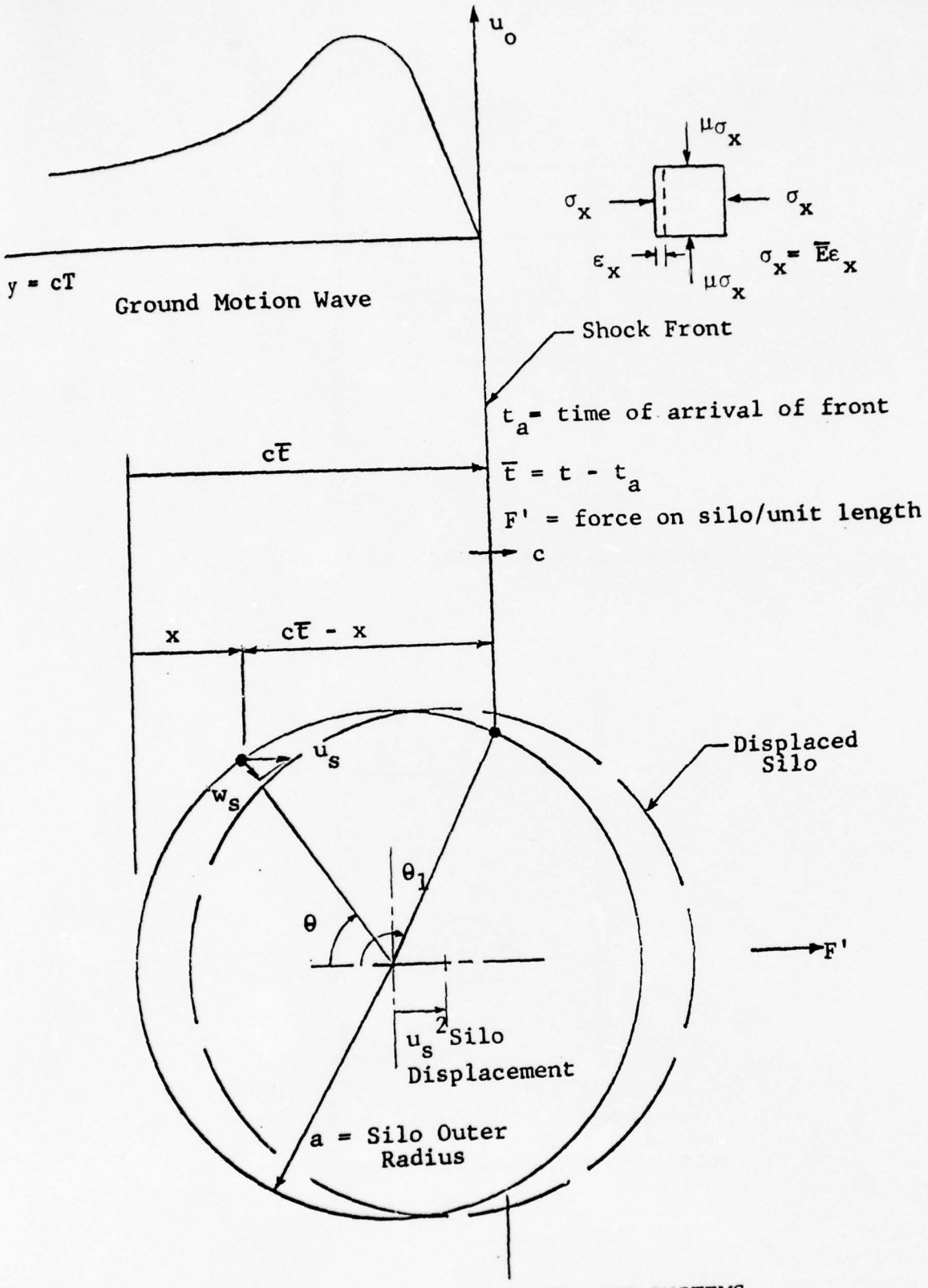

FIG. 41 STRESS WAVE AND SILO COORDINATE SYSTEMS

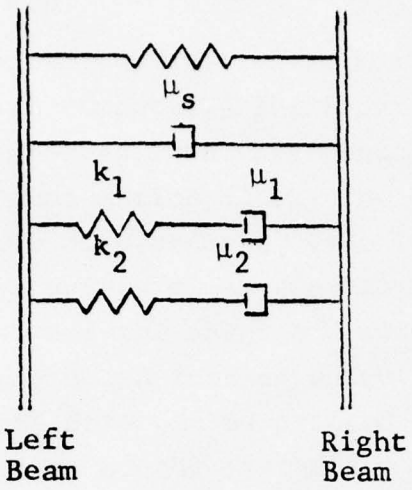

(a) Force Transmission Connector

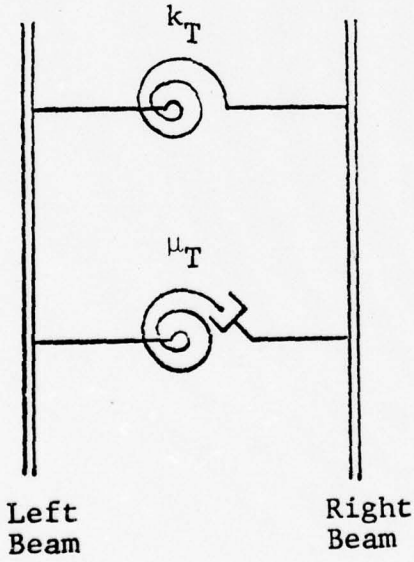

(b) Moment Transmission Connector

FIG. 42 TYPES OF INTERBEAM CONNECTIONS ALLOWED IN CURRENT PROGRAM

moment connections are provided for in the form of simple torsion spring-dashpots (Fig. 42b).

The computer program was written in FORTRAN IV language for the IBM 7094 digital computer. The input required to the code can be generally grouped into three categories: beam data, connection data and ground motion data. The typical output from the code consists of the displacement, velocity and acceleration of each beam at various points along the beam, applied loads and moments to the members, and the shear and moment developed in each beam along its length. A further output option is provided to the user in that this data can be printed out at various intervals through the course of the system's motion, or only maximum values can be printed at the end of the run.

APPENDIX

STRESS WAVE PROPAGATION INTO A REGION OF CHANGING MODULUS OF DEFORMATION

by

A. H. Wiedermann

Paper presented at Ground Shock Calculation Meeting, the RAND Corporation, Santa Monica, California, October 26-28, 1965

I. INTRODUCTION

The study of the propagation of stress waves in soils and rocks is vital to the design of buried protective structures against nuclear attack. The in situ soil properties are generally poorly defined, however, some general characteristics have been established. Wilson and Sibley (Ref. 14) have developed a procedure for selecting the constrained modulus and the strain recovery for typical surface soil conditions. The constrained modulus can increase rapidly with depth in several hundred feet and change by several orders of magnitude. The strain recovery, on the other hand, varies from approximately 60 percent at the surface to 100 percent at depths of the order of 100 ft. The density of the soil is relatively constant, increasing slightly with increasing depth. Figure 43 presents some data for two actual construction sites.

The following analysis was performed in order to obtain an estimate of the effect that the region of increasing modulus of deformation has upon the variables of the transient stress field which results from the application of a suddenly applied load, such as is experienced by the soil during a nuclear attack. The following model was selected because its specific properties permits one to obtain simple analytical expressions and thus rapidly provide approximate, but reasonable estimates of the soil motions.

This paper treats both one-dimensional nonsteady wave propagation into a region of changing modulus of deformation and a corresponding two-dimensional quasi-steady problem. This paper will summarize the procedures used and the results obtained recently by the author. A more detailed discussion is given in two recent papers, Ref. 15 and 16.

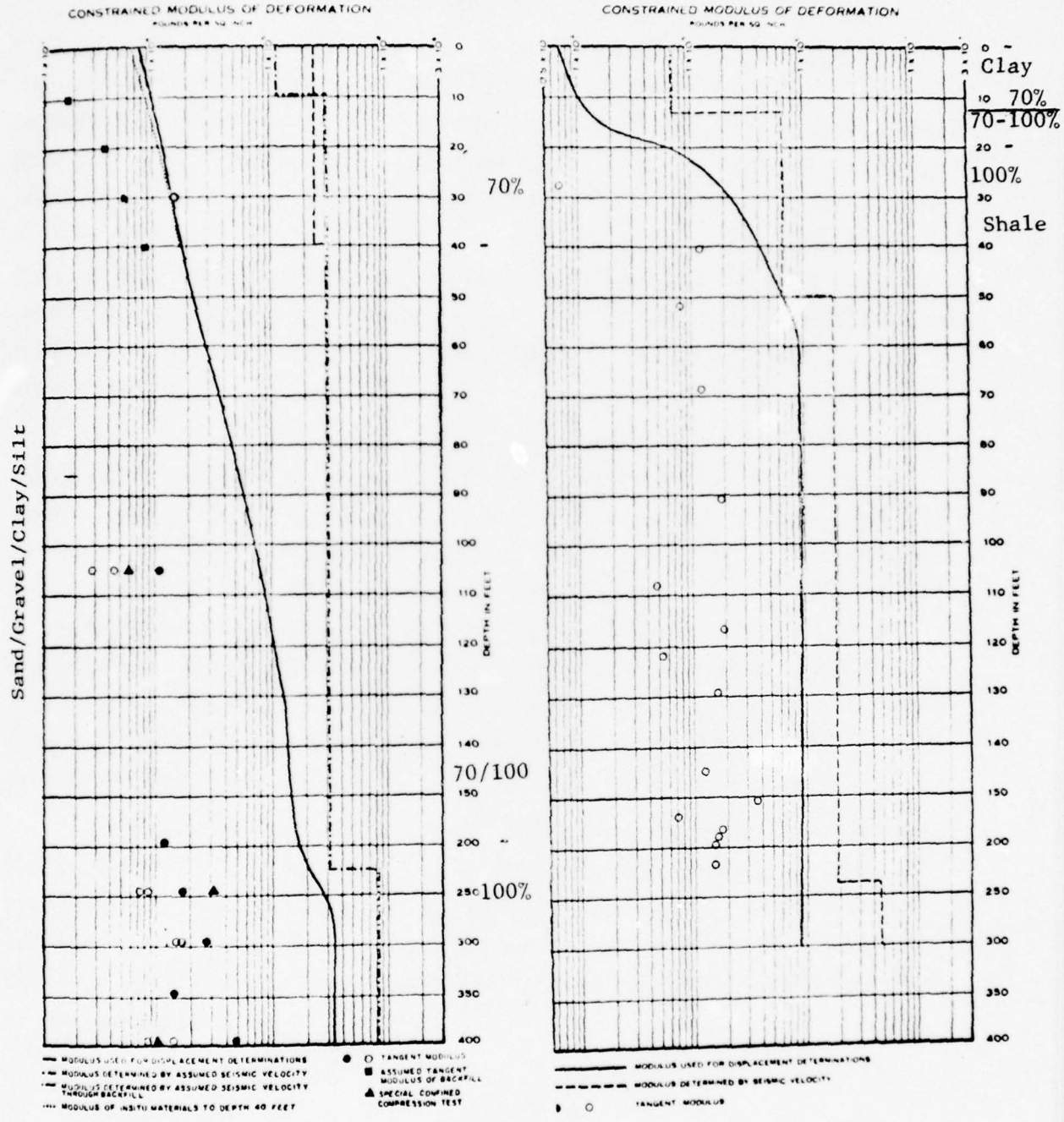

FIG. 43 STRESS WAVE PROPAGATION DATA FOR TWO CONSTRUCTION SITES

II. ONE-DIMENSIONAL NONSTEADY STRESS WAVE PROPAGATION

This section deals with one-dimensional propagation of stress waves into a region of changing modulus of deformation. The constrained modulus of deformation of the soil, M, is assumed to vary with depth, x, (measured from the surface), in any manner. More specific variations of the modulus will be treated in subsequent sections of this paper. Furthermore, the density of the soil is assumed to be constant at a value ρ_o. This latter assumption is not essential to the development of some of the results which follow, however, it does permit considerable simplification. A linear and reversible equation of state or stress-strain law was selected.

In general, we will consider a semi-infinite half space which is subjected to impulsive loads (stress) at the surface (x=o). Disturbances will propagate down into the medium and interact with the moduli gradients. The assumption of a linear and reversible stress-strain law, together with a seismic velocity which is dependent upon position, leads to characteristics or disturbance paths in the wave diagram which are self similar. Furthermore, the initial disturbance or shock front is uncoupled from the interior of the wave as well as from subsequent disturbances at the boundary.

The interaction of a stress wave with an interface across which the modulus changes from M to $M+\Delta M$ will result in the transmission and reflection of two stress waves. The incident and reflected wave will propagate at a velocity c, whereas the transmitted wave will propagate at a velocity $c+\Delta c$ corresponding to the modulus $M+\Delta M$.

The characteristic equations for each of the waves can be solved and one obtains the following results:

$$\Delta\sigma = -\rho_o c \Delta u \tag{1}$$

and

$$\frac{\Delta\sigma}{\sigma} = \frac{1}{2}\frac{\Delta c}{c} = \frac{1}{4}\frac{\Delta M}{M}, \quad (\Delta M << M) \tag{2}$$

where $\Delta\sigma$ and Δu are the changes in stress and particle velocity across the interface.

In the limit as $\Delta M \rightarrow 0$, Eq. (1) becomes

$$\frac{d\sigma}{du} = -\rho_o c = -\frac{\sigma}{u}$$

which when integrated, yields

$$\sigma u = \text{Constant} = \sigma_o u_o$$

where σ_o and u_o are values from some reference state S_o, say the initial value at the surface (x=o). The hodograph diagram, Fig. 44 illustrates the locus of these shock front states. Integrating directly the limiting forms of Eq. (2) yields

$$\frac{\sigma}{\sigma_o} = \left(\frac{c}{c_o}\right)^{\frac{1}{2}} = \left(\frac{M}{M_o}\right)^{\frac{1}{4}} = \left(\frac{u}{u_o}\right)^{-1} \tag{3}$$

where c_o and M_o refer to state S_o.

It will be of interest to compare the results of Eq. (3) with the case of a modulus discontinuity of finite magnitude, viz.

$$\frac{\sigma'}{\sigma_o} = \frac{2}{1 + \frac{c_o}{c_1}} = \frac{2}{1 + \sqrt{\frac{M_o}{M_1}}}$$

which in the limit for a rigid boundary ($M_1 \longrightarrow \infty$) yields a reflection coefficient (for stress) of $\sigma_r / \sigma_o = 2$. The case of a continuously varying modulus from M_o to M_1 yields much larger reflection coefficients for both stress and particle velocities. If $M_1 / M_o = 100$, which is not uncommon in geologic materials then $\sigma_1 / \sigma_o = 3.16$ and in the limit as $M_1 \longrightarrow \infty$, $\sigma_1 \longrightarrow \infty$. This comparison is illustrated in Fig. 44.

The results of the previous paragraphs permit us to compute the initial state behind the shock front as it propagates in the nonhomogeneous medium. This information is of value since the maximum stresses and velocities generally occur at the shock front for many practical problems. However, for this same class of problem the details behind the front are also of considerable interest.

In numerically examining the stress field behind a shock wave moving into a region of increasing modulus and generated by a step surface load, it appeared that the particle velocity was relatively independent of time. This suggested that perhaps there exists a variation of modulus M(x) for which the particle velocity is only a function of time. We will seek to determine such a modulus variation. Since the problem is linear and the principle of superposition is valid it is only necessary to determine the response of the medium to a step load (stress) applied to the surface. The response of the medium to a more general surface load can then be obtained by suitable integration processes.

The field equations are:

$$\frac{\partial u}{\partial t} + \frac{1}{\rho_o} \frac{\partial \sigma}{\partial x} = 0 \qquad (4)$$

$$\frac{1}{c^2} \frac{\partial \sigma}{\partial t} + \rho_o \frac{\partial u}{\partial x} = 0 \qquad (5)$$

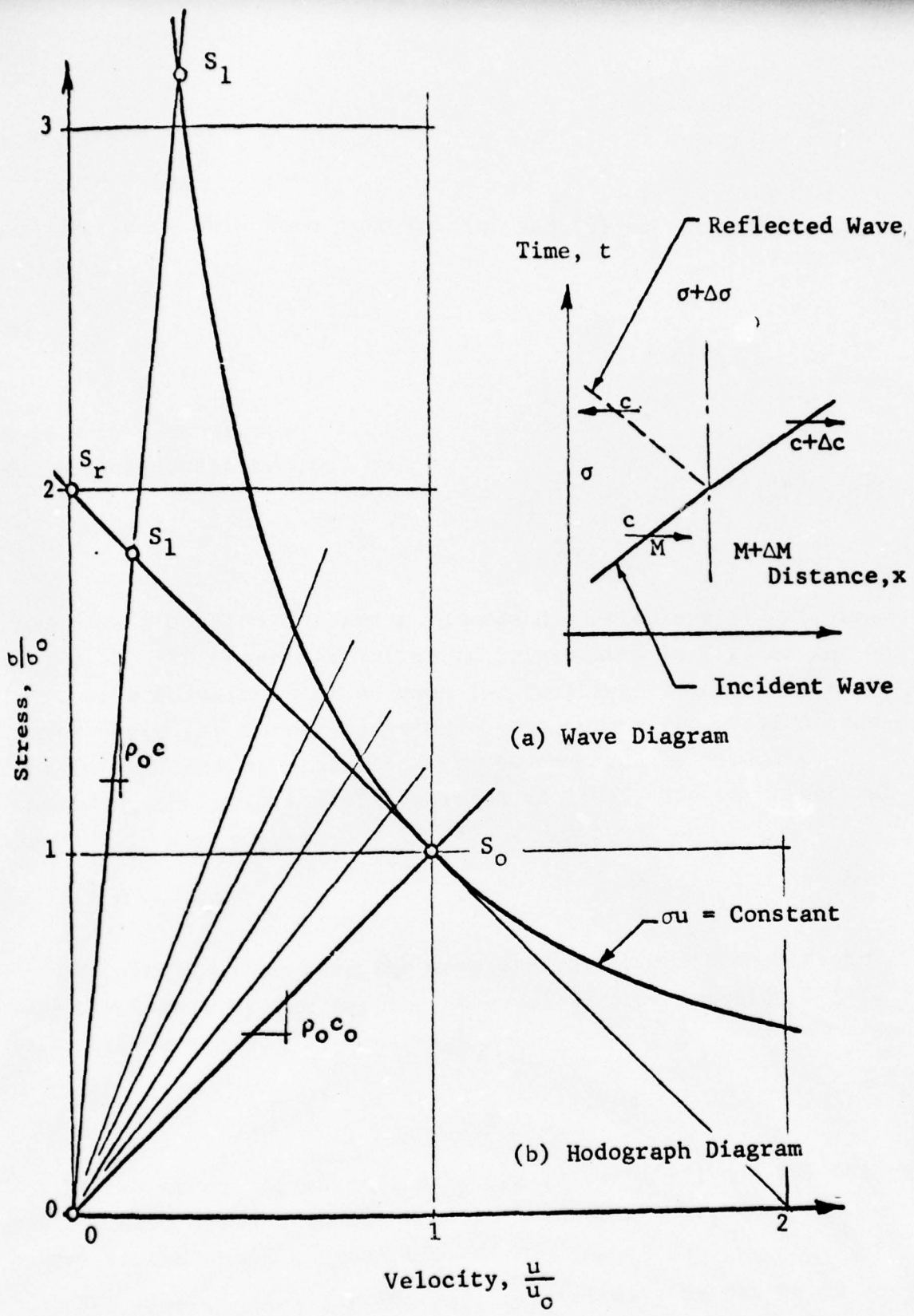

FIG. 44 INTERACTION OF STRESS WAVE WITH MODULUS GRADIENT

If we assume that:

$$\sigma = \sigma\ (x)$$

and substitute this form into Eq. (4) and (5) we obtain

$$\sigma = \sigma_o \pm ax$$

and

$$u = u_o \mp \frac{at}{\rho_o}$$

where a is a constant.
The modulus variation must be

$$\frac{M}{M_o} = (1 \pm \frac{x}{b}) = (1 \pm \zeta)$$

where b is a constant. Time t is made dimensionless by defining $\tau = t\ c_o/b$. This basis solution is illustrated in Fig. 45 and 46. The inverse solution will be used for treating reflected wave systems where the stress waves propagate into a region of decreasing modulus. The displacements can be computed by directly integrating the velocity with respect to time. The shock arrival time, τ', is given by

$$\tau' = \frac{\zeta}{1 + \zeta}$$

We will now consider the more general boundary condition where the stress at the surface is equal to some function G (τ). The stress varies as

$$\frac{\sigma(\zeta, \tau)}{\sigma_o} = (1 + \zeta)\ \ G(\tau - \tau')$$

that is the stress is magnified by the factor $(1+\zeta)$ and has the same normalized shape as the applied load at the boundary but delayed by the shock arrival time τ'.

The general form for the particle velocity is not quite as simple. We can write the velocity in the following form.

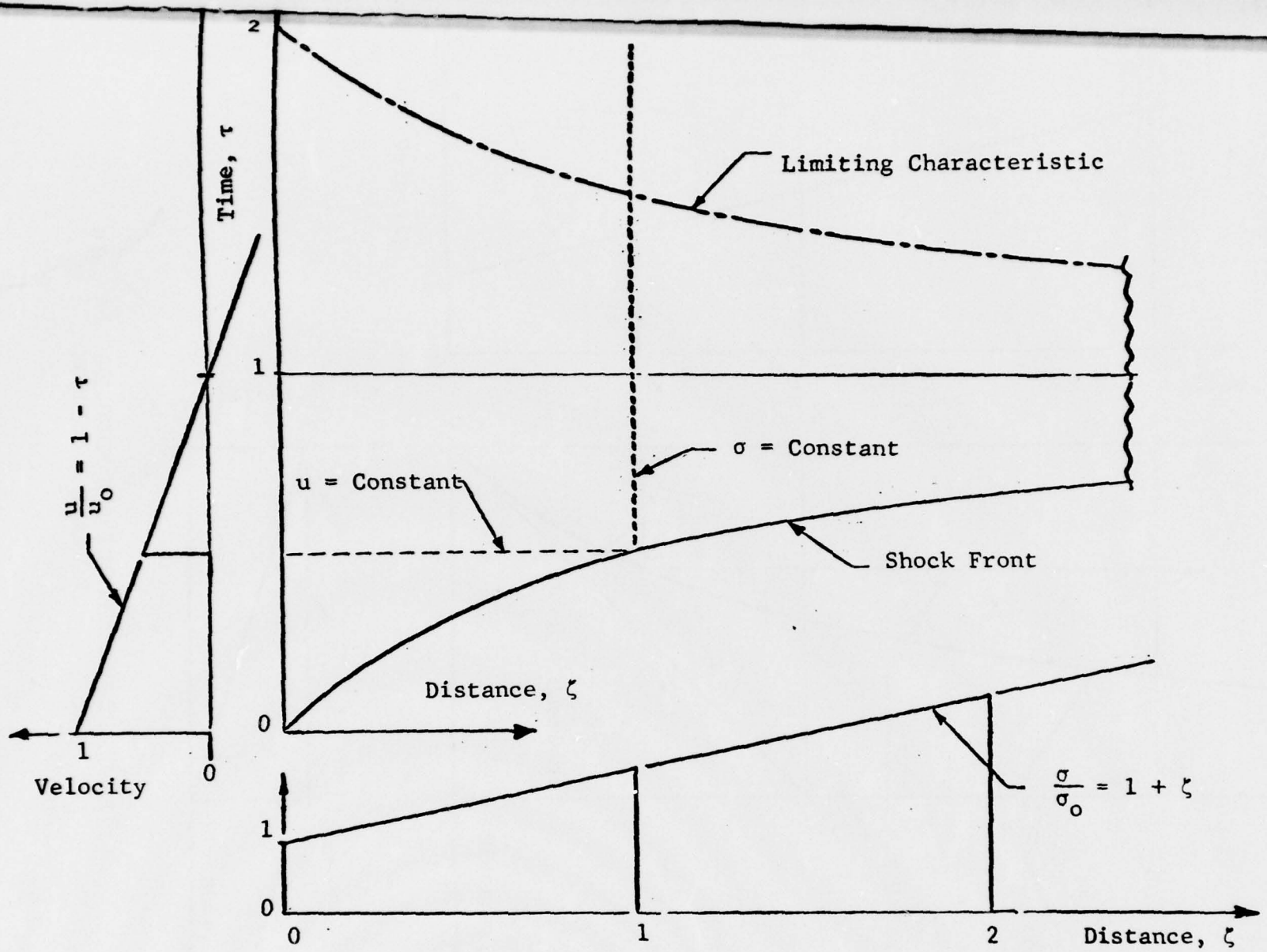

FIG. 45 SOLUTION FOR FOURTH POWER MODULUS VARIATION

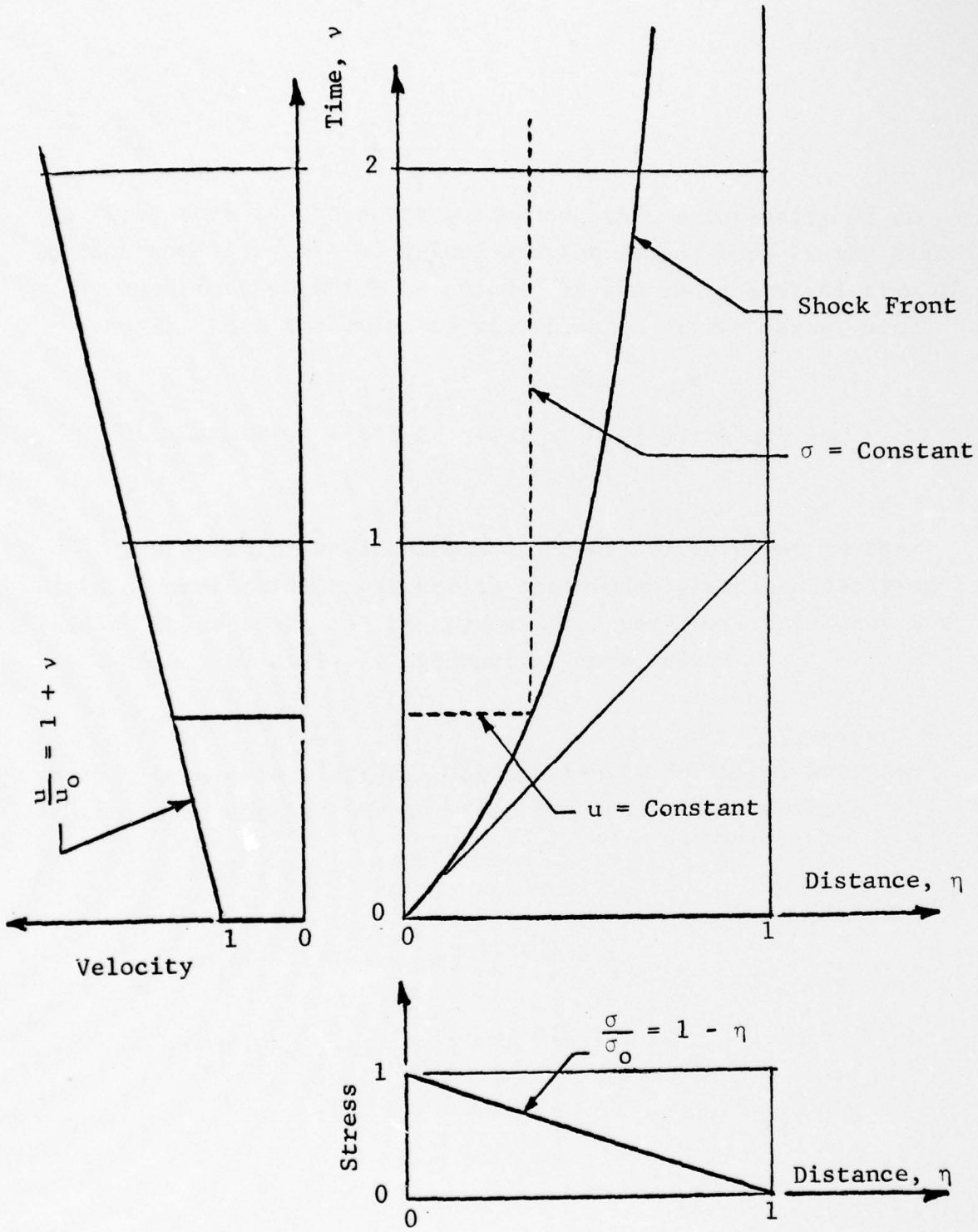

FIG. 46 SOLUTION FOR INVERSE FOURTH POWER MODULUS VARIATION

$$\frac{u}{u_o} = (1 - \tau') - (\tau - \tau')$$

The first term is the contribution due to the intensity of the surface load (or initial value) and the second term is the time decay contribution which is delayed by the shock arrival time τ'. In general, then the velocity will consist of two parts, viz.

$$\frac{u(\zeta, \tau)}{u_o} = (1 - \tau')\, G(\tau - \tau') - \int_{\tau'}^{\tau} G(\tau - \tau')\, d\tau$$

The dynamic surface loads which are of interest to the field of protective construction are suddenly applied decaying loads. These loads can be approximated very well, at least for early times, by a simple exponential form, viz.

$$G(\tau) = e^{-\alpha\tau}$$

where α is a decay factor. The previously indicated integrations can be carried out to yield the following results

$$\frac{\sigma}{\sigma_o} = (1 + \zeta)\, e^{-\alpha(\tau - \tau')}$$

$$\frac{u}{u_o} = \left[(1 - \tau') + \frac{1}{\alpha}\right] e^{-\alpha(\tau - \tau')} - \frac{1}{\alpha}$$

$$\frac{s}{s_o} = \frac{2}{\alpha}\left[(1 - \tau') + \frac{1}{\alpha}\right]\left[1 - e^{-\alpha(\tau - \tau')}\right] - \frac{2}{\alpha}(\tau - \tau')$$

where:

$$s_o = \frac{b}{2}\,\frac{\sigma_o}{M_o}$$

Some typical displacement results are shown in Fig. 47. The response of the soil exhibits a definite bounce characteristic. The effect of the decaying surface wave decreases with depth since the response of the soil at depth increases. For a step pulse the soil reaches a maximum displacement s_m which falls off as the inverse square of the depth variable,

$$\frac{s_m}{s_o} = \left(\frac{1}{1+\zeta} \right)^2$$

The fourth power fit of the modulus variation appears to be a reasonable approximation for surface and near surface soil conditions. However, at greater depths the modulus generally approaches a constant value. The results of the previous paragraphs can be used to construct relatively simple analytical relations to describe the response of a media of this more complicated modulus distribution. To illustrate this we have selected a modified modulus form which consist of a fourth-power increase to a depth ζ_1 and then a region of constant modulus, M_1. This is illustrated in Fig. 48. We will derive the response of the medium to a step load at the surface of intensity σ_o. Again the response of the medium to a more general input $G_o(\tau)$ can be obtained by suitable integrations.

The propagation of the shock front will occur as in the basic solution and result in the generation of a reflected and transmitted disturbance at $\zeta = \zeta_1$. This disturbance will reverberate between $\zeta = 0$ and $\zeta = \zeta_1$ and define a number of distinct solution zones. These are illustrated and defined in Fig. 49. It should be noted that the zones in the constant modulus portion of the medium are regions of simple waves. This fact results in a simple relationship between the stress and the particle velocity.

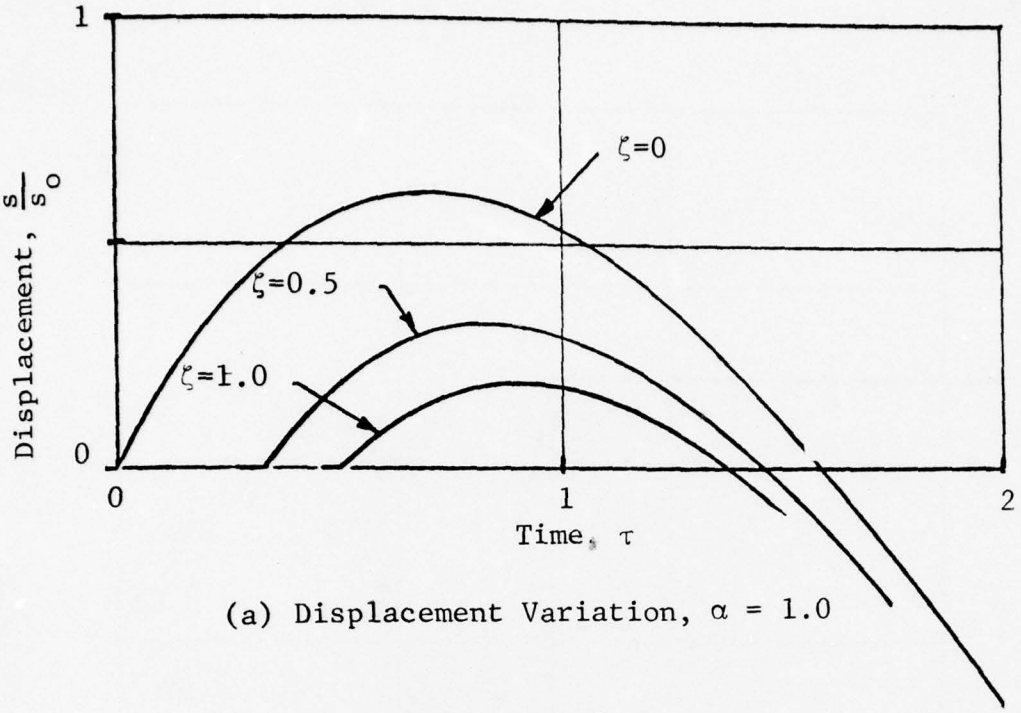

(a) Displacement Variation, $\alpha = 1.0$

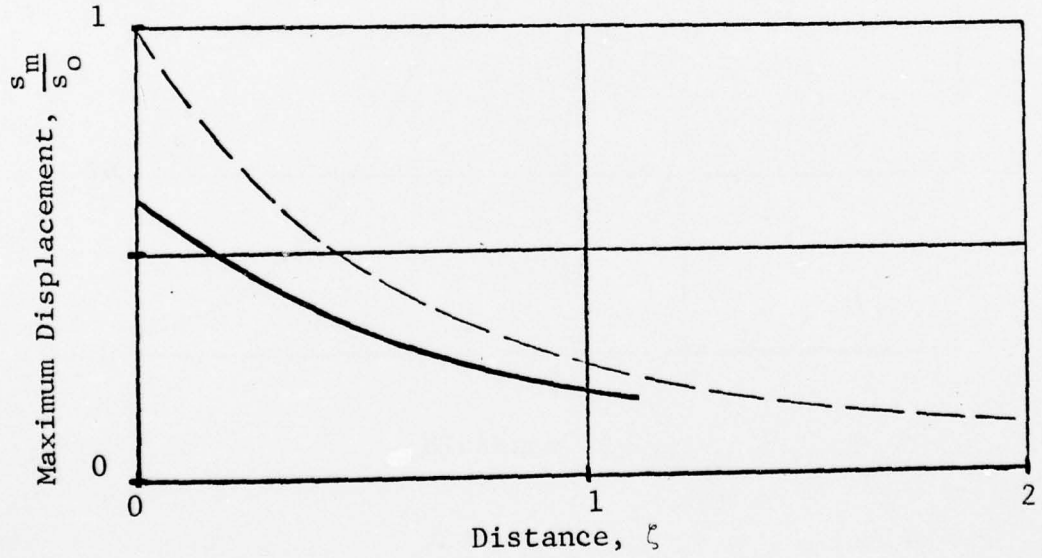

(b) Maximum Displacement, $\alpha = 1.0$

FIG. 47 DISPLACEMENT VARIATION AND MAXIMUM DISPLACEMENT

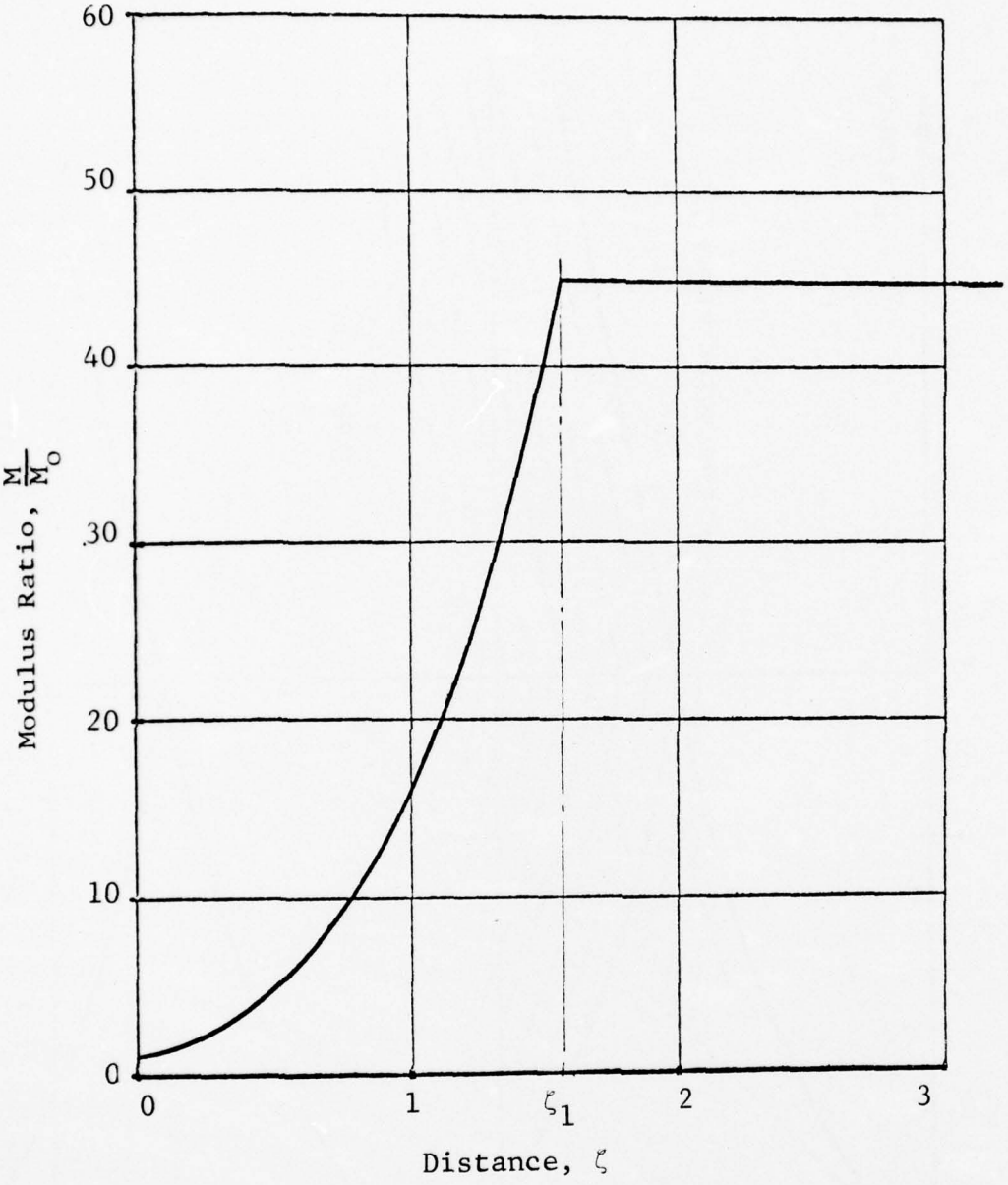

FIG. 48 MODIFIED MODULUS FORM

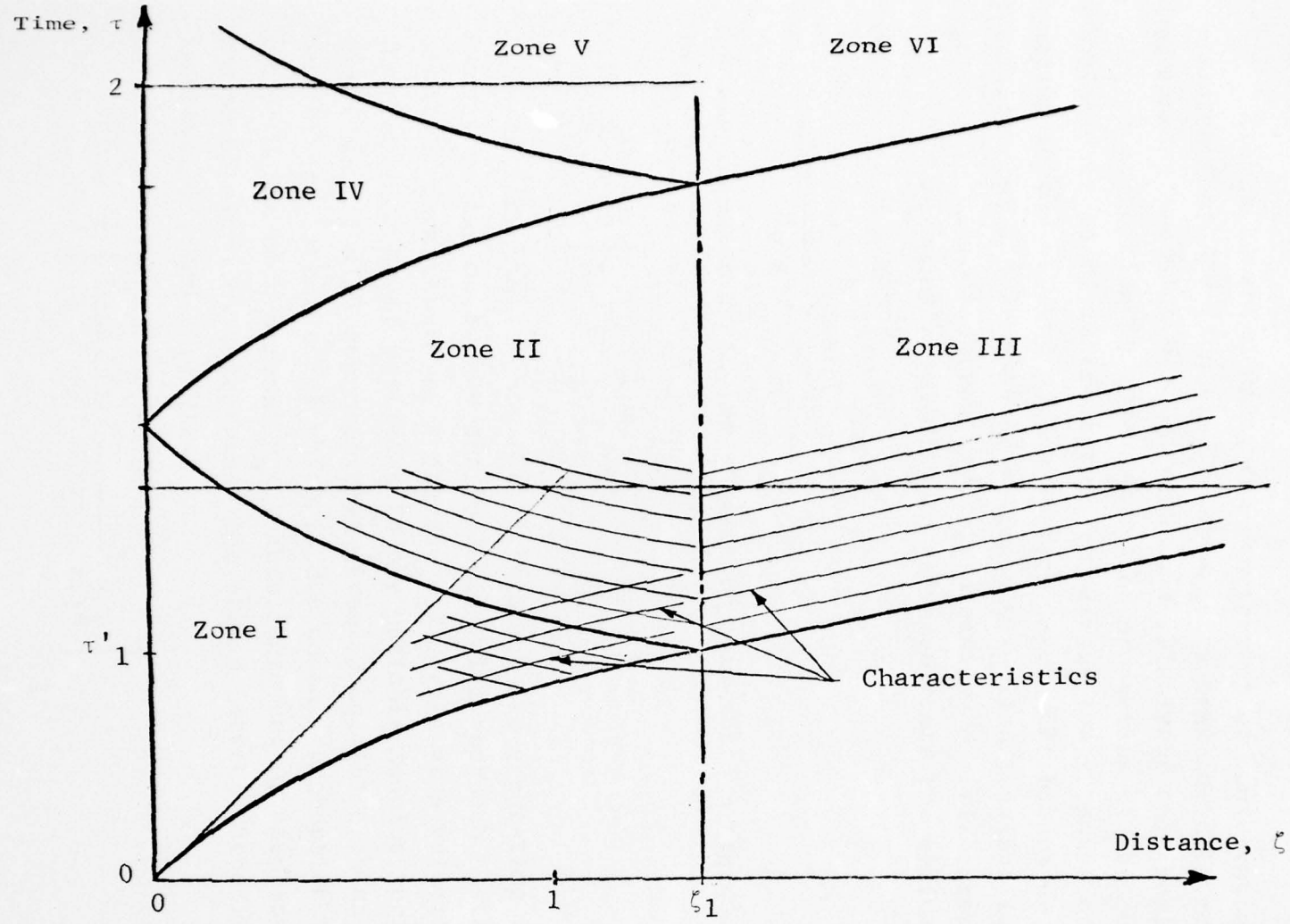

FIG. 49 WAVE DIAGRAM, MODIFIED MODULUS FORM

The solution has been constructed for the first four zones. Typical displacements are presented in Fig. 50.

It can be shown using the requirement of conservation of momentum that the long time behavior of a semi-infinite region of constant modulus M_1 , covered by a relatively thin region of varying properties is governed by the properties of the constant region. It is of interest then to examine the response of the medium in the absence of the surface layer. As before we will consider the simple case of a suddenly applied constant load of intensity σ_o . A stress wave of intensity σ_o will propagate into the medium at a velocity c_1 and accelerate the medium to a velocity u^*, where

$$u^* = \frac{\sigma_o}{\rho_o c_1}$$

The displacement s^* at the surface of this uniform region will be

$$\frac{s^*}{s_o} = 2\left[\frac{1}{1+\zeta_1}\right]^2 \cdot \tau \qquad (6)$$

At late times, when the disturbances reverberating in the surface region decay the entire region will approach a static condition (compressed by a stress σ_o) moving at a velocity u^* . The displacement of particles in the variable modulus region ($0 \leq \zeta \leq \zeta_1$) will approach that given by Eq. (6) plus an increment of displacement $\Delta\hat{s}$ which is due to the compression of the entire media to a stress σ_o . This increment of displacement can be obtained by integrating the strain between the point of interest, ζ , and ζ_1, viz.

$$\frac{\Delta\hat{s}}{s_o} = \frac{2}{3}\left[\frac{1}{(1+\zeta)^3} - \frac{1}{(1+\zeta_1)^3}\right]$$

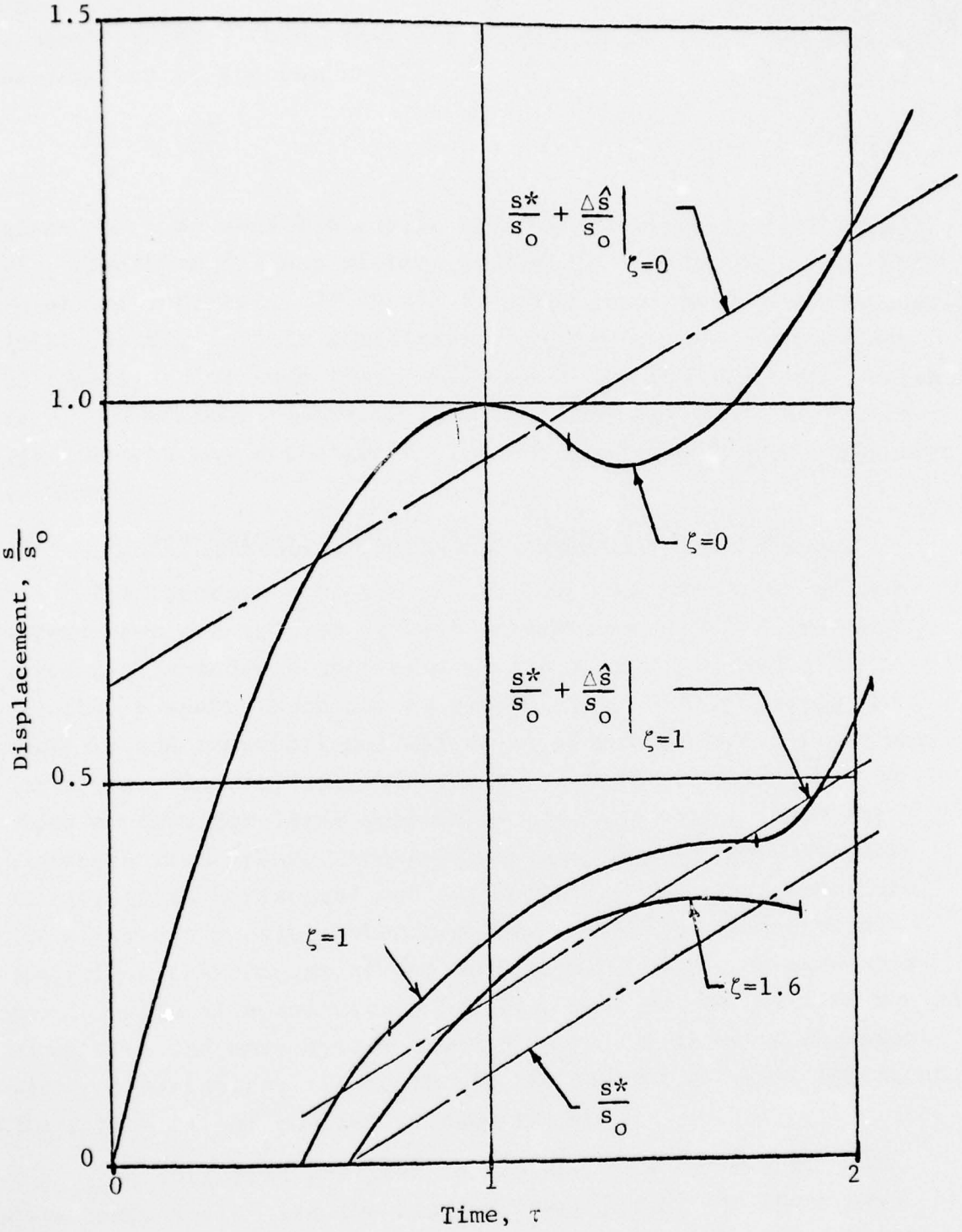

FIG. 50 DISPLACEMENTS, MODIFIED MODULUS FORM, $\zeta_1 = 1.6$

We would expect, then, that the displacements would approach a value given by the sum

$$\frac{s^{\star}}{s_o} + \frac{\Delta\hat{s}}{s_o} \qquad (7)$$

where the time variable equals zero at the shock arrival time, τ' . Equation (7) was plotted in Fig. 50 corresponding to the points of interest. It should be noted that the medium responds quite rapidly to this equilibrium condition. The oscillations will persist for some time, which is as yet undetermined. Furthermore, the maximum excursion from this equilibrium or reference displacement may not occur during the first four zones which were examined.

III. TWO-DIMENSIONAL QUASI-STEADY STRESS WAVE PROPAGATION

The importance of the multidimensional character of the stress wave propagation is well established, however, in many cases the dependence upon some of the spatial variables is relatively weak. Much can be gained then, in simplifying the analysis and computational effort by dropping these unimportant variables. The superseismic region of the air-induced ground shock problem for large weapons is one such case. Since the distances from ground zero are generally large, the divergence effects (both horizontal and vertical) are small. Furthermore, the air blast pressure waveform changes slowly. Under these conditions the complex stress wave problem can be reduced to a two-dimensional quasi-steady problem; that is, an observer moving along with the wave system views the problem as being dependent upon two variables, the depth and the distances behind the front. The latter is, of course, related to time.

The following analysis is divided into two parts. The first part deals with the basic interaction of the shock wave or disturbance front with a modulus discontinuity, and develops a differential equation governing the strength with a hydrodynamic as well as with an elastic model. The second part

presents a basic or exact solution for the pressure and velocity fields behind the shock wave, however, it is limited to the hydrodynamic model. Thus for this case, both the horizontal and the vertical displacements are known. The results of the first part permit one to evaluate the differences between the behavior of an elastic and a hydrodynamic media at the disturbance front and establish a measure of the importance of the shear capacity of the media to influence the stress and the motion in the media.

A linear and reversible stress-strain law was selected as in the previous one-dimensional nonsteady analysis. The wave diagram for the quasi-steady problem is illustrated in Fig. 51.

We can now examine the interaction of the disturbance front with a modulus discontinuity. Figure 52 illustrates this interaction for both the hydrodynamic and the elastic models.

For the hydrodynamic model the shock wave, S_i, will interact with the interface, I, across which the bulk modulus changes from M to M+ΔM. This interaction will generate a reflected shock wave S_r which will propagate back up into Region (1) and a transmitted wave S_t which will propagate into the undisturbed region.

The solution of this interaction yields, (after letting $\Delta M \rightarrow 0$)

$$\frac{dp}{p} = \frac{1}{2} \frac{dc}{c} \left[\frac{U^2}{U^2 - c^2} \right]$$

which when integrated results in the following stress amplification relation:

$$\frac{P}{P_o} = \left\{ \left(\frac{M}{M_o} \right) \left[\frac{\Lambda^2 - 1}{\Lambda^2 - \frac{M}{M_o}} \right] \right\}^{\frac{1}{4}}$$

where $\Lambda = \frac{U}{c_o}$.

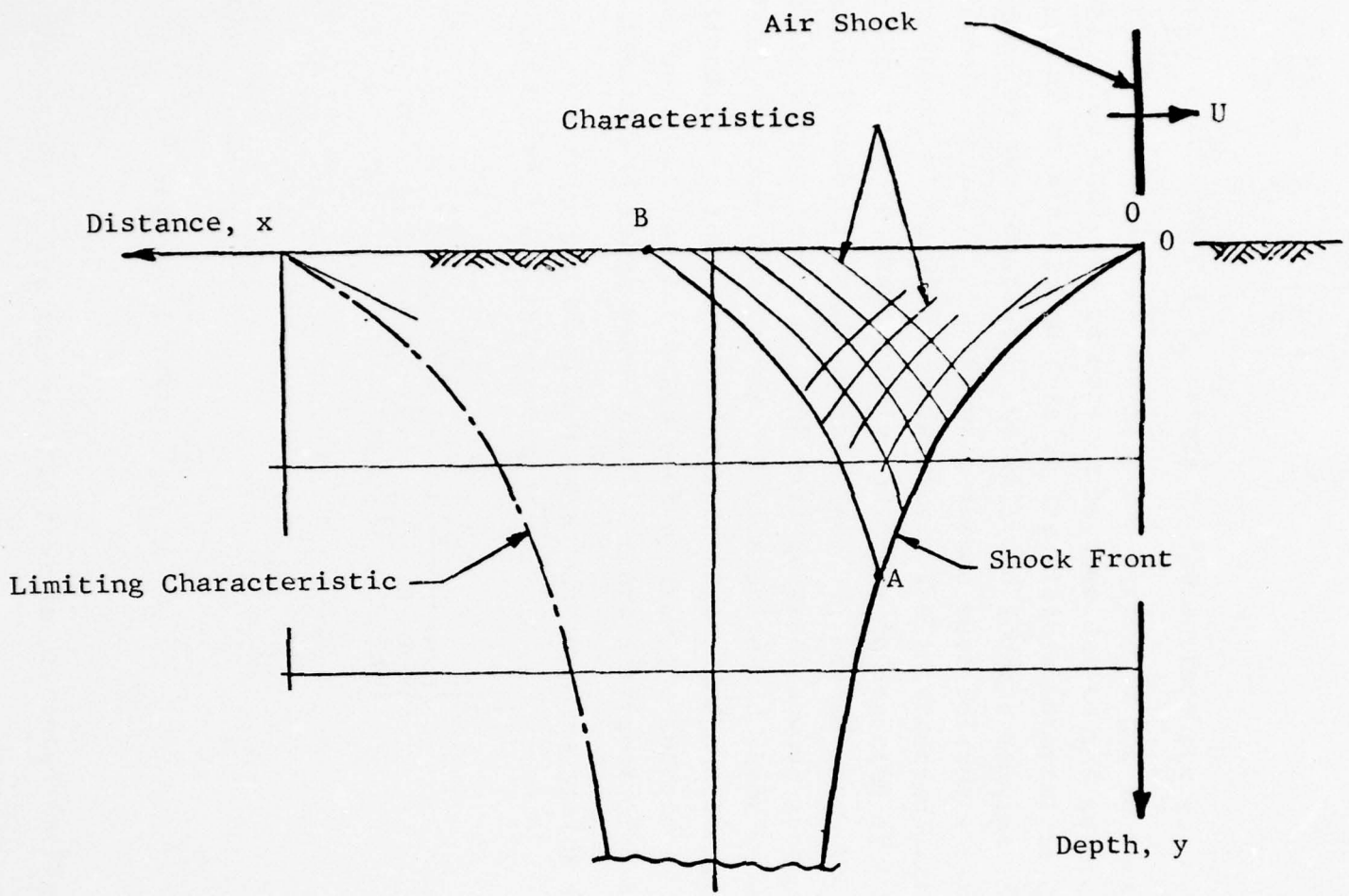

FIG. 51 WAVE DIAGRAM, TWO-DIMENSIONAL QUASI-STEADY MOTION

Furthermore the vertical (u) and horizontal (v) particle velocities are

$$\frac{P}{P_o} = \frac{u}{u_o} = \left(\frac{v}{v_o}\right)^{-1}$$

where the subscript $(\ )_o$ refers to the surface state.

The same kind of analysis was performed for an elastic media. The analysis is more cumbersome due to the more complex nature of an elastic material. The elastic material is characterized by two constants. We will use Young's modulus, E and Poisson's ratio , ν . We will assume that Poisson's ratio is a constant, along with the density. The interaction pattern for this case is shown in Fig. 52. The interaction of a dilatation of P wave, P_i with an interface, I, across which Young's modulus varies from E to E+ΔE will generate a wave system consisting of four other waves. A dilatation and shear wave will be transmitted into the undisturbed region and a dilatation and shear wave will be reflected back up from the interface. The dilatation and shear wave velocities are functions of E and ν.

The solution of this interaction problems yields (after letting $\Delta E \longrightarrow 0$ and integrating):

$$\frac{\sigma}{\sigma_o} = \left\{\left(\frac{E}{E_o}\right)\left[\frac{\Lambda^2 - 1}{\Lambda^2 - \left(\frac{E}{E_o}\right)}\right]\left[\frac{\Lambda^2 - a}{\Lambda^2 - \frac{E}{E_o}}\right]\right\}^{\frac{1}{4}}$$

where: $a = \dfrac{1 - 2\nu}{1 - \nu}$

ν = Poisson's ratio

A typical result for the elastic case is presented in Fig. 53.

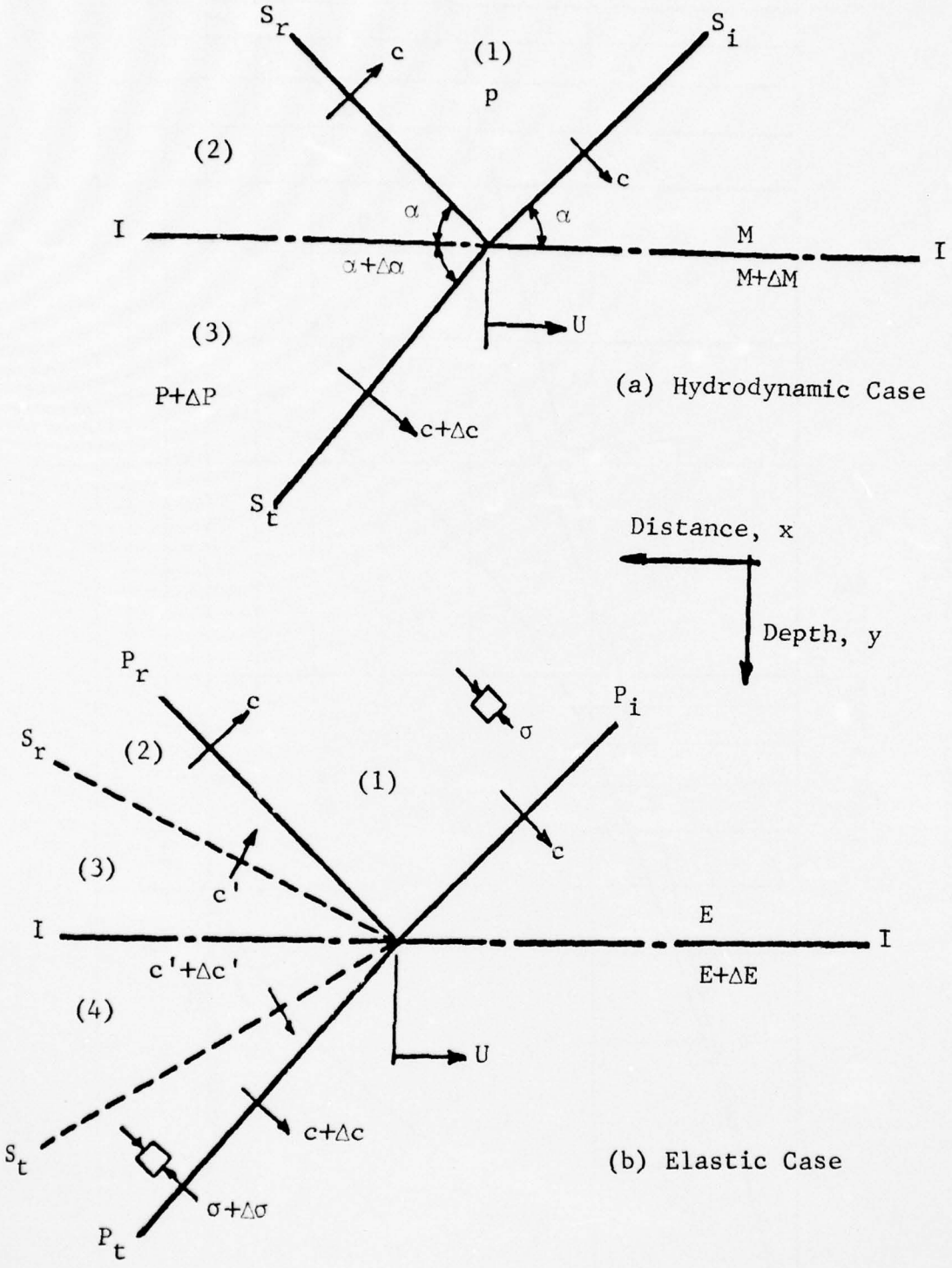

FIG. 52 INTERACTION AT MODULUS DISCONTINUITY

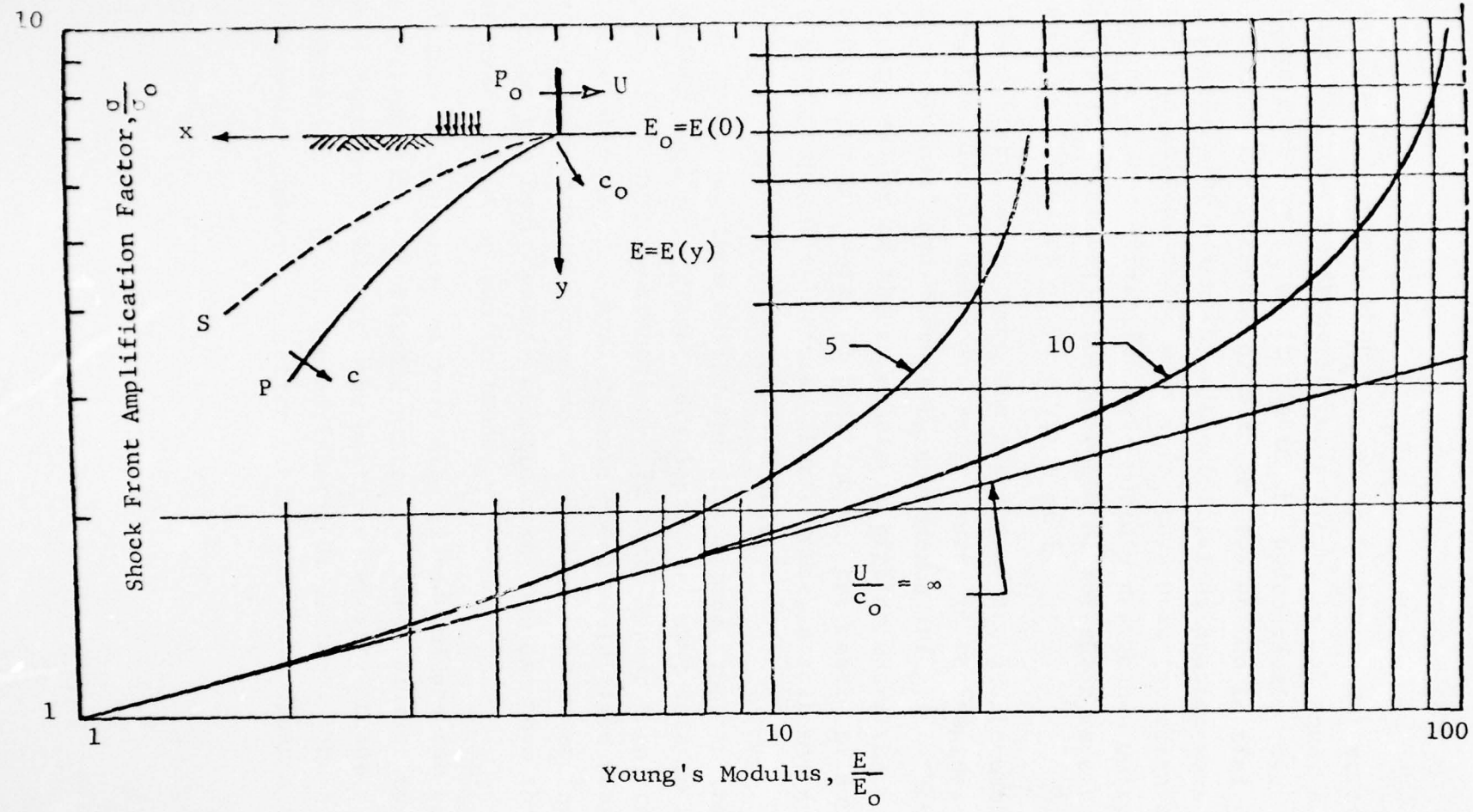

FIG. 53 TWO-DIMENSIONAL QUASI-STEADY ELASTIC MODEL

It should be noted that σ_o , which is the normal stress behind the disturbance front at the surface, is not equal to the surface pressure p_o as it was in the hydrodynamic case. This is due to the presence of a shear wave at the initial loading point. The strength of the initial dilatation wave σ_o/p_o and the initial shear wave τ_o/p_o have been investigated. The strength of the dilatation wave rapidly approaches unity when $U/c_o > 2$. Similarily the strength of the shear wave becomes small as U/c_o increases above a value of 2.

The differences between the results of the hydrodynamic model and the elastic model are small except in the regions where U/c_o is small and where E/E_o approaches $(U/c_o)^2$. These are extreme regions of the superseismic problem where the wave front approaches the vertical position and the onset of subseismic wave propagation occurs. Furthermore, a soil may not obey either one of the fundamental models.

The ground motions behind the disturbance front in the superseismic region represent very important input data to the design of protective construction. It would appear then, that an exact solution to the hydrodynamic model would yield reasonably accurate information on ground motions. Since the governing equation for the hydrodynamic elastic case, one can hope that such an exact solution can be found.

Figure 51 presents the wave diagram and defines the coordinate system. This coordinate system is fixed relative to the moving disturbance, that is, the particle velocity in the undisturbed region is U (in the horizontal direction). The basic equations which govern the motion behind the shock front are:

AD-A040 180 IIT RESEARCH INST CHICAGO ILL F/G 18/3
A BIBLIOGRAPHY ON THE RESPONSE OF EARTH MEDIA AND BURIED STRUCT--ETC(U)
JUN 67 R L CHIAPETTA, C J COSTANTINO DACA39-67-C-0015
UNCLASSIFIED WES-CR-3-168 NL

2 OF 2
AD
A040 180

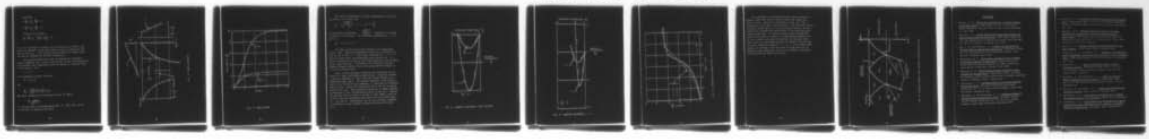

END
DATE FILMED
6-77

Momentum:

$$U \frac{\partial u}{\partial x} + \frac{1}{\rho_o} \frac{\partial p}{\partial x} = 0$$

$$U \frac{\partial v}{\partial x} + \frac{1}{\rho_o} \frac{\partial p}{\partial y} = 0$$

Conservation of Mass:

$$\frac{U}{c^2} \frac{\partial p}{\partial x} + \rho_o \left[\frac{\partial u}{\partial x} + \frac{\partial v}{\partial y} \right] = 0$$

Since the equations are linear we can consider the special case where the pressure at the free surface (y=0) is constant at the initial value p_o . The solution for any arbitrary surface load can then be obtained by suitable integration.

The solution obtained in the one-dimensional nonsteady problem suggests that a similar form exist for this two-dimensional quasi-steady case, especially since the former is a special case of the latter. Let:

$$p = p\ (y)$$

This assumption yields, as before

$$P = P_o \pm Ay$$

and

$$\frac{M}{M_o} = \frac{\Lambda^2\ (1 + \zeta)^4}{(\Lambda^2 - 1) + (1 + \zeta)^4}$$

The basic solution is illustrated in Fig. 54, where

$$\eta = \frac{x}{b} \frac{1}{\sqrt{\Lambda^2 - 1}}$$

The modulus form is illustrated in Fig. 55. This form can be fitted well to existing site data.

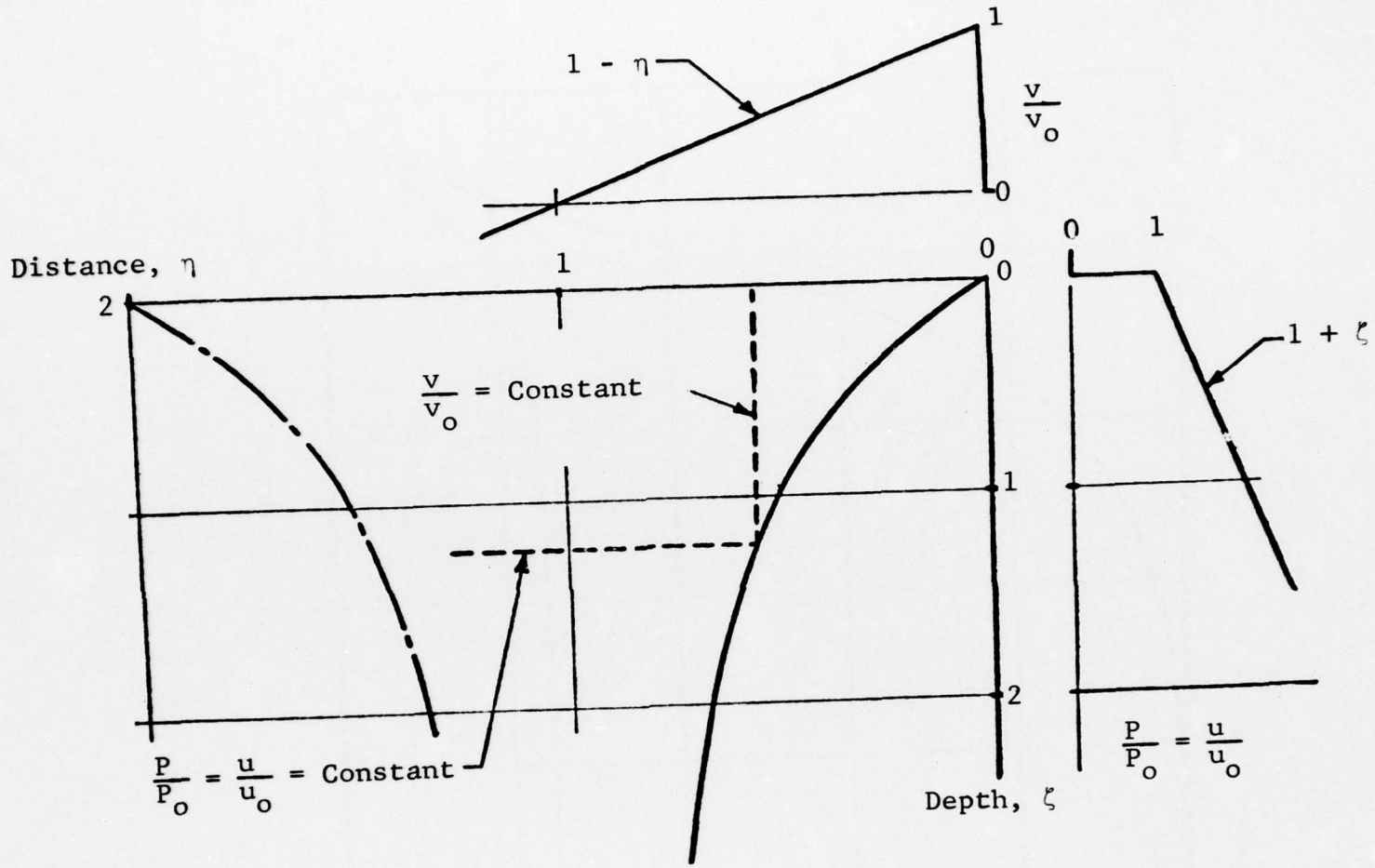

FIG. 54 BASIC SOLUTION

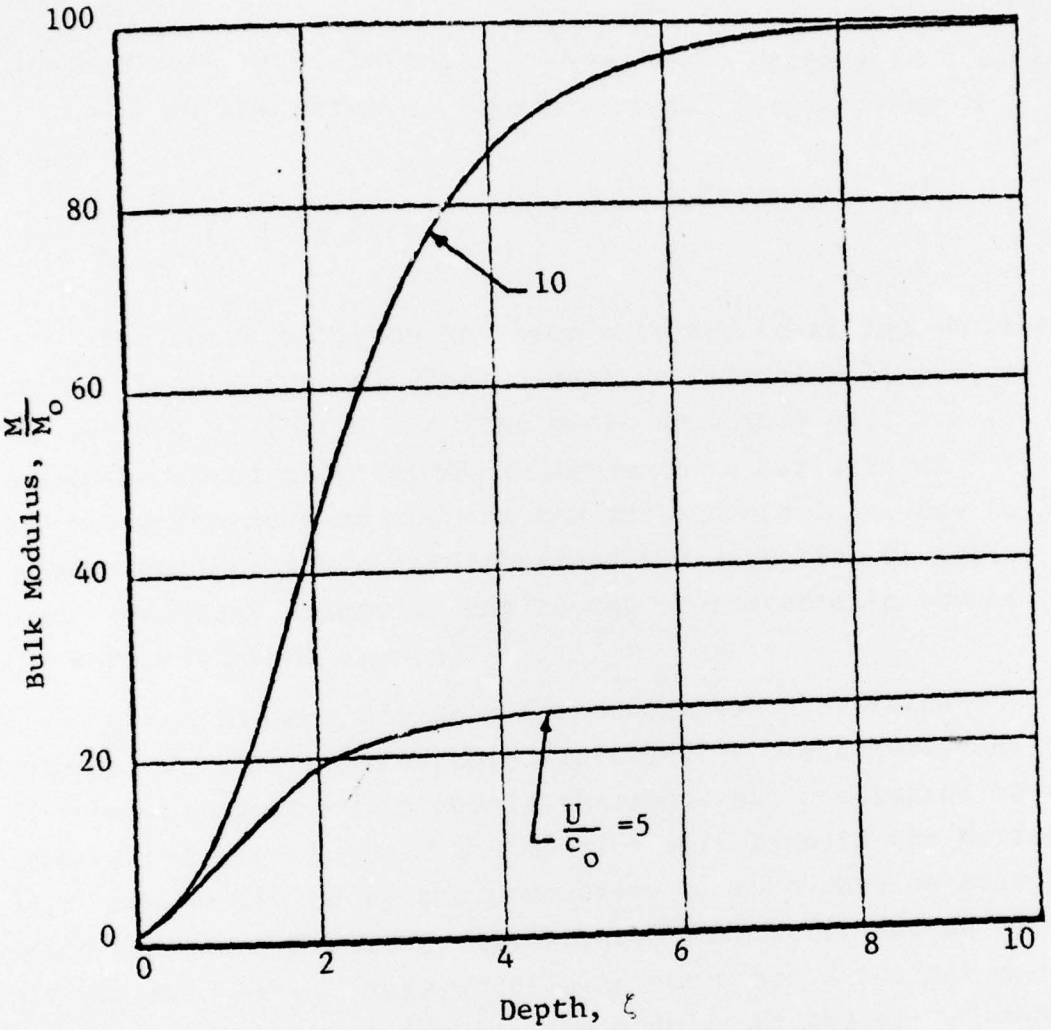

FIG. 55 MODULUS FORM

The vertical displacement; being representative of all of the results, is of the form.

$$\frac{s}{s_o} = 2\left[\frac{\sqrt{\Lambda^2 - 1}}{\Lambda}(\tau-\tau') - (\tau^2 - \tau'^2)\right]$$

The parametric coefficient $\frac{\sqrt{\Lambda^2 - 1}}{\Lambda}$ appears in a variety of places in the results. The horizontal displacement r, is given by:

$$\frac{r}{s_o} = (1 + \zeta)(\tau-\tau')$$

The basic solution has been extended to an exponential surface load. Typical displacement results are illustrated in Fig. 56 and 57 for $\alpha = o$ (the basic solution) and $\alpha = 1$. It should be noted that the trajectories of the particle at $\zeta = 1$ are not influenced as much as the surface particle, due to their rather rapid response. Furthermore the direction of motion changes rapidly primarily due to the characteristic bounce of the softer surface layer.

Since in many geologic formations the properties of the material at some considerable depth become relatively uniform, it becomes important to couple the above basic solution to a homogeneous base layer. The modulus variation in the surface layer can be fitted by the parameter, b, such that an acceptable match is made. Figure 58 illustrates such a fit for an actual missile silo site. This particular curve has a surface modulus M_o identical to the corresponding modulus at the site. However, the matching does not have to be done in this manner, hence we actually have two parameters with which to fit the field data (i.e., M_o and b). Furthermore, we can also tolerate a modulus discontinuity at the interface between the base and surface layer.

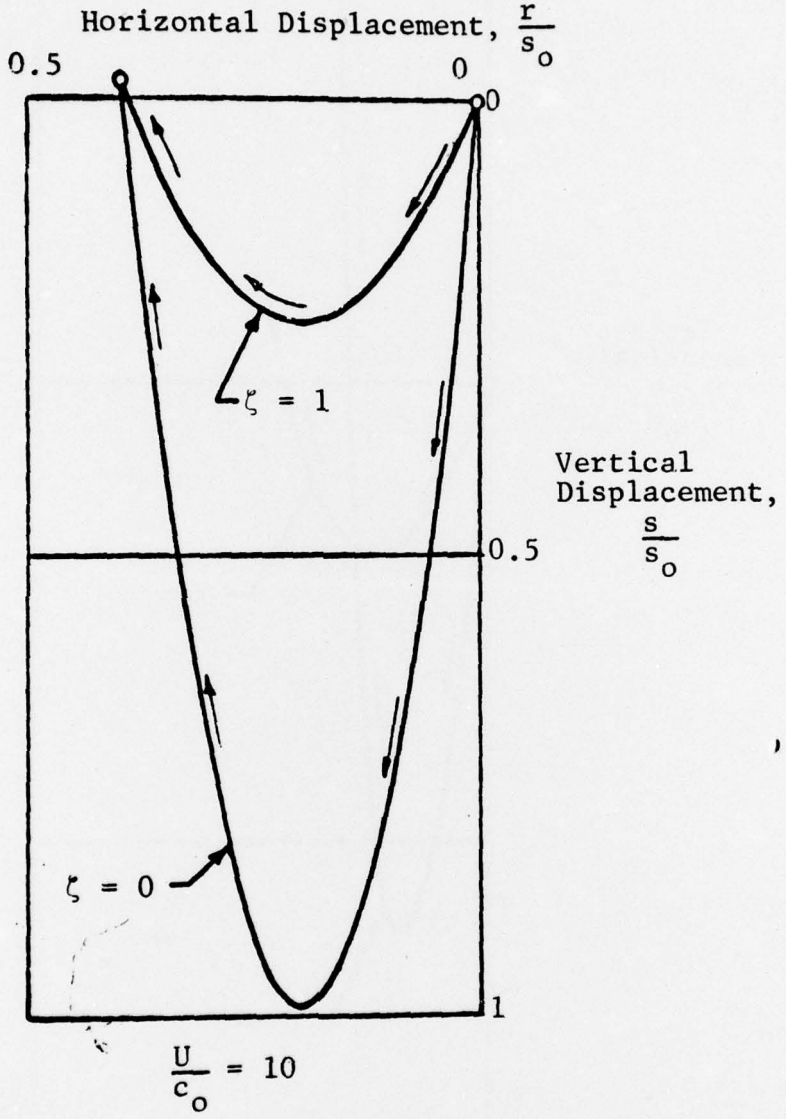

FIG. 56 PARTICLE TRAJECTORY, BASIC SOLUTION

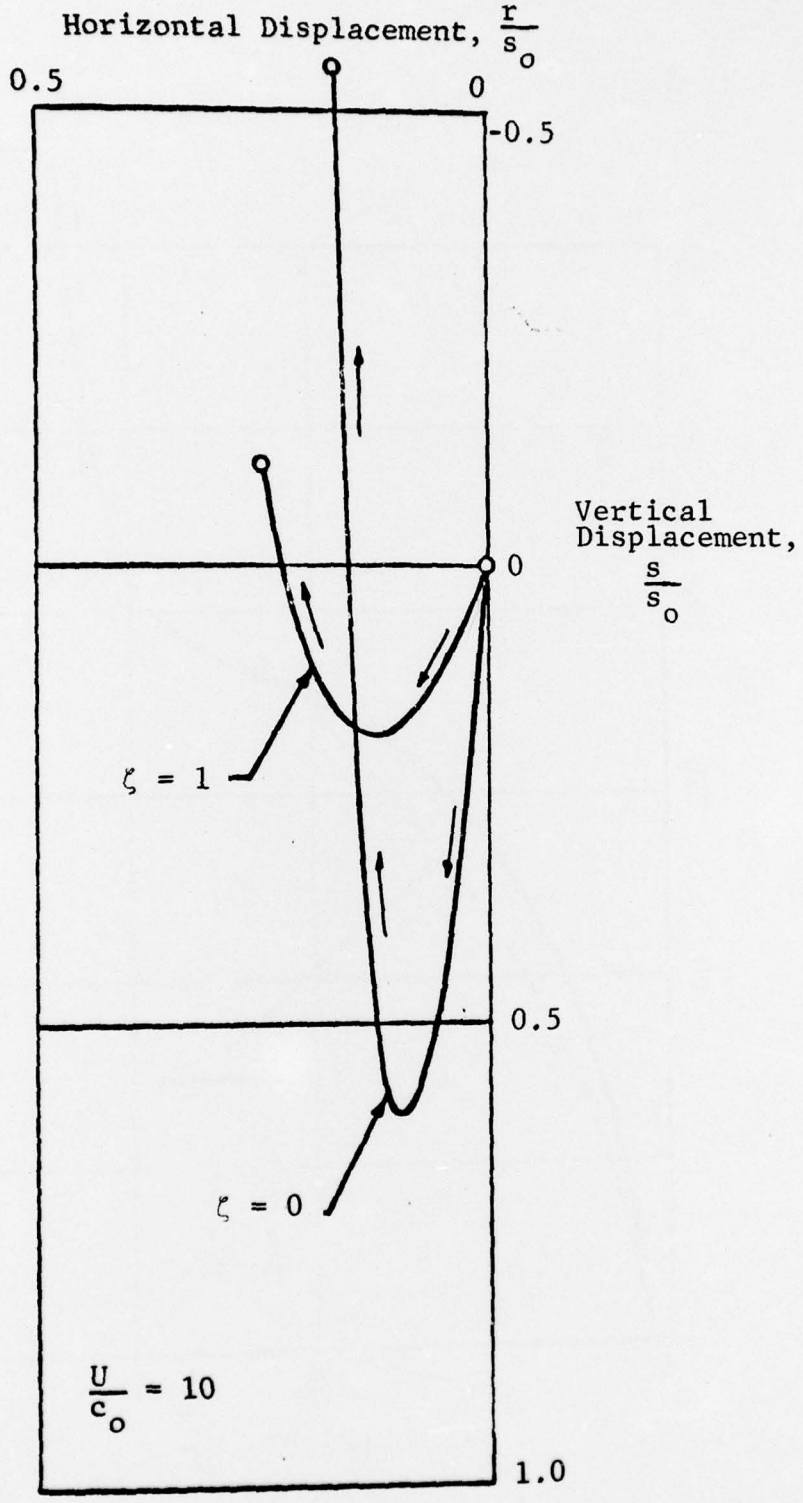

FIG. 57 PARTICLE TRAJECTORY, $\alpha = 1$

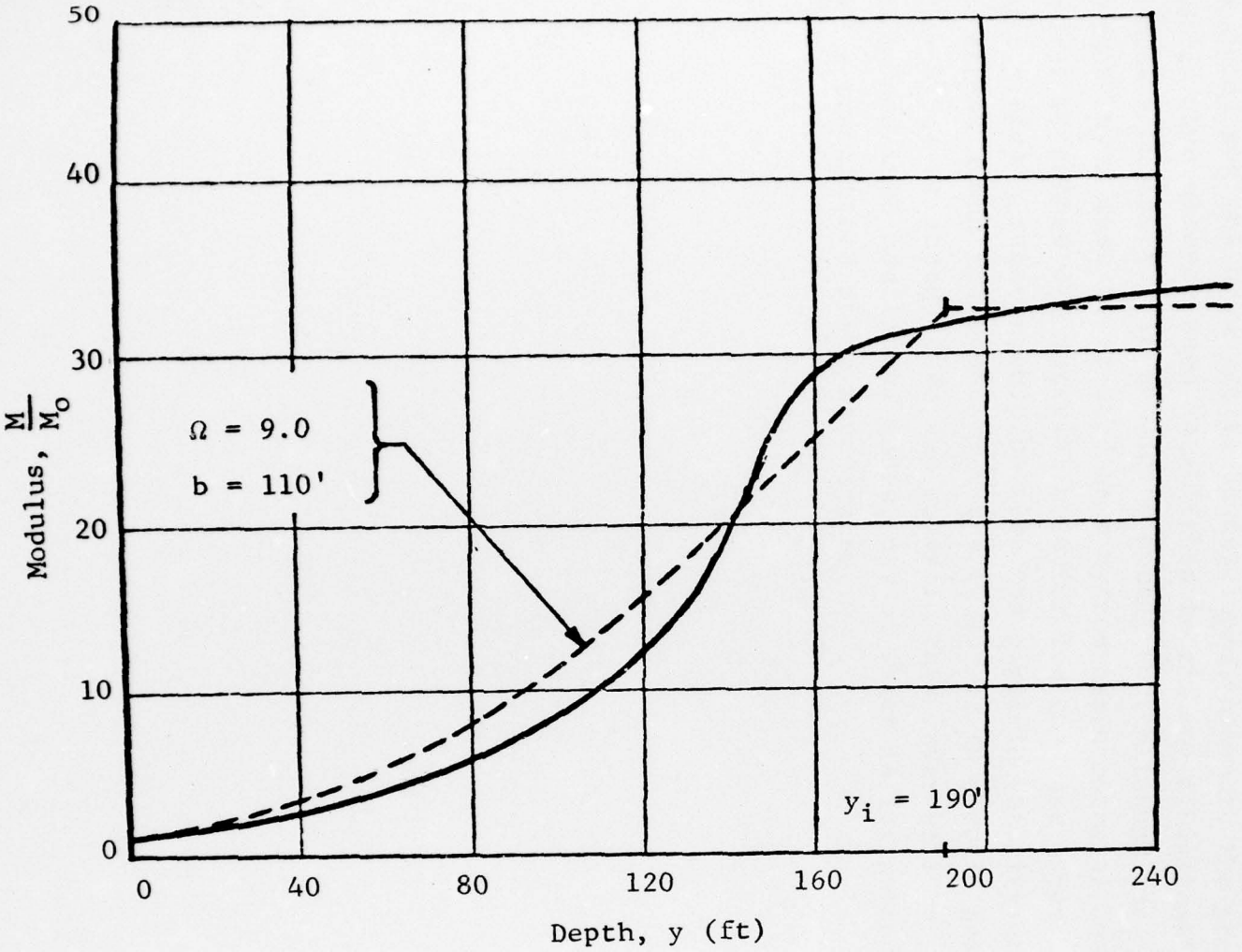

FIG. 58 COMPARISON OF MODULUS FORM WITH FIELD DATA

The existance of a homogeneous base layer introduces a definite major wave pattern which divides the region into descrete zones. These are illustrated in Fig. 59. Zone I corresponds to the basic solution given. The solutions for the remaining regions have yet to be developed, however, the procedures have already been established in the one-dimensional nonsteady analysis. It should be noted, that although the surface layer must be treated as a hydrodynamic material one is free to choose any material behavior for the base layer which yields a relationship between the particle velocity and the stress along its boundary ($\zeta = \zeta_1$). If an elastic base material is selected, then the zones in this layer will be subdivided into additional zones, one of which is influenced by the transmitted shear wave system.

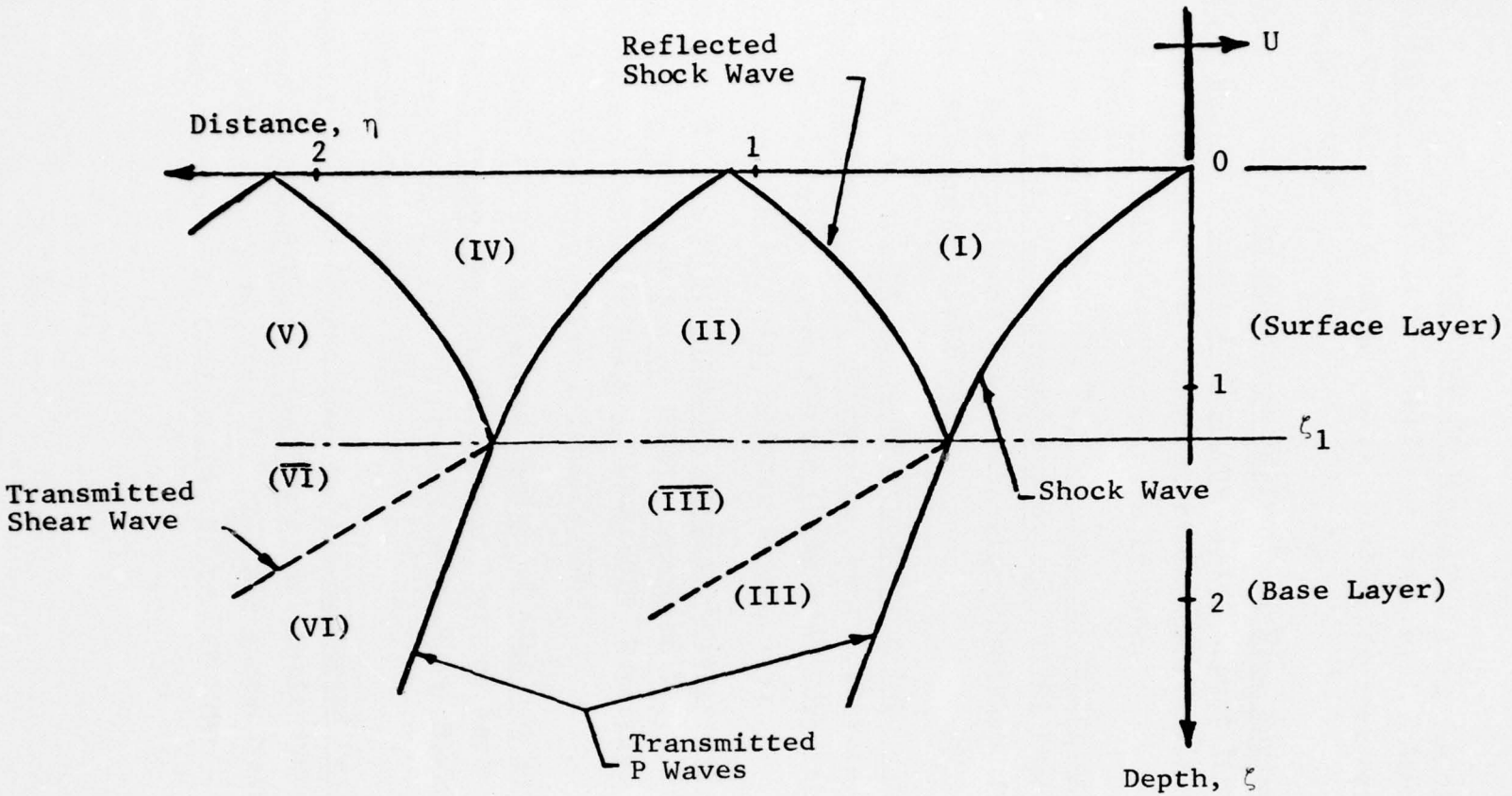

FIG. 59 MODIFIED MODULUS WAVE PATTERN, ELASTIC BASE LAYER

REFERENCES

1. Eichler, J. B., Stress Wave Propagation in Elastic-Plastic Compactable Media, IITRI-578P21-10, Vol. 4, for Atomic Energy Commission Contract AT(11-1)-578, Project Agreement 21, June 1966

2. Eichler, T. V., Ground Shock Environment From Surface and Shallow-Buried Nuclear Explosions, IITRI Report T6094, for U.S. Army Engineer R & D Laboratory Contract DA-44-009-AMC-661 (T), Fort Belvoir, Virginia, July 1965

3. Ash, J. E. and Eichler, T. V., A Theory of Cratering for Multiple Nuclear Underground Explosions, IITRI Report T6094, for U.S. Army Engineer R & D Laboratory Contract, Fort Belvoir, Virginia, April 1964

4. Wiedermann, A. H., Stress Wave Propagation Into a Region of Changing Modulus of Deformation, Paper presented at Ground Shock Calculation Meeting, the RAND Corporation, Santa Monica, California, October 26-28, 1965

5. Robinson, R. R., Miscellaneous Studies Relating to Wave Propagation Through Soils, IITRI Report M6177, for Corps of Engineers Contract DACA 39067-C-0015, Waterways Experiment Station, Vicksburg, Miss., January 1967

6. Costantino, C. J., Automated Design of Advanced Hardened Facilities Study, Ballistic Systems Division Report TR-66-256, Vol. I, Air Force Systems Command, Norton AFB, California, September 1966

7. Wachowski, A. and Costantino, C. J., Automated Design of Advanced Hardened Facilities Study, Ballistic Systems Division Report TR-66-256, Vol. II, Air Force Systems Command, Norton AFB, California, September 1966

8. McDowell, E. L., Deviatoric Effects in High-Intensity Stress Waves, IITRI Report M6097, for Air Force Weapons Laboratory Contract AF29(601)-6696, Kirtland Air Force Base, New Mexico, June 1966

9. Robinson, R. R., Hardness Levels for Titan II As-Built 100,000 Gallon Water Tank for Silo Response Analysis Shock Input, IITRI Report M6144, for Air Force Ballistic Systems Division Contract P.O. (04-694)-66-12, Norton AFB, California, June 1966 (Secret)

10. Miller, C. A., Vertical Interaction Code Programmer's and User's Manual, IITRI Report M6142, September 1966

11. Costantino, C. J. and Marino, R. L., Response of Cylindrical Shell Encompassed with Isolation Material to a Plane Pressure Pulse, IITRI Report M6096, for Air Force Weapons Laboratory, June, 1965

12. Costantino, C. J., Study of Advanced Missile Support-Isolation Systems, IITRI Report M6091, Part I, for Air Force Ballistic System Division Contract AF04(694)-569, January 1965, (Secret)

13. Wachowski, A. and Costantino, C. J., Study of Advanced Missile Support-Isolation Systems, IITRI Report M6091, Part 2, for Air Force Ballistic System Division, Contract AF04(694)-569

14. Wilson, S. D. and Sibley, E. A., Ground Displacements from Air-Blast Loading, Proc. A.S.C.E., December 1962

15. Wiedermann, A. H., Stress Wave Propagation Into a Region of Changing Modulus of Deformation, March 1965 (unpublished)

16. Wiedermann, A. H., Some Comments on Two-Dimensional Quasi-Steady Stress Wave Propagation Into a Region of Changing Modulus of Deformation, September, 1965 (Unpublished)